STUDY OF SOME HEAVY-ION INDUCED REACTIONS BELOW 7 MeV/NUCLEON

ABSTRACT

OF THE

THESIS

SUBMITTED FOR THE AWARD OF THE DEGREE OF

Doctor of Philosophy

IN

EXPERIMENTAL NUCLEAR PHYSICS

BY

TAUSEEF AHMAD

Under the Supervision of

DR. ISAR AHMAD RIZVI

(Reader)

DEPARTMENT OF PHYSICS
ALIGARH MUSLIM UNIVERSITY
ALIGARH (INDIA)

2008


Azad Library

ABSTRACT

The main purpose of the thesis is to shed light on the heavy-ion (HI) reaction mechanisms involved in the formation of the observed evaporation residues. The thesis explores the dynamics of HI induced reactions (mainly complete and incomplete fusion) by measuring the excitation functions(EFs) for a large number of residues produced in $^{12}C + ^{93}Nb$, $^{12}C + ^{52}Cr$ and $^{16}O + ^{115}In$ systems at energies near and well-beyond the Coulomb barrier. The measured EFs for various residues in these systems have been compared with the statistical model code PACE 2, based on Hauser-Feshbach theory. In order to show the difference between our data and the earlier reported values (in the case of $^{12}C+ ^{93}Nb$ system) we have also compared our new measurements with the ALICE-91 whereas the earlier researcher has compared the results with old version ALICE. Further, to separate the relative contributions of the complete and the incomplete fusion in $^{12}C+^{93}Nb$ system, the Recoil Range Distributions (RRDs) of several residues have also been measured.

From the point of view of Physics, the different reaction mechanisms of HI collisions and their dependence on the available laboratory energies are of great interest. Ever since Incomplete Fusion (ICF) reactions in HI collisions have been observed at relatively low bombarding energies, the study of mechanisms of these reactions has gained momentum. Moreover, the ICF reactions are considered to be a promising route to populate high spin states in heavy residues using moderate heavy–ion beams (A $\leq$16) even at low bombarding energies. In view of all these developments the study of the ICF dynamics may provide key parameters to determine optimum irradiation conditions for the production of radio-active ion beams (RIBs). In order to explain the ICF reactions, several dynamical models, such as the Sum-rule model, the Break- up Fusion (BUF) model, the Promptly Emitted Particles (PEPs) model etc., have been proposed. However, none of

these models has succeeded in explaining all the features of ICF reactions at energies below 10 MeV/ nucleon. Hence the ICF reactions continue to be an active area of investigation. Such an investigation may be fruitful if it aims at systematizing the ICF dynamics by using the precise experimental data covering a wide range of the periodic table and energies.

In this context, an accurate measurement and analysis of the EFs of nuclear reactions are of immense importance. It is the shape of the EFs which reveals the reaction mechanism. For instance, the slowly descending tail of the EFs is a direct signature of the pre-equilibrium emission. A comparison of experimentally measured EFs with the theoretical model calculations indicates an agreement and /or disagreement which serve as a clue for the understanding of reaction mechanism of CF and/or ICF. This is not the only criterion we have used for determining the CF and/or ICF mechanism but RRDs (in the case of $^{12}C+^{93}Nb$ system) have also been used as a criterion to characterize the aforesaid mechanisms.

Apart from being beneficial to the area of HI reactions, the study of the EFs is useful from the point of view of nucleo-synthesis. Moreover, there is a growing need of a comprehensive understanding of EFs so that the production of isotopes used in medicine may be maximized. Besides, the values of EFs play a significant role in the study of thin layer activation (TLA) technique. In addition to these applications, the EFs are also in demand for the development of accelerator driven subcritical reactors popularly known as energy amplifiers.

In order to study HI reaction mechanism, the experiments were carried out at Inter-University Accelerator Centre (IUAC), New Delhi, India. In our experiments three different types of targets viz., ^{93}Nb, ^{52}Cr and ^{115}In were prepared either by rolling machine or by the vacuum–evaporation technique. The Al foils, prepared by rolling machine, were used as energy degraders in the EF measurements. To characterize the thickness of each

target, we used gravimetry for ^{93}Nb and the alpha transmission method for ^{52}Cr and ^{115}In. Three different stacks of samples were irradiated for different time spans keeping in view the half-lives of the yields, the melting point of the target element and also the thickness of the targets. After the irradiation, the exposed stack was taken out of General Purpose Scattering Chamber (GPSC) using In-vacuum Transfer Facility (ITF). Then, the gamma–ray spectra of activated target foils were recorded by counting the target and catcher foils together using a high resolution (≈2 keV for 1332 keV γ ray of ^{60}Co) high purity Ge (HPGe) detector of 100 cm^3 active volume coupled to a PC based multichannel analyzer employing FREEDOM software. The dead time for counting was kept less than 10% by adjusting the target detector separation in these measurements and proper account of the dead time was taken in the calculations. Various peaks observed in these spectra were assigned to different reaction residues on the basis of their characteristic energy of gamma-lines as well as measured half-lives. The activation technique which is popular for its sensitivity, selectivity and simplicity, was employed in these measurements. The RRDs of several residues at ≈ 80 MeV incident beam energy have also been measured using recoil catcher technique and off-line gamma ray spectrometry. In order to measure the RRDs, the yield was calculated by way of dividing the cross-section by thickness of each catcher foil.

The experimentally measured EFs for ^{12}C and ^{16}O induced reactions were compared with the theoretical predictions made on the basis of model code PACE2. By way of such a comparison, we have extracted some important information about the complete and the incomplete fusion process in heavy–ion reactions. The considerable enhancements of the experimentally measured EFs for some reactions clearly indicate that these reaction channels are populated not only via the complete fusion but also through the incomplete fusion process. The analysis of RRDs confirms the presence of contributions from the ICF reactions. The range distributions clearly show three separable components, which are attributed to complete fusion of ^{12}C, incomplete fusion of ^{8}Be and incomplete

fusion of ^{4}He, with the target. The determined relative contributions (shown in %) of the CF and the ICF indicate that the ICF plays an important role in the population of different reaction products involving direct α-cluster and Be emission at energies below 7 MeV/nucleon. Moreover, the direct reactions are also found to be significant in the population of radio-nuclides ^{93}Mo^{m} and ^{92}Nb^{m}.

The present thesis consists of five chapters. In the first chapter, a general introduction of HI induced reactions and related topic is presented. A brief review of the work reported in this thesis is also given in this chapter. The second chapter focuses on the essential experimental details for studying HI reactions at IUAC and the derivation of cross-section formulation. The measurements of EFs for thirty reactions namely ^{93}Nb (C, 2n)^{103}Ag, ^{93}Nb (C, 3n) ^{102}Ag, ^{93}Nb(C, 4n) ^{101}Ag, ^{93}Nb(C, p3n)^{101}Pd, ^{93}Nb (C, p4n)^{100}Pd, ^{93}Nb(C, p5n)^{99}Pd, ^{93}Nb(C, 2p2n)^{101}Rh , ^{93}Nb(C,αn)^{100}Rh, ^{93}Nb(C,α2n)^{99}Rh, ^{93}Nb(C,αp3n)^{97}Ru, ^{93}Nb(C,αp5n)^{95}Ru,^{93}Nb(C,2αn)^{96}Tc,^{93}Nb(C,2α2n)^{95}Tc,^{93}Nb(C,2α3n)^{94}Tc,^{93}Nb(C,2αp3n)^{94} Mo^{m} , ^{93}Nb(^{12}C,^{13}C)^{92}Nb^{m} , ^{52}Cr (C, 2n) ^{62} Zn, ^{52}Cr (C, p2n) ^{61} Cu, ^{52}Cr (C, p3n) ^{60}Cu, ^{52}Cr(C,α3n) ^{57}Ni, ^{52}Cr(C,α4n) ^{56}Ni, ^{52}Cr (C, α p3n) ^{56}Co, ^{52}Cr (C, α p4n) ^{55} Co, (C, α3pn) ^{56} Mn,^{115} In (O,p3n)^{127}Ba, ^{115} In (O,p4n)^{126}Ba , ^{115} In (O, α)^{127}Cs, ^{115} In (O,α2n)^{125}Cs, ^{115} In (O, αp3n)^{123}Xe, and ^{115} In (O, αp5n)^{121}Xe have been enumerated in the third chapter. It is worth mentioning here, that sections 3.4 and 3.5 of the same chapter comprise of the measurement of forward recoil range distributions (RRDs) and the uncertainties in the measurements respectively. The essential input parameters for evaluating EFs using computer codes ALICE-91 and PACE2 are discussed in the fourth chapter. The last chapter contains the experimental results and their analyses using the above-mentioned codes.

STUDY OF SOME HEAVY-ION INDUCED REACTIONS BELOW 7 MeV/NUCLEON

THESIS

SUBMITTED FOR THE AWARD OF THE DEGREE OF

Doctor of Philosophy

IN

EXPERIMENTAL NUCLEAR PHYSICS

BY

TAUSEEF AHMAD

Under the Supervision of

DR. ISAR AHMAD RIZVI

(Reader)

DEPARTMENT OF PHYSICS
ALIGARH MUSLIM UNIVERSITY
ALIGARH (INDIA)

2008

Dedicated

To my

Parents

Dr. Isar Ahmad Rizvi
Reader

DEPARTMENT OF PHYSICS
Aligarh Muslim University
Aligarh-202002 (India)
Phone: 91- 0571- 2701001(Off.)
91- 0571- 2703125(Res.)
Mobile: 91- 9412505988
Fax: 91- 0571- 2701001
E-mail: isarrizvi@hotmail.com

CERTIFICATE

Certified that the work presented in this thesis entitled **"Study of some heavy ion induced reactions below 7 MeV/nucleon"** is the original work of **Mr. Tauseef Ahmad** done under my supervision.

(ISAR AHAMAD RIZVI)
24.9.08

Acknowledgements

At the outset I have great pleasure in acknowledging my deep sense of gratitude to my supervisor, ***Dr. Isar A. Rizvi****, Reader in the Department of Physics. AMU, Aligarh for his invaluable guidance, unfailing help and encouragement during the course of this work. The whole of the work bears imprints of his balanced criticism and scholarly approach. He has always been kind enough to have access to his precious time for discussions despite his busy schedule and preoccupations with unfailing personal affection and interest. I am also deeply indebted to* ***Prof. A.K. Chaubey****, my former Supervisor and Ex-Chairman of the Department from whom I got the initial inspiration to continue this research.*

I am highly beholden to ***Prof. Muhammad Zafar****, Chairman and* ***Prof. Muhammad Irfan****, former chairman, Department of Physics, for providing me the necessary research facilities required for this work.*

I also wish to thank ***Prof. Amit Roy****, Director, Nuclear Science Centre, New Delhi for providing me the experimental facilities and hospitality during my stay at NSC. I must acknowledge the Pelletron crew for providing the good quality beam. Thanks are due to NSC personnel especially* ***Mr. Rakesh Kumar*** *(Scientist- C) and* ***Ms. K.S. Golda****, our local experiment co-coordinator (LEC). I am obliged to* ***Er. Abhilash****, Lab. Assistant of Target laboratory, NSC, New Delhi for providing technical help in the preparation of samples required for the experiment.*

My special thanks are due to my teachers particularly ***Dr. M. Shoeb*** *who read this manuscript, made useful suggestions. His critical comments*

have greatly improved the quality of contents of the same. I also express sincere obligations to ***Dr. Avinash Agarwal*** *and* ***Dr. Manoj K. Sharma*** *for their help and valuable suggestions at various stages of this work.*

I am always owed, from my inner core to friends and research scholars particularly ***Mr. Pushpendra P. Singh*** *of this department for invaluable cooperation and constant encouragement.*

Special mention must be made of my parents, especially my father ***Mr. Nisaruddin Sahib,*** *my maternal uncle* ***Mr. M. Mohsin,*** *wife, family members and relatives who showered their blessings, affections and provided me moral and material support at every stage. Finally, I am also thankful to my son* ***Mr. M. HARIS*** *who ofently prayed for the completion of this work.*

Ahmad 24/9/08

(Tauseef Ahmad)

Contents

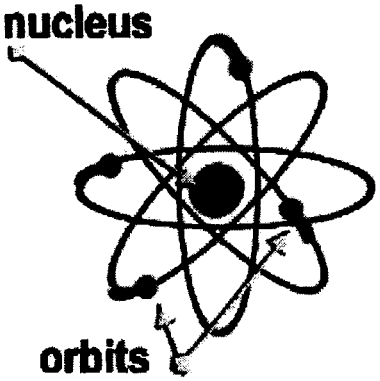

Chapter - I

INTRODUCTION

The beginnings of nuclear physics may be traced to the discovery of radioactivity in 1896 by Becquerel, who noticed that well-wrapped photographic plates were blackened when placed near certain minerals. In 1911 , Rutherford performed a series of experiments by bombarding a piece of gold foil with positively charged particles emitted from a radioactive source and showed that an atom consists primarily of empty space surrounding a well-defined central core, called nucleus. The nucleus residing at the centre of an atom is a very unusual entity. It binds electrons around it, carries almost the whole of the mass, ~ 99.95 % but occupies an extremely tiny space. Thus the nucleus is an object with very high matter density consisting of neutrons and protons. The basic nuclear constitution was understood after the discovery of the neutron by Chadwick in 1932 [1]. The nucleus, over the past several decades, has attracted the attention of physicists by displaying very divergent properties ranging from highly collective to single particle behavior. Nature has thus provided through this quantum object, an ideal laboratory to study interesting behavior of a strongly interacting multi-fermion system. Since the nucleus being a quantal system, one has to extract information indirectly by comparing experimental results with proposed theoretical models. One of the ways of extracting the character of nuclear interactions and the structure of nuclei is the study of nuclear reaction mechanism.

In a nuclear reaction, as shown in Fig.1, properties of entrance and exit channels are well-defined but what exactly happens at the time of the interaction of the colliding partners is not well-understood. Since the nuclear reaction takes place in a very short time (10^{-20}-10^{-16} sec), it can not be visualized directly. In 1936, Bohr was the first to propose the compound nucleus (CN) theory [2] to explain the nuclear reaction mechanism. In CN reaction, the projectile of sufficient kinetic energy interacts with the target nucleus, leading to the formation of quasi-bound intermediate complex systems (i.e. bound configuration of the target nucleus and the projectile nucleus). The compound nucleus reaction mechanism is believed to be a two stage process: the first stage is the capture of the projectile by the target forming a composite nucleus and the second one is the subsequent decay of the

composite nucleus. It is further assumed that the total energy of the projectile is shared among all the nucleons of the composite nucleus leading to thermodynamic equilibrium. After a long time, a sufficient amount of energy may be accumulated on one of the nucleons or on a group of nucleons to make these escapes. The basic assumption of the CN theory is that since the time lapse between the formation of the composite nucleus and its decay is too large ($\approx 10^{-16}$ sec), no trace is left to decide its mode of formation. In 1950, Ghoshal [3] experimentally verified the validity of Bohr's independent hypothesis.

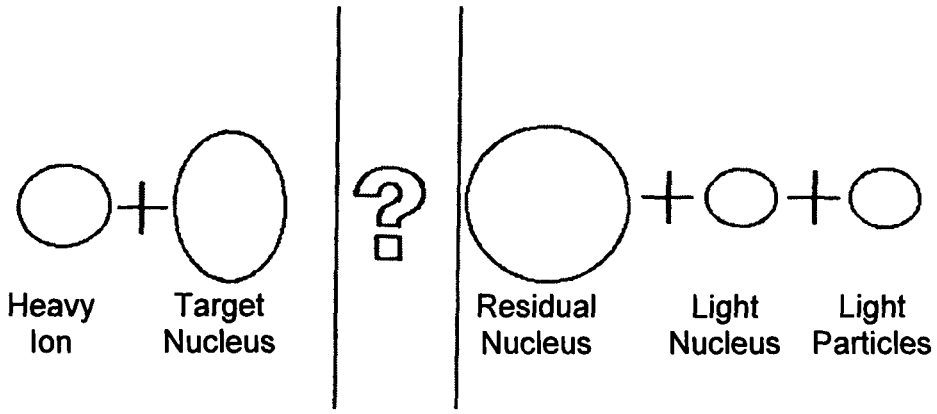

Fig.1. Pictorial Representation of a Nuclear Reaction.

On the other hand, the direct reactions occur on a time scale of the same order as it takes for the projectile to traverse the target nucleus (i.e. $\approx 10^{-22}$ sec.). Hence, the CN and the direct reaction process may be distinguished on the basis of the interaction time. The direct reaction may further be classified into stripping and its inverse, pick-up reactions. In the CN reaction the emission of particles/ clusters takes place after reaching the thermodynamical equilibrium. However, it has been inferred from the results of a large number of experiments [4, 5, 6] that the emission of particles / clusters may also take place even before the thermodynamic equilibrium of the compound system has been reached. The particles which are emitted before the equilibration of the composite system are called pre-equilibrium (PE) particles and the process is referred to as PE or pre- compound reaction mechanism.

The study of nuclear reactions is not only an important subject in its own right, but it is significant also for its impact on related fields of investigation and for its rich variety of applications. In this context the measurement and the calculation of the cross-section of

nuclear reactions as accurate as possible and the understanding of reaction mechanism is of immense importance. The study of the nuclear reactions got a big boost with the advent of advanced accelerators and detectors which opened many possibilities for exploring new aspects of nuclear behavior. Using a wide variety of projectiles and bombarding energies, one can hope to achieve a more detailed understanding of the dynamics of nuclear collisions casting a new light on to the temporal evolution of quantal systems and yielding a fertile testing ground for theories of many-body systems, chaotic regime dynamics and the statistical mechanics of strongly interacting, finite systems. At the same time, one can investigate the properties and the decay modes of nuclear systems. Advanced instrumentation plays a key role in these investigations. Besides, the obvious implications of an improved understanding of nuclear behavior, reaction mechanism studies leave profound impact on other areas of science. In particular, thermodynamic information concerning the behavior of nuclear system derived from these investigations can shed light on the nuclear equation of state. This yields important input relevant to problems in nuclear astrophysics such as the big bang, stellar evolution and the dynamics of supernova explosions.

In India, experimental research in heavy-ion physics started in late nineties with the availability of heavy-ion beams of suitable energy ranges. The interest has renewed in recent past with the establishment of the heavy-ion Pelletron accelerator facilities at IUAC, New Delhi and at TIFR, Mumbai. Heavy-ion is generally used to mean a nucleus heavier than the helium. Heavy-ion physics deals with the phenomena that occur when two nuclei are brought into contact such that the nuclear forces are felt by each other. The study of heavy-ion induced reactions starts with the extrapolations from the existing knowledge of nuclear structure and reactions, their generalization or modification in order to encompass new experimental findings.

The study of heavy-ion reactions is quite complicated because of large Coulomb barrier between the interacting nuclei. The angular momentum of heavy-ions with respect to the centre of mass is very large and therefore, it is possible to produce nuclei at high excitation energy and high spin states. Therefore, it is necessary to study heavy-ion induced reactions to understand reaction mechanism. Further, the de-Broglie wavelength depends on the mass (m) of projectile as:

$$\lambda\!\!\!^{-} = \frac{1}{2\pi}\left[\frac{h^2}{2m.E_{lab}}\right]^{1/2} \qquad \text{------1}$$

where E_{lab} is kinetic energy of the incident particle in the laboratory frame. The small de-Broglie wavelength for large (m) of the projectile helps in treating the heavy-ion collision semi-classically. The semi classical nature of HI reaction makes it possible to give general description of their classical characteristics, particularly their relative motion along quite well defined orbits in terms of the closest distance between the interacting nuclei (r_{min}), which is related to the impact parameter(b) given as :

$$r_{\min} = \frac{b}{\sqrt{\left[1 - \frac{V(r_{\min})}{E_{CM}}\right]}} \qquad \text{-----2}$$

where, $V(r_{\min})$ is the nuclear potential acting between the interacting nuclei and E_{CM} is the centre of mass energy.

Apart from properties referred to above the heavy-ion reactions have also been used for synthesis of super heavy elements (SHE). During the process of synthesis of SHEs several new reaction mechanisms like deep in elastic collision (DIC), quasi-fission, fast-fission; incomplete fusions (ICF) were discovered [7]. It was pointed out by Conlon [8] that the heavy ion beams can be used to produce an extremely thin layer of activity by direct nuclear reaction. Since the heavy ion beam loses energy very fast in materials, it produces a very thin layer of activity in the surface. For example, thin layers for 15 MeV proton, 40 MeV α and 110 MeV ^{16}O in copper are 480 μm, 244 μm and 40 μm respectively. These reactions are useful for the study of thin layer activation technique (TLA) [9].

Depending on the impact parameter a great variety of phenomena can arise in heavy-ion collisions. A typically classical picture [10] of heavy-ion interaction representing different processes at different impact parameters is shown in Fig.2. Some of the important processes are: elastic scattering (the Coulomb region with $r_{min} > R_N$), deep inelastic scattering (region with $R_F < r_{min} \leq R_{DIC}$), transfer reactions (the peripheral region with $R_{DIC} < r_{min} \leq R_N$), fusion reaction (the fusion region with $0 \leq r_{min} \leq R_F$), where $R_F = 1.0\left(A_1^{1/3} + A_2^{1/3}\right)$. A qualitative description of different reaction processes is given in Fig. 3, where the range of angular-momenta *(l)* involved for the various processes is indicated.

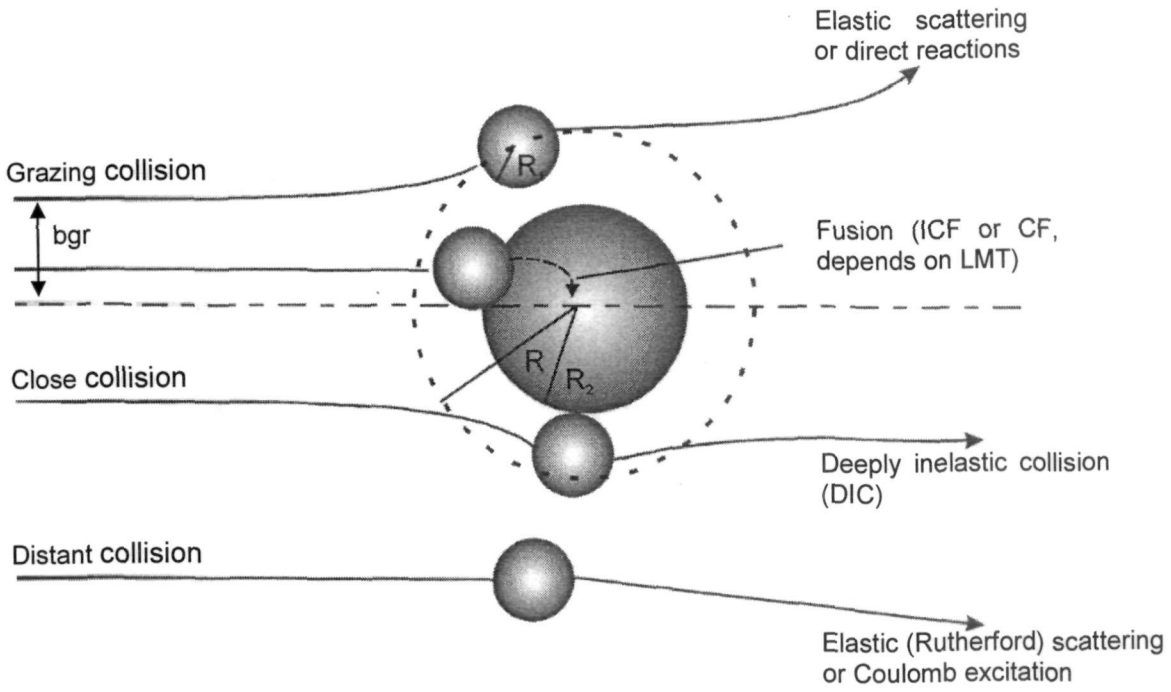

Fig.2. Classical picture of heavy-ion interactions.

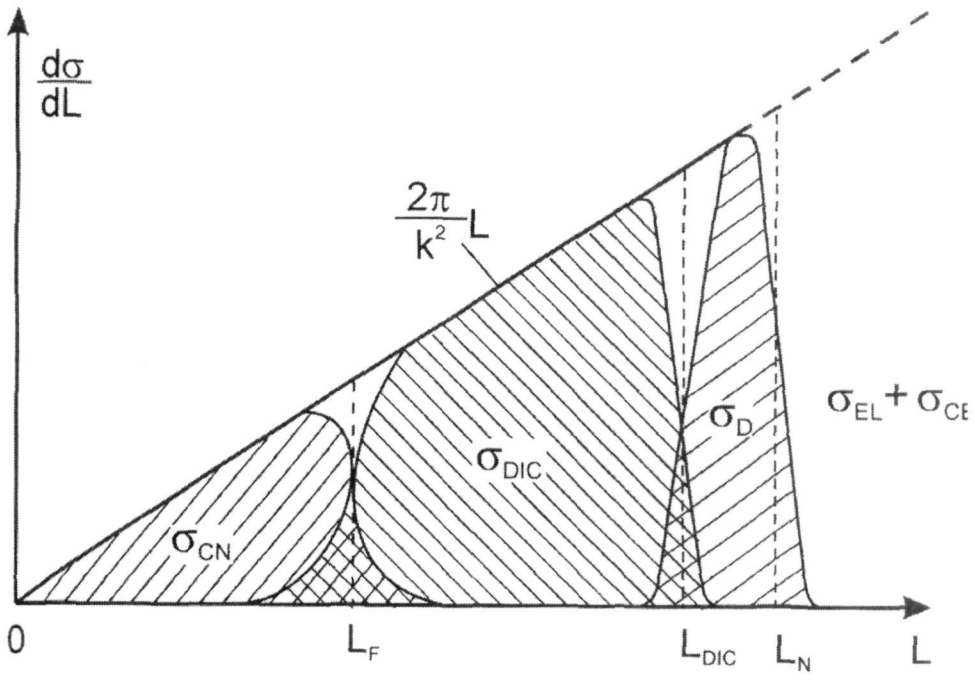

Fig. 3. Schematic illustration of L - dependence of partial cross- section.

In gentle encounters, the two nuclei barely touch each other and essentially keep their identity; one can study the interplay between the degrees of freedom of the two nuclei, with a possibility of varying the physical situation in a practically unlimited number of ways. By appropriately selecting targets and projectiles one may be able to specifically excite different degrees of freedom and search for new ones. On the other hand, collisions bringing the two nuclei into a more intimate contact lead to a combined nuclear matter system which at a later stage may look like a normal nucleus strongly deformed and excited to a state of very high angular momentum. The transition from the situation where the two nuclei maintain their identity to the state in which these become a composite system is expected to be a main theme of research in the field of heavy- ion physics.

The two ions interact only through the Coulomb fields for large impact parameter; consequently, elastic scattering takes place. For the grazing impact parameter b_{gr}, the tails of the nuclear wave functions overlap and processes like inelastic scattering and / or nucleon transfer may take place. Further reduction in the impact parameter results in considerable overlap of the wave functions of two interacting nuclei and the relative kinetic energy is converted into internal excitation before the two separate into target and projectile like systems. Such processes are termed as deep inelastic collisions (DIC) and are likely to take place at energies of a few MeV/ nucleon above the Coulomb barrier.

The two ions may come within the range of nuclear interactions on further lowering the values of the impact parameter. Classically, a nuclear interaction can take place, if the centre of the mass energy of two ions exceeds the Coulomb barrier. Since there is a large over lap between the wave functions of the two interacting nuclei, the projectile may fuse with the target and a number of nuclear reactions may occur. In the present work we are interested in this regime. Some of the possible reaction mechanisms that may occur in this regime are described in the following paragraphs.

The projectile may completely fuse with the target at low incident energies and for lower values of the impact parameter. Consequently, the entire linear as well as angular momentum is transferred to the composite nucleus. This system is far from statistical equilibrium as a large part of its excitation energy is in the form of an orderly collective translational motion of the nucleons of the projectile and the target. The orderly motion

gradually transforms into chaotic thermal motion mainly through a sequence of two-body interactions. This thermalization process takes place till composite system reaches a state of thermal equilibrium resulting in the formation of a compound nucleus. Once the thermal equilibrium is reached, the accumulation of sufficient energy on a single nucleon or cluster of nucleons may only occur by a random and improbable sequence of events. Thus, such a process favors the emission of low energy particles after a long time.

The angular momentum of the projectile at higher incident energies and relatively larger impact parameters is too large for the composite system to hold together .In such cases only a part of the projectile may fuse with the target nucleus and the remaining part gets stripped off. This results in the incomplete fusion (ICF) of the incident heavy ion.

Incomplete fusion reactions are fast binary processes in which the part of the projectile fuses with the target, while the remainder continues its flight with the approximate beam velocity. The subsequent decay of the residual nucleus is characteristic of fusion evaporation. In contrast to the DIC, in which total kinetic energy of the colliding nuclei is dissipated into intrinsic excitations, incomplete fusion reactions proceed on a faster time scale and thus closely resemble direct reactions. The ICF reactions were first observed by Kaufmann and Wolfgang [11] in the system $^{16}O + {}^{103}Rh$ at laboratory energy 100 MeV. Subsequently Britt and Quinton [12] and Gallin et al. [13] observed these phenomena with the low Z heavy- ion as the projectile. The study of the ICF by particle-γ coincidence by Inamura et al. [14] contributed a great deal to the understanding of underlying dynamics. Bimbot et al. [15] carried out the pioneering work on the excitation functions, angular distributions and differential recoil range to study the transfer of alpha particle and ^{8}Be, to the target, in $^{12}C+{}^{197}Au$ system. Some of the important features of ICF are:

(i) The ICF contributes a significant fraction to the reaction cross section in the case of low Z projectiles and high Z targets.

(ii) The forward mean ranges of recoils show relatively smaller depths in the stopping medium than those of complete fusion residues, strengthening the concept of fractional momentum transfer.

(iii) Out-going projectile-like fragments are mainly concentrated in the forward cone and their energy spectrum essentially peak at the projectile velocity [12].

(iv) The spin distributions of evaporation residues populated via the ICF are found to be distinctly different as observed for the complete fusion process [14, 16].

In order to explain some of the above features several dynamical models have been proposed. Some of these are: the Sum-rule model [17], the Break- up Fusion (BUF) model [18] and the Promptly Emitted Particles (PEPs) model [19]. Morgenstern et al. [20, 21] correlated the probability of incomplete fusion reaction to the entrance channel mass asymmetry. However, none of these models succeeded in explaining all the features of ICF reactions, and it continues to be an active area of investigations [22-28]. The Sum-rule model [17] assumes that the various ICF channels are localized in the angular momentum space above the critical angular momentum for the complete fusion of the projectile and the target. The model gives cross sections for products arising not only from the ICF and quasi-elastic transfer reactions but also from the complete fusion. The break- up fusion model [18] explained the ICF in terms of the break- up of the projectile in the nuclear field of the target nucleus followed by the fusion of one of the fragments with the target nucleus. This model uses the distorted wave born approximation (DWBA) to calculate the shapes of energy spectra and angular distribution of a projectile-like fragment. However, it is unable to give the absolute cross sections, due to lack of information about the spectroscopic form factors of the continuum states of the product nuclei. According to the promptly emitted particle model [19], the particles transferred from the projectile to the target nucleus are assumed to get accelerated in the nuclear field of target nucleus and hence, acquire extra velocity to escape.

Generally, the existing models have been used to explain the experimental data obtained at projectile energies E/A $\geq$ 10 MeV. However, so far, no theoretical model which can provide a satisfactory fitting to the ICF reaction data at energies 5-7 MeV / nucleon is available. Some studies, however, showed the onset of the ICF process at $\approx$ 5-7 MeV/ nucleon. Parker et al. [29] observed the ICF even at E/A $\approx$ 6 MeV using low Z heavy- ions. Recently, there is a renewed interest in the study of the ICF dynamics after the observation of these reactions at relatively low bombarding energies [30-32]. Moreover, the ICF reactions are considered to be a promising route to populate high spin states in heavy residues using moderate heavy–ion beams (A $\leq$16) even at low bombarding energies [33-35]. The

study of the ICF dynamics in the view of all these developments may provide key parameters to determine optimum irradiation conditions for the production of radio-active ion beams (RIBs) [36,37]. As such, in order to have a better understanding of the ICF dynamics, precise experimental data covering a wide range of the periodic table and energies are required.

In view of the availability of limited data covering only a few projectile- target combinations at E/A $\approx$ 5-7 MeV, our group has undertaken a program of precise measurement and analysis of excitation functions (EFs), recoil range distributions (RRDs) and spin distributions of residues populated via complete and/or incomplete fusion using the particle-γ coincidence technique for various projectile–target combinations over a wide range of projectile energy. From the point of view of Physics, the shape of EFs reveals the reaction mechanism. For instance, the slowly descending tail of the EFs is a direct signature of the pre-equilibrium emission. The study of excitation functions is also important from the point of view of nucleo–synthesis [38]. The importance of the excitation function also lies in the fact that with ever increasing use of radioactive isotopes in various applied fields, there is a growing demand to provide the knowledge of the excitation functions of nuclear reactions in order that the production of the selected isotopes could be maximized. The excitation functions of nuclear reactions leading to suitable products are very important to be known for the yields of products before their TLA application in a particular material. These EFs are also in demand for the development of accelerator driven subcritical reactors popularly known as energy amplifiers [39]. The measurement of the excitation function has been done using the activation technique [40] which is popular for its sensitivity, selectivity and simplicity. The main advantage of this technique is the possibility of measuring EFs for the production of a large number of residues in a single irradiation, thereby reducing beam time requirements. Another way to characterize the CF and/or ICF processes is the measurement of forward recoil ranges, even when a single reaction product is populated via several mechanisms. The linear momentum transfer (LMT) is the signature of the interaction of the projectile and the target nucleus and hence can be used to probe the reaction dynamics associated with the different reaction products.

In the present work, as a part of the ongoing program to explore the dynamics of heavy-ion induced reactions (mainly complete and incomplete fusion), an attempt has been made to measure the excitation functions for a large number of residues produced in ^{12}C + ^{93}Nb, ^{12}C + ^{52}Cr and ^{16}O + ^{115}In systems at energies near and well-beyond the Coulomb barrier. To the best of our knowledge, the EFs for ^{52}Cr and ^{115}In targets are being reported for the first time. However, the measurements of EFs for the ^{12}C + ^{93}Nb system have been carried out by earlier two groups [41, 42], show discrepancies to a large extent; hence precise and accurate measurements are still needed. The measured EFs for various residues in these systems are compared with the statistical model code PACE 2 (based on Hauser-Feshbach theory) [43]. In order to show the contrast between our data and earlier reported values [41, 42](in the case of ^{12}C+ ^{93}Nb system), we have also compared our new measurements with the latest version ALICE-91 [44] whereas Misaelides [41] compared his findings with theoretical predictions made by a modified version [45] of the statistical model code ALICE [46]. Further, to separate the relative contributions of the complete and the incomplete fusion in ^{12}C+^{93}Nb system, the RRDs of several residues were also measured. The experiments were carried out at Inter-University Accelerator Centre (IUAC), New Delhi, India. The details of experiments and measurements are given in chapter II and III respectively. Chapter IV is devoted to the description of computer codes. The Results and analysis of the present measurements are discussed in chapter V. The references are given at the end of each chapter.

References

[1] J. Chadwick, Proc. Roy. Soc., **A 36,** 692 (1932).

[2] N. Bohr, Nature **137**, 344 (1936).

[3] S.N. Ghoshal, Phys. Rev. **80,** 839 (1950).

[4] M. Blann, Phys. Rev. Lett. **27,** 337 (1971).

[5] I.A. Rizvi, Ph.D. Thesis (Unpublished), AMU, Aligarh, India (1988).

[6] Avinash Agarwal et al., Phy. Rev. **C 65**, 034605 (2002).

[7] U. Mosel, Heavy Ion Fusion Reactions in Treatise in Heavy Ion Science, ed. A. Bromely (1986).

[8] T.W. Conlon, Contemp. Phys. **23**, 353 (1982).

[9] D. P. Chowdhury et al., Nucl. Instrum. Methods **B 211**, 288 (2003).

[10] P.E. Hodgson, Introductory Nuclear Physics, Clarendon Press, Oxford (1997).

[11] R. Kaufmann and R. Wolfgang, Phys. Rev. **121**,192 (1961).

[12] H.C. Britt and A.R. Quinton, Phys. Rev. **124**, 877 (1961).

[13] J. Gallin et al., Nucl. Phys. **A 159**, 161 (1970).

[14] T. Inamura et al., Phys. Lett., **68 B**, 51 (1977).

[15] R. Bimbot et al., Nucl.Phys.**A189,** 193 (1972).

[16] P. P. Singh et al., DAE-BRNS, Nucl. Phys. Symp. **51**, 361 (2006).

[17] J. Wilczynki et al., Nucl. Phys. **A373**, 109 (1982).

[18] T. Udagawa and T. Tamura, Phys. Rev. Lett. **45**, 131 (1980).

[19] J.P. Bondrof et al., Nucl. Phys. **A333,** 285 (1980).

[20] H. Morgenstern et al., Phys. Rev. Lett.**52**, 1104 (1984).

[21] H. Morgenstern et al., Z.Phys.**A324**, 443 (1986).

[22] E. Gadioli et al., Eur. Phys. J.**A17**, 195 (2003).

[23] L. J. Mudau et al., Nucl.Phys.**A761**, 190 (2005).

[24] B. Becker et al., Eur. Phys. J. **A18**, 639 (2003).

[25] E. Z. Buthelezi et al., Eur. Phys. J. **A28**, 193 (2006).

[26] M. Cavinato et al., Phys. Rev. **C 52**, 2577 (1995).

[27] C. Birattari et al., Phys. Rev. **C 54**, 3051(1996).

[28] Valery Zagrebaev and Walter Greiner, J. Phys. **G 34**, 1(2007).

[29] D. J. Parker et al., Phys. Rev **C 39**, 2256 (1989).

[30] Manoj K. Sharma et al., Nucl. Phys. **A 776,** 83 (2006).

[31] Pushpendra P. Singh et al., Phys. Rev. **C 77**, 014607(2008).

[32] D. Singh et al., J. Phys. Soc. Jpn.**75**, 104201(2006).

[33] P. Walker and G. Dracoulis, Nature (London) **399,** 35 (1999).

[34] S.M. Mullins et al., Phys. Lett. **B 393**, 279 (1997).

[35] M. Kaci et al., Phys. Rev **C 56**, 600 (1997).

[36] C. Rubbia et al., Reports CERN/AT/95-94 (ET).

[37] M. M. Mustafa et al., Appl. Rad. Isoto. **62**, 419 (2005).

[38] M.R. Anderson et al., Nucl. Phys. **A 405** (1983) 170.

[39] C. Rubbia et al., Conceptual Design of a fast Neutron Operated High Power Energy Amplifier, Report CERN/AT/95-94 (ET) 1995.

[40] R. C. Koch, Activation Analysis Handbook, Academic Press, New York and London (1960).

[41] P. Misaelides, Radio chim. Acta **28**, 1 (1981).

[42] B.S. Tomar et al., Z. Phys. **A 343**, 223 (1992).

[43] A Gavron, Phys. Rev. **C21**, 230 (1980).

[44] M. Blann, ALICE-91, LLNL/IAEA/NEA Data Bank France (1991).

[45] I.S. Grant, (Private Communication).

[46] M.Blann, J. Bisplinghoff, Report C00-3494-27, University of Rochester, N.Y. (1975).

Chapter - II

In the present work, activation technique [1] has been used for measuring the EFs for a large number of evaporation residues produced in ^{12}C + ^{93}Nb, ^{12}C+ ^{52}Cr and ^{16}O+ ^{115}In systems at the energies below 7 MeV/nucleon. In order to separate the relative contributions of the CF and the ICF in the ^{12}C + ^{93}Nb system, RRDs of various evaporation residues have also been measured at ≈ 80 MeV. These experiments were carried out using 15 UD Pelletron accelerator facilities at the Inter-University Accelerator Centre (IUAC), New Delhi, India.

2.1 Pelletron Accelerator

A schematic diagram of IUAC Pelletron is shown in Fig.2.1. The IUAC Pelletron is a 15 UD tandem Van de Graff electrostatic accelerator. It is capable of accelerating any ion from proton to uranium (except of the inert gases) in the energy range from a few tens of MeV up to a few hundred MeV, depending on the ion species. The accelerator is installed in a vertical geometry in a stainless steel tank, which is 26.5 m high, and 5.5 m in diameter. In the middle of the tank there is a high voltage terminal, which can hold potential from 4 to 16 MV. The terminal is connected to the tank vertically with ceramic–titanium accelerating tubes. The tank is filled with a high di-electric constant SF_6 gas at 6-7 atm. pressures to insulate the high voltage terminal from the tank wall. A potential gradient is maintained through the accelerating tubes from ground potential at the top to the terminal and from the terminal to the ground potential at the bottom of the tank. Negative ions of suitable energy from source of negative ions by cesium sputtering (SNICS) ion source are injected into the accelerator and are accelerated towards the positive terminal. [2].

In the first stage of acceleration, singly charged – ve ion from the ion source are accelerated from ground potential to the terminal at the high potential V. The energy gained in the process is eV. Then the beam is made to pass through a stripper where the ions are stripped off the electrons thereby making these + ve ions. The average charge of the ion depends upon the type of the ion and the terminal voltage.

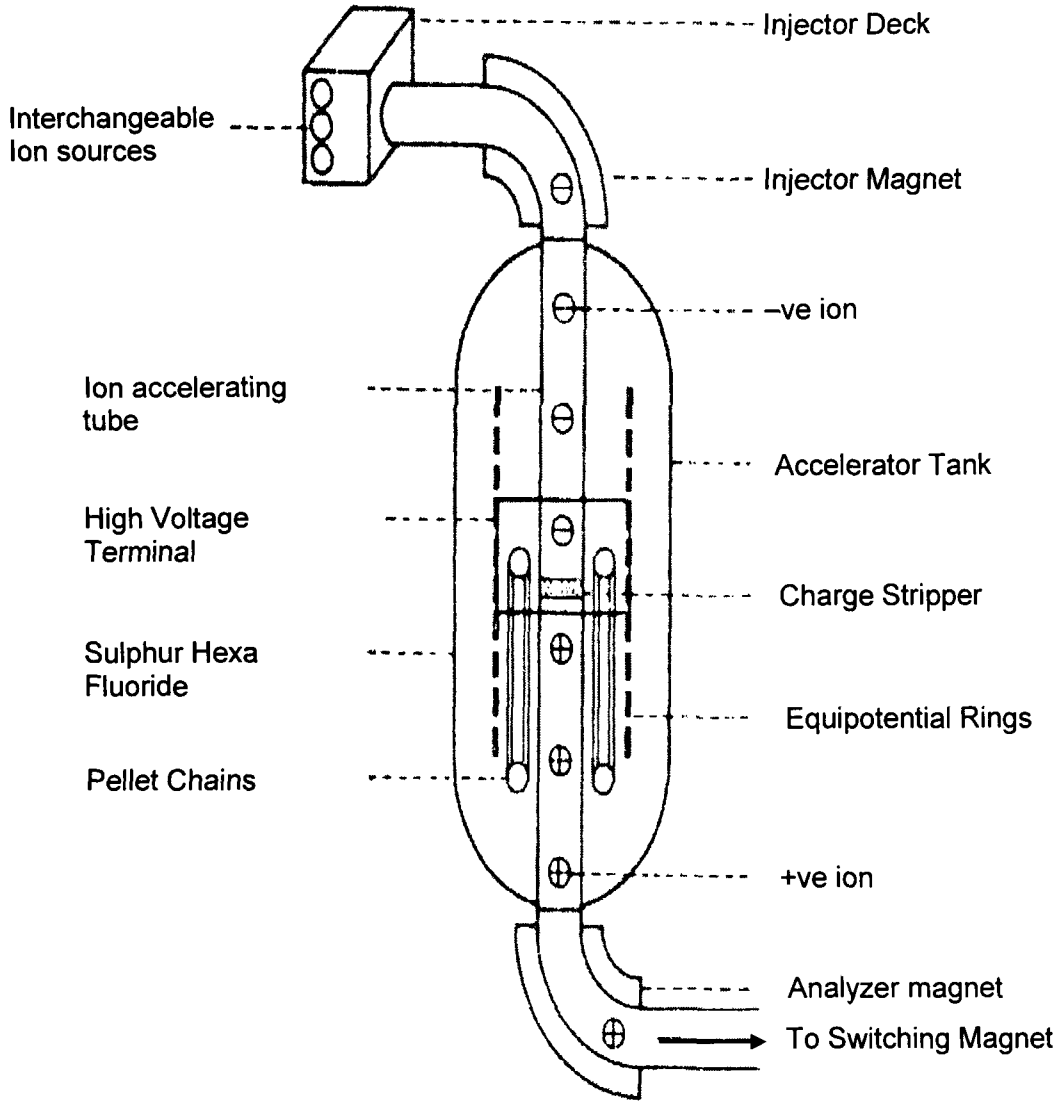

Fig.2.1 A schematic diagram of Pelletron at IUAC, New Delhi, India

If *qe* is the charge on the +ve ions after passing through the stripper foil, the energy gained by accelerating it from the terminal to the ground potential is *qeV*. Thus, after passing through the two stages of the acceleration, the final energy of the ion in *eV* is given by

$$E = (q + 1)\ eV \qquad \text{.....2.1.1}$$

These high-energy ions are then passed through the analyzing magnet and energy slit which selects the particular ions of the desired energy. By switching magnet the beam of ions are then directed towards the desired experimental area.

2.2 Target Preparation and the Characterization

The targets used in the present work, were either self–supporting or prepared by vacuum evaporation on thin Al-foils. For excitation function measurements, three different types of materials (^{93}Nb, ^{52}Cr and ^{115}In) were used in targets fabrication.

Self –supporting ^{93}Nb targets of thickness ~ 2.02 mg/cm^2 were prepared by rolling natural niobium of purity better than 99.9%. The rolling technique is the most efficient method to prepare self supporting targets. Mechanical rolling was done by sandwiching the material between the mirror polished stainless steel sheets of 1mm thickness and size 7 cm x 5 cm. The surfaces of the sheets were cleaned with acetone to obtain purity and uniformity in the thickness of the target. The distance between the two rollers was gradually decreased in many steps to obtain the desired area. The target thickness was determined by gravimetry. The minimum thickness that can be achieved by sandwich rolling is up to 500μg/cm^2. Rolling is by far the most conservative process with regard to material loss in preparing thin targets. To prevent target foil sticking on the sheets paraffin was sometimes used as a lubricant. The rolling machine at the Target Division of IUAC, New Delhi., where the targets were prepared, is shown in Fig. 2.2.1.

Targets of enriched isotope of ^{52}Cr (83.79%) of thickness 364.32 μg/cm^2 were prepared by the vacuum evaporation technique. The ^{52}Cr material was deposited on the Al foils of thickness 0.90-1.87mg/cm^2. In the target, the Al–backing serves as energy degrader as well as backing material.

Spectroscopically pure with purity 99.99% indium targets (abundance ^{113}In = 4.3% and ^{115}In = 95.7%) of thickness ≈ 1 mg/cm^2 were also made by vacuum evaporation technique on aluminum backing of thickness ≈2 mg/cm^2 . The aluminum foils were cut into pieces of 1.5 x 1.5 cm^2 and fixed on the aluminum holders having concentric hole of ≈ 1 cm diameter. The indium targets were then formed by heating the material via resistive heating method in the vacuum chamber and allowing the indium vapor to condense on the aluminum backing mounted on the aluminum holders.

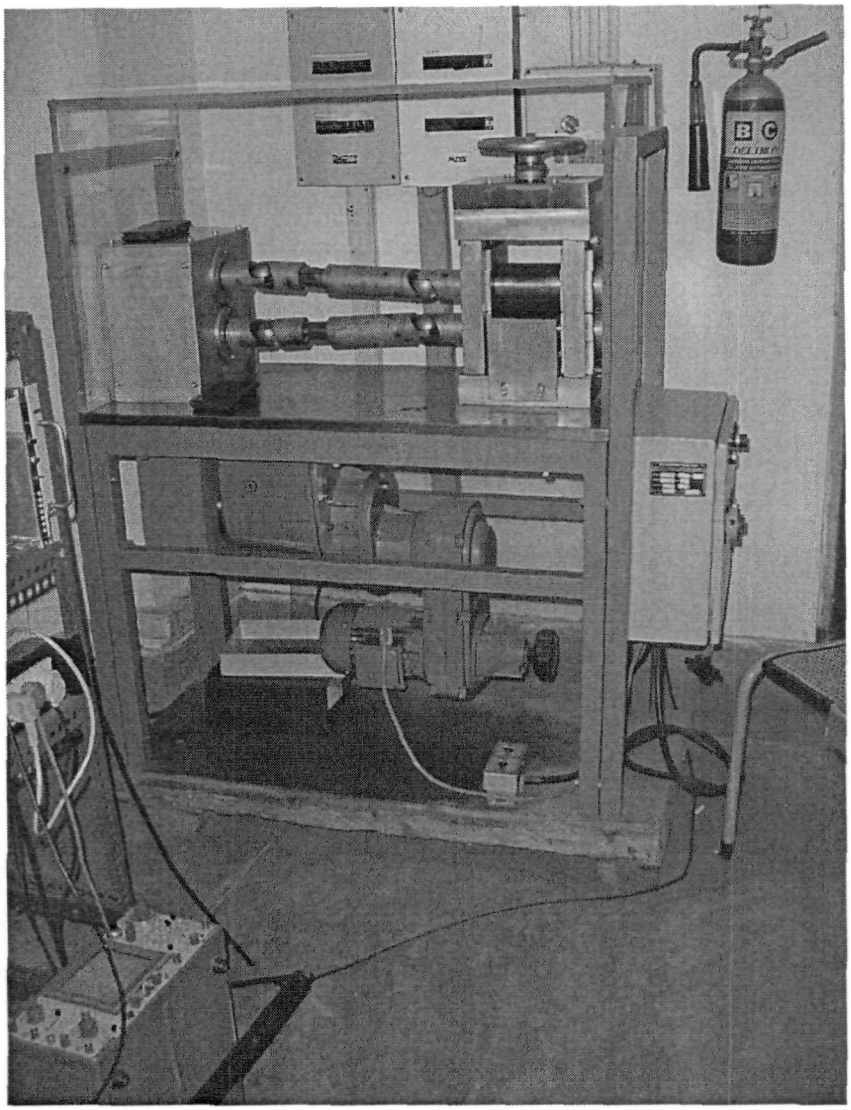

Fig. 2.2.1. Rolling Machine at Target Laboratory, IUAC, New Delhi

For recoil range measurements, thin targets of metallic niobium (^{93}Nb) of thickness 100 μg/cm^2 were prepared by vacuum evaporation on to thin Al-foils of thickness 2.164 mg/cm^2. A stream of 13 aluminum catcher foils having thicknesses ranging from 102 to 113 μg /cm^2, prepared by the same technique, was used to stop the recoiling products.

The vacuum evaporation unit used at IUAC is shown in Fig.2.2.2. The thickness of each target was determined by the α- transmission method which is based on the measurement of the energy lost by α particles while passing through the sample. The 5.485 MeV α-particles from ^{241}Am source were used for this purpose. In the case of vacuum evaporation method, as a check, the target thicknesses were also measured with the quartz thickness monitor and were found to be within range of 5% of the transmission method.

2.3 Irradiation

The stacked foil activation technique is generally used for the study of charged particle reaction cross-sections [3]. In this technique, a number of target foils are arranged to form a stack. Energy degrader foils can be used in between the target foils to obtain the desired projectile energies. In a single run, a number of target foils can be irradiated to different projectile energies using this technique. In the present investigation, for EFs measurement three different stacks were irradiated separately for different times keeping in view the half-lives of interest. A brief description of each stack is as follows:

A stack consisting of five targets of ^{93}Nb and four aluminium degraders (≈ 2.08 mg/cm^2) was irradiated by ^{12}C beam of energy ≈75 MeV for nearly six and half hours. During the exposure the charge state of beam was 6^+ with beam current ranging from 25nA to 30 nA. The second stack comprising of five target foils of ^{52}Cr with energy degraders was irradiated by $^{12}C^{6+}$ beam of energy ≈ 80 MeV for about 4 hours. The beam current was maintained ≈36-38 nA. The third stack consisting of six targets of ^{115}In was irradiated by ^{16}O (charge state 7^+) beam of energy ≈ 105.0 MeV. The irradiation was carried out for ≈ 8.0 hours and the beam current was maintained ≈ 8-10 nA.

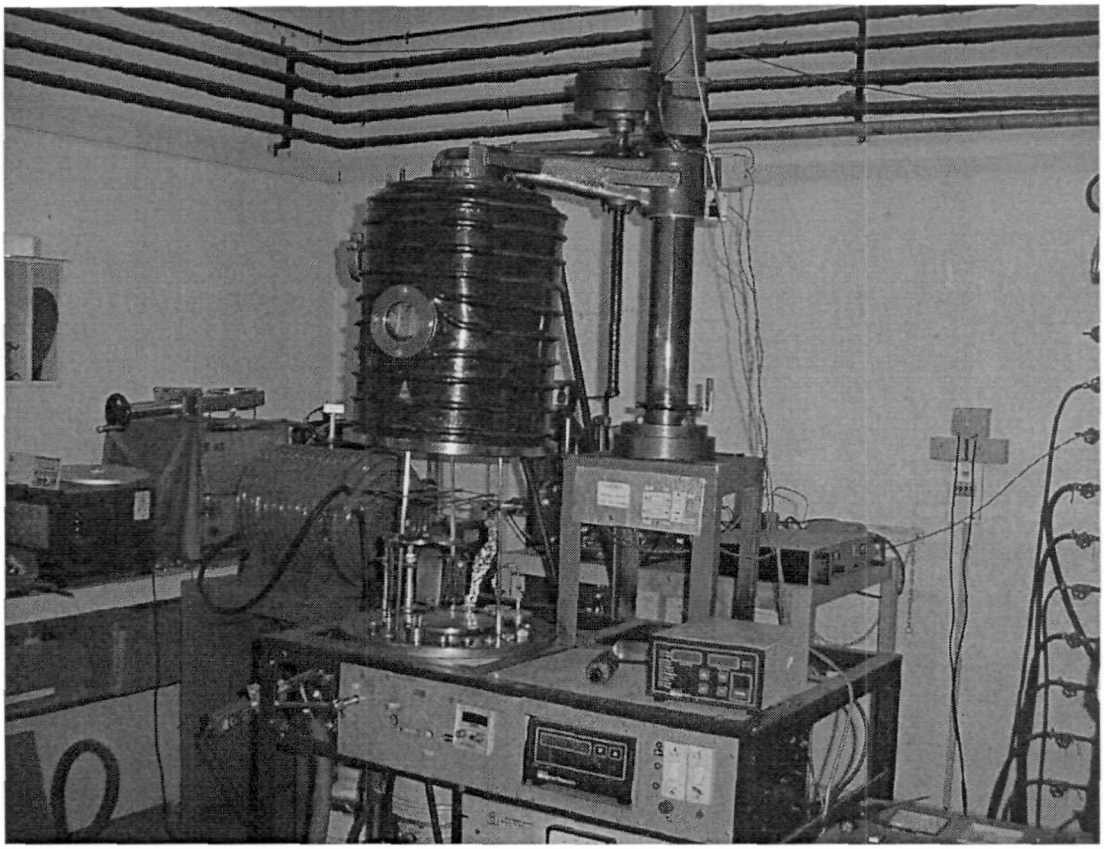

Fig.2.2.2 The Vacuum Evaporation Unit at IUAC, New Delhi

The irradiation was performed in General Purpose Scattering Chamber (GPSC) of 1.5 m diameter having In-vacuum Transfer Facility (ITF). ITF allows target shifting without disturbing the high vacuum and it works to minimize the time lapse between the stop of irradiation and beginning of the counting. The General Purpose Scattering Chamber is shown in Fig. 2.3.1.

The targets under investigation were first mounted on target ladder (as shown in Fig.2.3.2.) which was then placed inside the scattering chamber. The inner view of the scattering chamber is shown in Fig.2.3.3. Two surface barrier (SSB) detectors were also kept at $\pm 10°$ to the beam direction to monitor the flux of the incident beam. The experimental set-up is shown in Fig.2.3.4.

The mean energy of ^{12}C and ^{16}O-ion beams incident on half of the thickness of each foil in the stack was calculated from the energy range program SRIM-2006. The inherent energy spread in ^{12}C and ^{16}O beams was negligible. Moreover, when beam passes through the target the energy spread due to straggling may come into picture. However, the energy spread due to straggling, being insignificant [4, 5], has not been taken into account.

2.4 Calibration of Detector

The word calibration means "in accordance" with i.e. if the gamma rays expected to appear in the spectrum are well known in advance, the corresponding peaks can be readily identified by inspection. On the other hand the energy of any unknown gamma ray can be determined from the calibration curve. In order to identify the characteristic γ-rays of evaporation residues in the complex γ-ray spectra, a detector of good resolution and proper calibration is required. In fact it is the calibration of pulse height in terms of absolute gamma ray energy and is very important for proper identification of the photo-peaks in a gamma ray spectrum. Hence very high-resolution HPGe detector and standard sources having gamma energies that cover the complete range of the γ-rays expected during the experiments are indispensable. In the present measurements the multipoint calibration of γ-ray detector has been done using ^{152}Eu gamma standard source, as it emits γ-rays covering a wide energy range of 120 - 1530 keV. Table 2.4 lists the prominent γ-rays along with their absolute intensities, for the calibration of detector used in the present work.

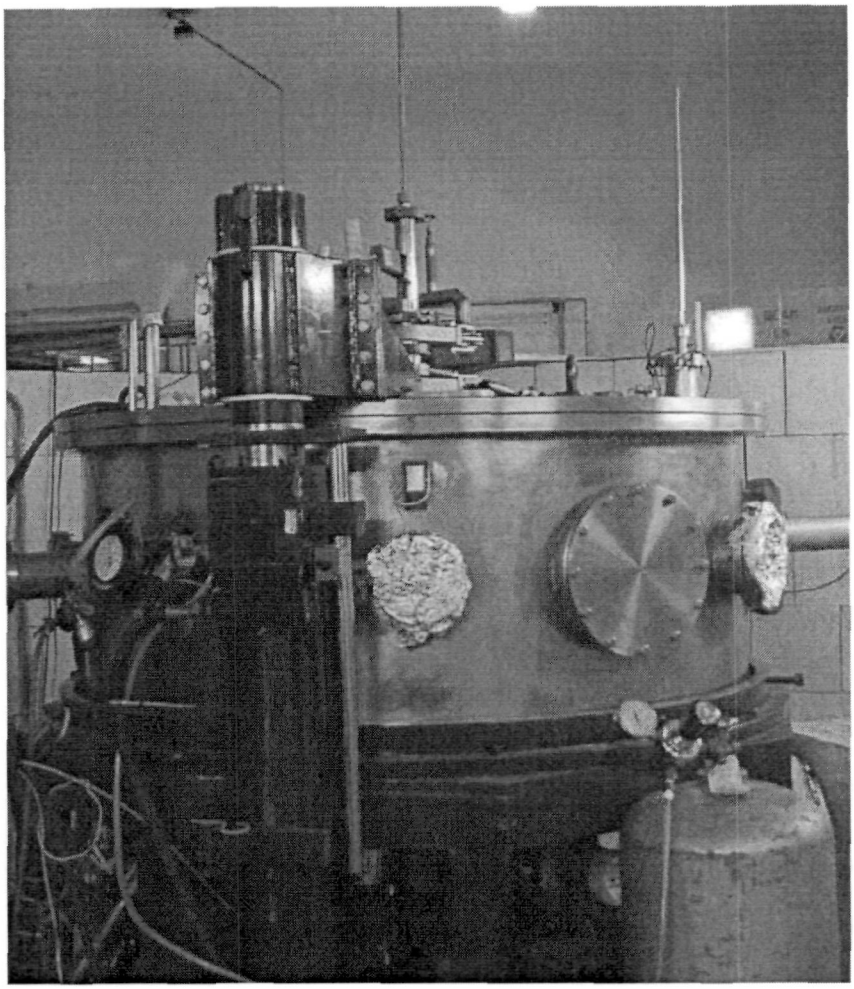

Fig.2.3.1 General Purpose Scattering Chamber (GPSC) at IUAC, New Delhi

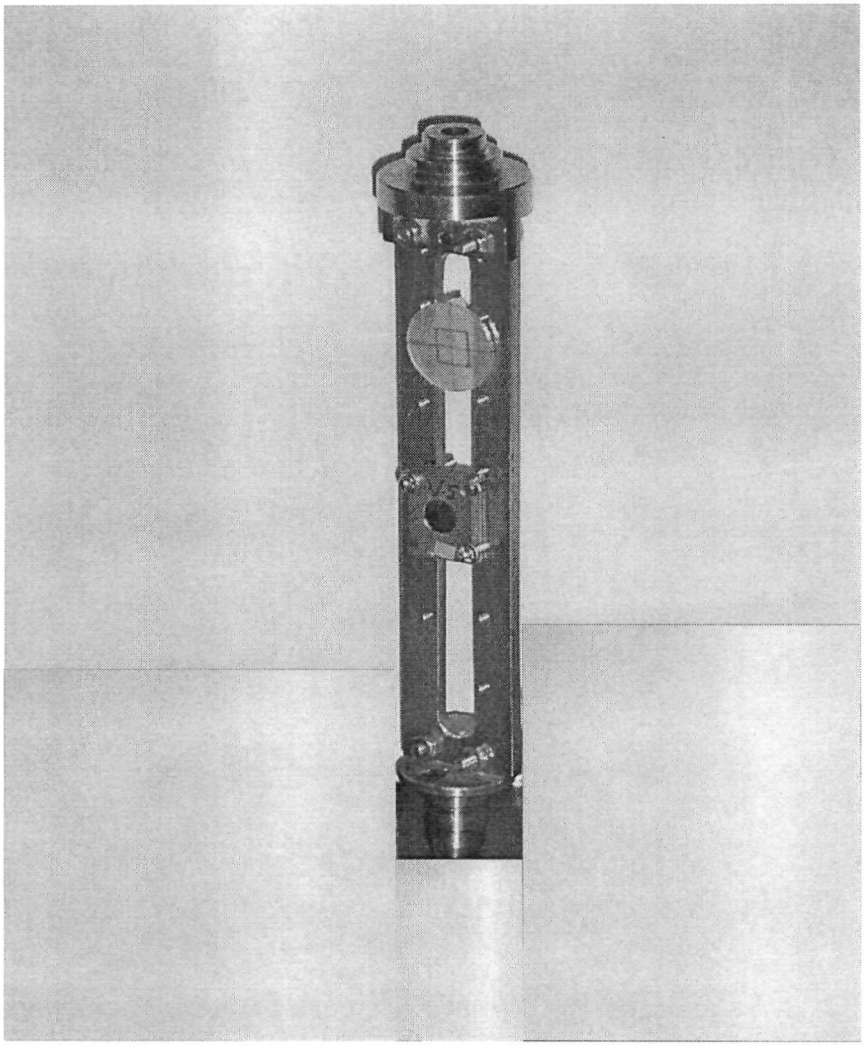

Fig. 2.3.2. Front view of the ladder on which targets were mounted.

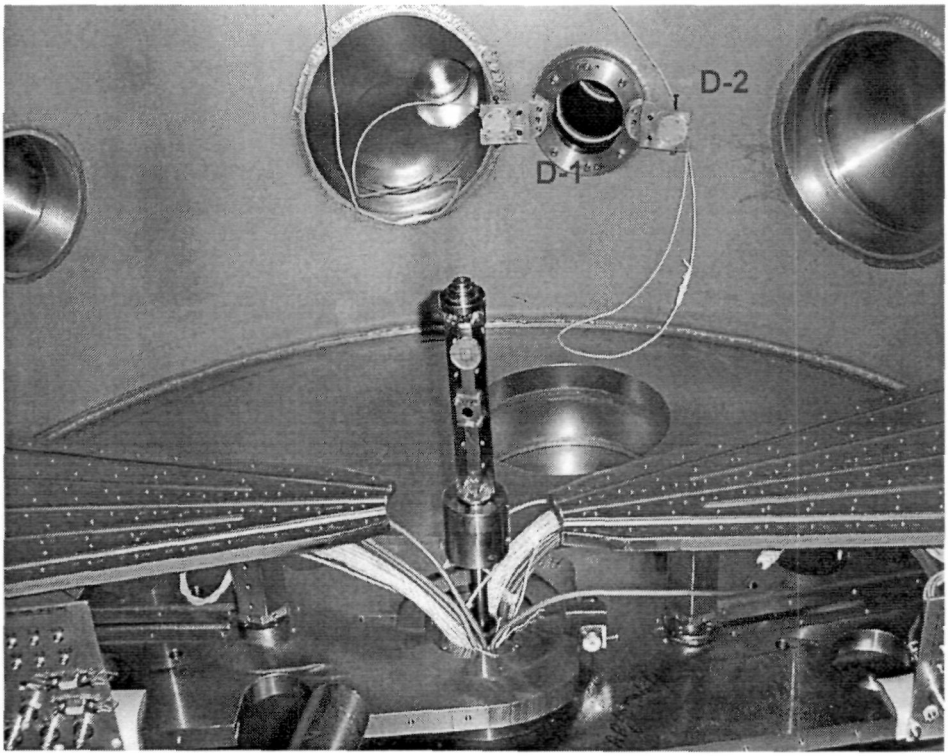

Fig. 2.3.3. Inner view of the Scattering Chamber

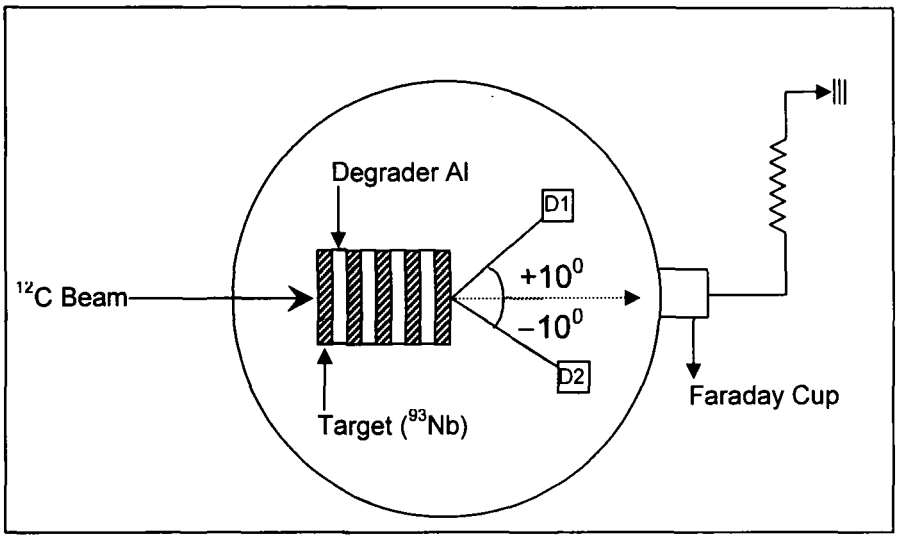

Fig. 2.3.4 The typical experimental set-up for heavy-ion irradiation

Table 2.4
Prominent gamma rays and their absolute intensities of ^{152}Eu source.

S.No.	Gamma-ray Energy (keV)	Absolute intensity (%)
1.	121.78	28.40
2.	244.69	7.51
3.	344.29	26.60
4..	411.0	2.23
5.	778.92	12.98
6.	964.11	14.50
7.	1086.0	13.60
8	1112.08	9.94
8.	1299.16	1.63
9.	1408.00	20.80

2.5 Measurement of Detector Efficiency

The detector efficiency is a measure of how many pulses occur for a given number of gamma rays. The definitions of efficiency in common use for gamma ray detectors are as under :

a. **Absolute Efficiency:** The ratio of number of counts produced by the detector to the number of gamma rays emitted by the source (in all directions). It is dependent not only on detector properties but also on the details of the counting geometry (primarily the distance from the source to the detector).

b. **Intrinsic Efficiency:** The ratio of the number of pulses produced by the detector to the number of gamma rays striking the detector. It no longer includes the solid angle subtended by the detector at the source as an implicit factor.

It is much more convenient to tabulate values of intrinsic rather than absolute efficiency because the geometric dependence is much milder for the former. A detector with known efficiency can be used to measure the absolute activity of a radioactive source. The determination of efficiency of detector using individual standard sources may introduce errors due to non-reproducibility of the geometry. These errors may be eliminated by using a single source emitting large number of γ-rays. A typical γ-ray spectrum of ^{152}Eu source used for this work is shown in Fig. 2.5.1.

The relation gives the intrinsic photo-peak detection efficiency of gamma point source

$$\epsilon = \frac{C.e^{\lambda t}}{S_0.\theta \cdot G} \qquad \ldots\ldots\ldots 2.5.1$$

where C is the count rate under the photo peak, λ is the decay constant of source, t is time lapsed between start of counting and the date of fabrication of standard γ--ray source, S_0 is strength of the source at the time of its manufacture, θ is Absolute intensity of relevant gamma ray and G is geometrical factor which is given by $\left(\frac{\Omega}{4\pi}\right)$ where Ω is solid angle in steradians subtended by the detector surface facing the source.

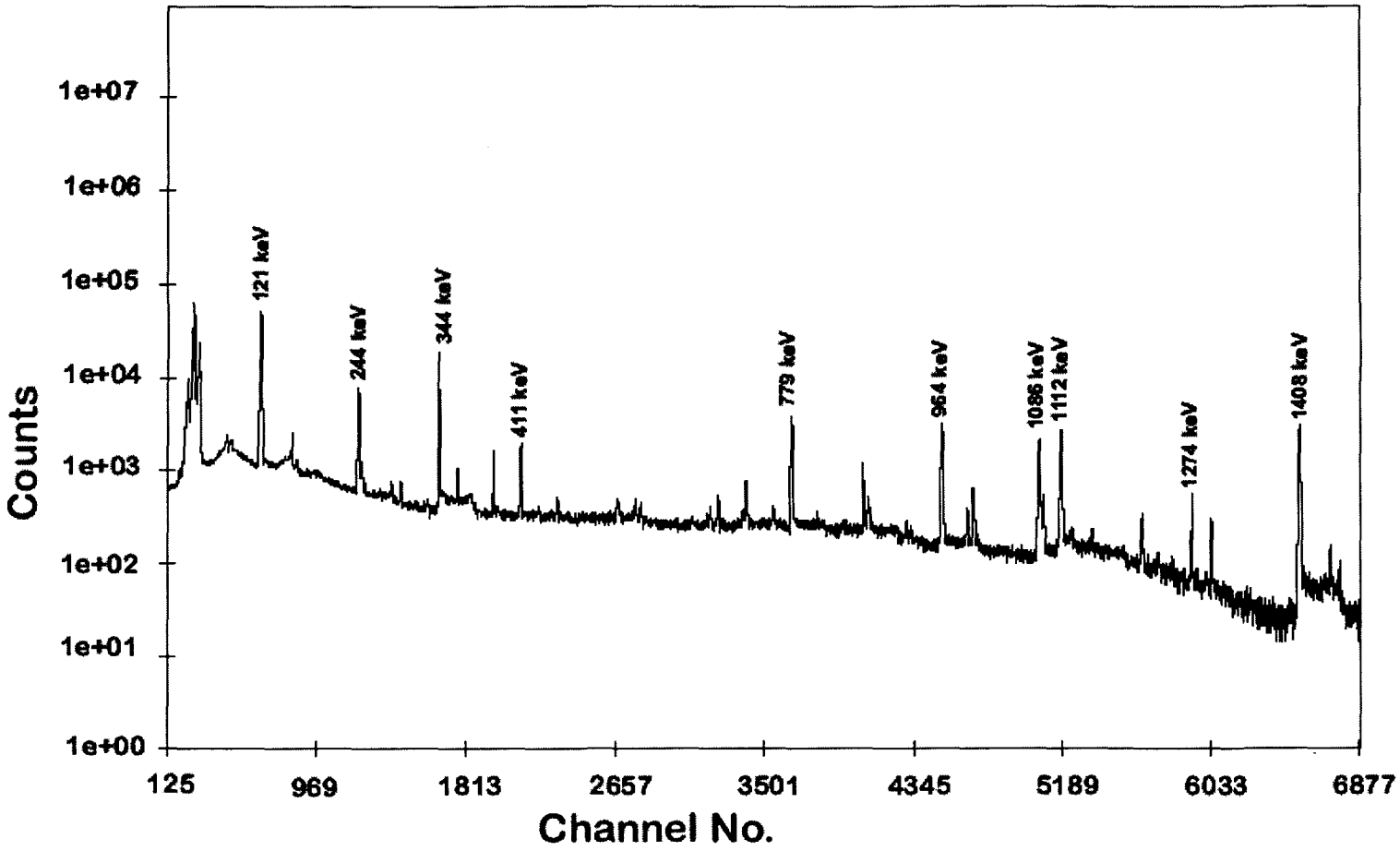

Fig. 2.5.1 A Typical γ-ray spectrum of ^{152}Eu source used for this work

In order to avoid the probable error in geometry factor, the relative efficiency was determined by using the relation,

$$\epsilon \cdot G = \frac{C.e^{\lambda t}}{S_0.\theta} \qquad \ldots\ldots\ldots 2.5.2$$

Depending upon the intensity of induced activity produced in the target foil / catcher, the source to detector distance in each case was kept different (whenever necessary), in order to keep the dead time of counting less than 10%. The values of $\epsilon \cdot G$ thus obtained were plotted as a function of energy using the program ORIGIN 6.0. A polynomial of degree 4 having the following form was found to give the best fit for these curves

$$\epsilon \cdot G = a_0 + a_1 x + a_2 x^2 + a_3 x^3 + a_4 x^4 \qquad \ldots\ldots\ldots 2.5.3$$

where a_0, a_1, a_2, a_3 and a_4 are the coefficients having different values for different source detector distances, x is the energy of characteristic gamma ray. The typical geometry dependent efficiency curves of the detector at various source- detector distances are shown in Fig. 2.5.2.

2.6 Recording of γ-Ray Spectra and Identification of Reaction Residues

In nuclear reactions, evaporation residues are produced in excited state by emission of charge particles/neutrons. These excited residual nuclei decays to their ground state by emitting characteristic γ-rays. In activation technique γ-activities produced in the irradiated targets/catcher foils were followed. As each isotope has a unique mode of decay and it comes to ground state by emitting characteristic γ-rays so identification of characteristics γ-rays and their intensity provides the measure of particular evaporation residue. The activation technique is a very powerful and, therefore, the cross-sections up to 1μb have been measured [6]. This technique is based on the discovery of artificial radioactivity [7]. Extremely high sensitivity, selectivity and the possibility of non-destructive analysis are some advantages of this technique.

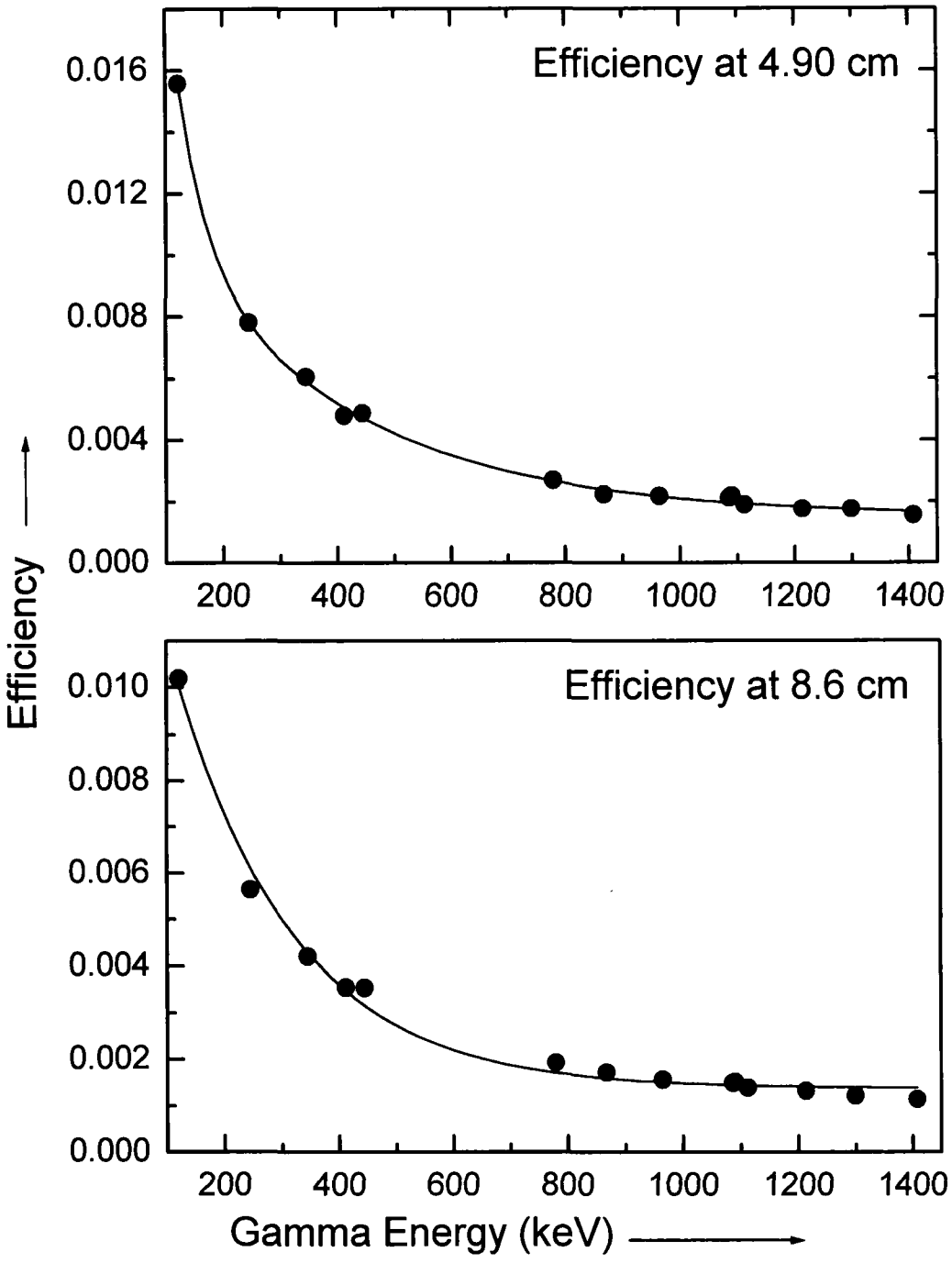

Fig. 2.5.2. Geometry Dependent Efficiency of the HPGe Detector

The activation technique involves identification and the measurement of the intensity of characteristic γ-rays emitted by the excited residual nucleus or by the daughter nucleus in the case of radioactive evaporation residues. Several activities may be induced in the sample and the catcher foil by irradiating these with the flux of heavy ions. The irradiation may be followed by off-line measurement of the activities induced in the target and catcher assembly. In such measurements, the γ-ray spectra of each sample were recorded at increasing times and radioactive residues were identified by their characteristic γ-rays as well as by their half lives. In some cases γ-rays emitted by two different residues were of nearly same energy. The concentration of each isotope in such cases was separated on the basis of their half-lives, by following the induced activities for a considerably long period.

Some of the radioactive residues are produced independently in the interaction of heavy ions. Others are produced in the decay of higher charge isobar precursor (cumulative yield) nucleus through β^+ emission, and/or electron capture. For such cases, cumulative cross-section has been measured if the half-life of precursor is considerably smaller than that of the residue, by analyzing the induced activities at times greater than about eight to ten half lives of the precursors. The cumulative cross-section of the given residue is the sum of (i) its independent production cross-section and (ii)cross-section for the independent production of its precursor multiplied by a numerical co-efficient which depends on the branching ratio for precursor decay to residue and the half lives of the precursor and the residue. In such case, the following decay analysis given by Cavinato et. al. [8] has been used in order to obtain the precursor decay contributions.

If a precursor P is formed with cross section σ_P during the irradiation , and decays with half- life $T^P_{1/2}$ and a branching ratio P_p , to a daughter nucleus D which is produced with cross-section σ_D during the irradiation and decays with half- life $T^D_{1/2}$, the cumulative cross section σ_C , for the production of the daughter is given by,

$$\sigma_C = \sigma_D + P_P \frac{T_{1/2}^{\ D}}{T_{1/2}^{\ D} - T_{1/2}^{\ P}} \sigma_P \qquad \text{.....2.6}$$

The branching ratio P_p has been taken from reference [9]. In certain cases, the radioactive residues emit γ-rays of more than one energy. The intensities of several gamma rays emitted from the same residue have been recorded and the production cross-section of the residue has been calculated from the observed intensities of gamma rays separately . The weighted average of the calculated cross-sections is taken as the measured cross-section [10].

The most important and major step in the experiment is the recording of the gamma ray spectra of the induced activities in the samples and catcher foils. The IUAC built data acquisition system FREEDOM was used to record the spectra. Keeping in view the appreciable count rate and low dead time of the detector counting geometry was chosen. HPGe detector was used to record the gamma ray spectrum because of very high-energy resolution ≈ 2 keV @1332 keV of ^{60}Co. The good energy resolution of these detectors not only helps to separate very closely spaced gamma ray peaks, but also nicely detects the weak gamma rays of discrete energies when superimposed on a broad continuum. The γ-ray spectrum of each foil was recorded at increasing times and analyzed in order to identify the photo-peaks of the interest produced due to various residual nuclei. Typical γ-ray spectra of ^{93}Nb irradiated by ^{12}C at ≈75 MeV and ≈ 47 MeV are shown in Fig.2.6.1. Similarly, the observed γ-rays spectra for ^{12}C + ^{52}Cr system at ≈ 80 MeV and for ^{16}O +^{115} In system at ≈ 105 MeV are shown in Figs. 2.6.2. and 2.6.3 respectively. Various peaks in the spectra correspond to different residues produced via different reaction channels. The γ-ray energy of some important peaks is indicated in these spectra.

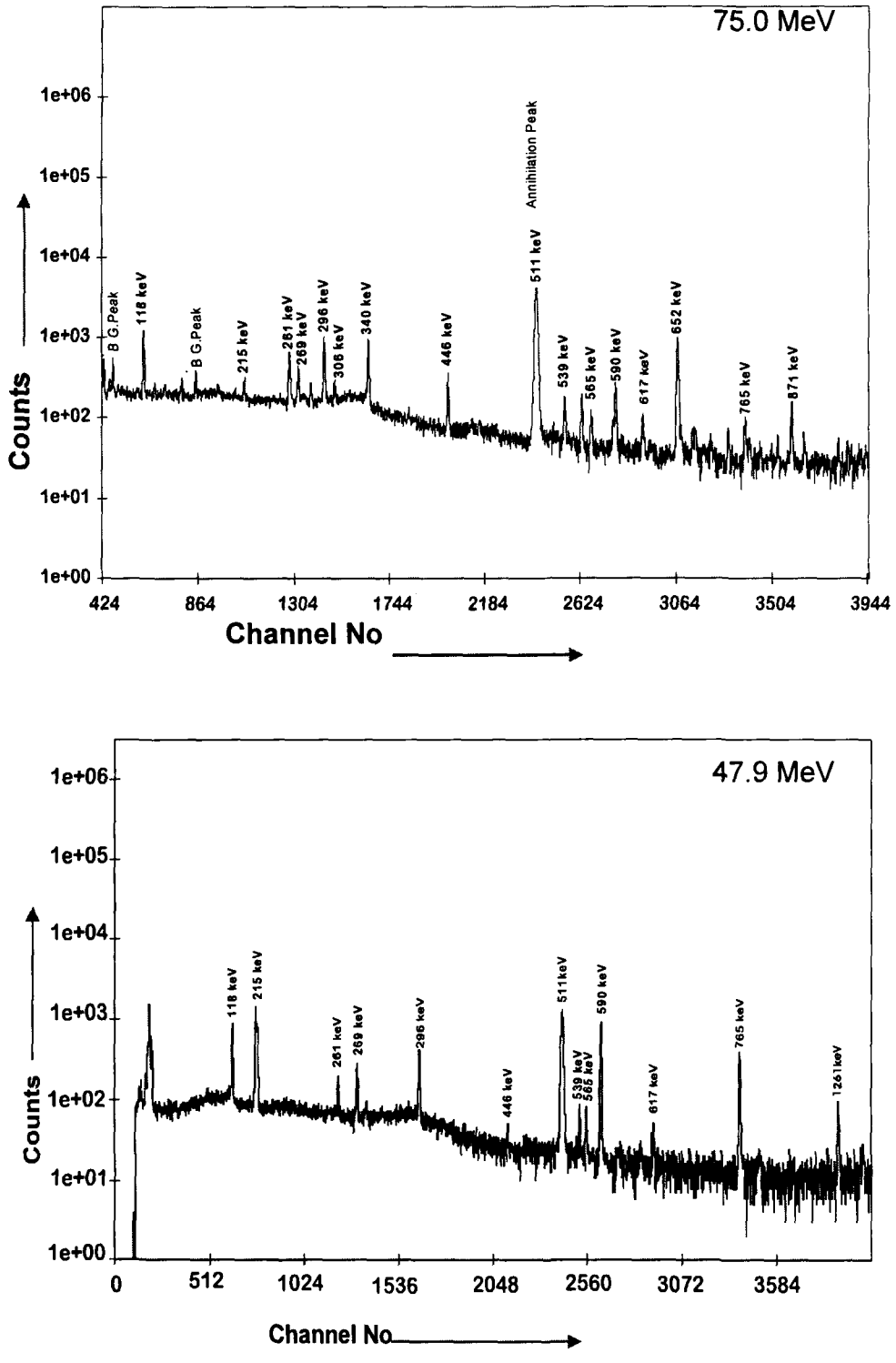

Fig. 2.6.1 Observed γ-ray spectra for $^{12}C+ ^{93}Nb$ system at ≈75 and ≈ 47 MeV respectively.

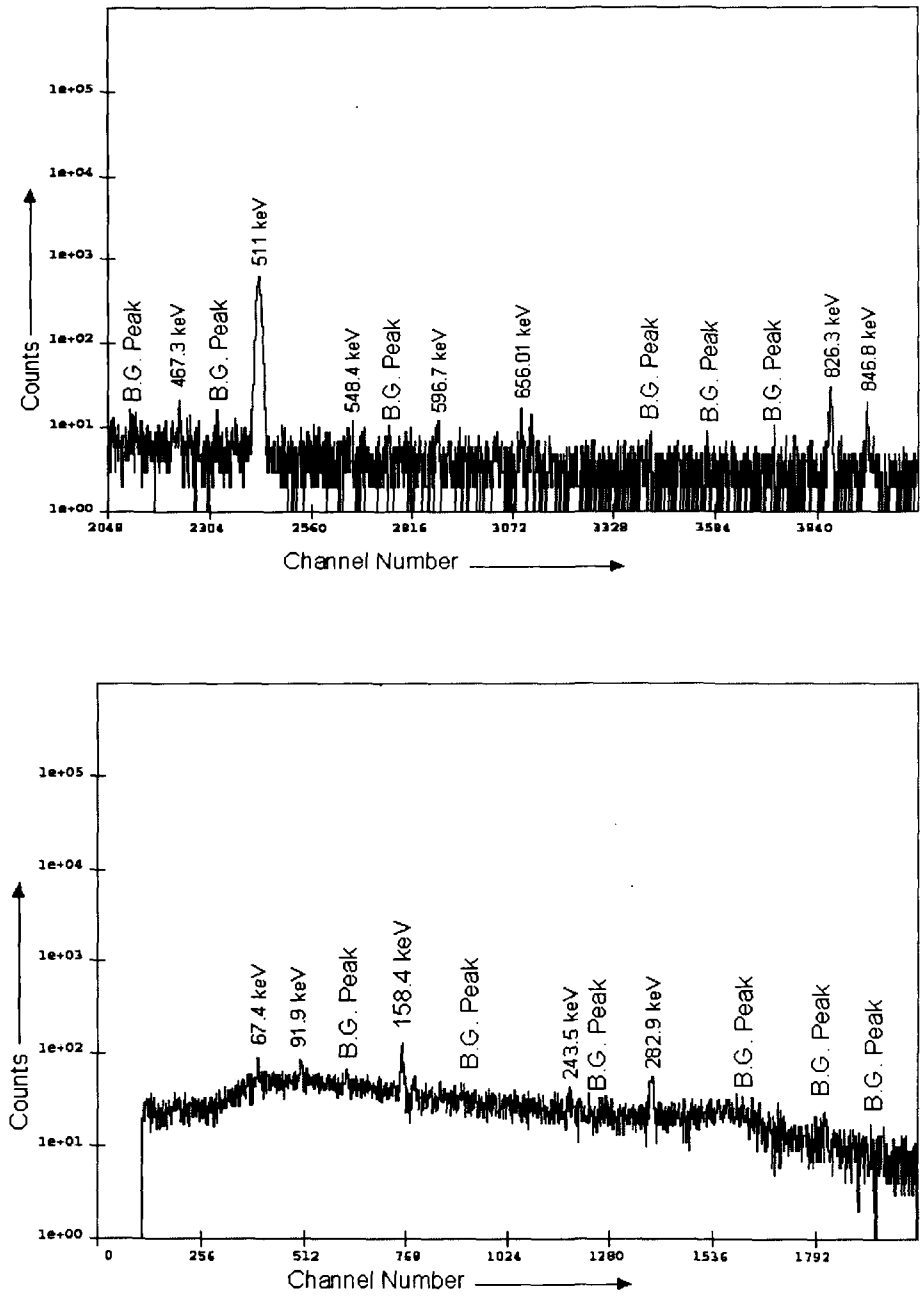

Fig. 2.6.2 Observed γ-ray spectra for $^{12}C+ ^{52}Cr$ system at ≈ 80 MeV .

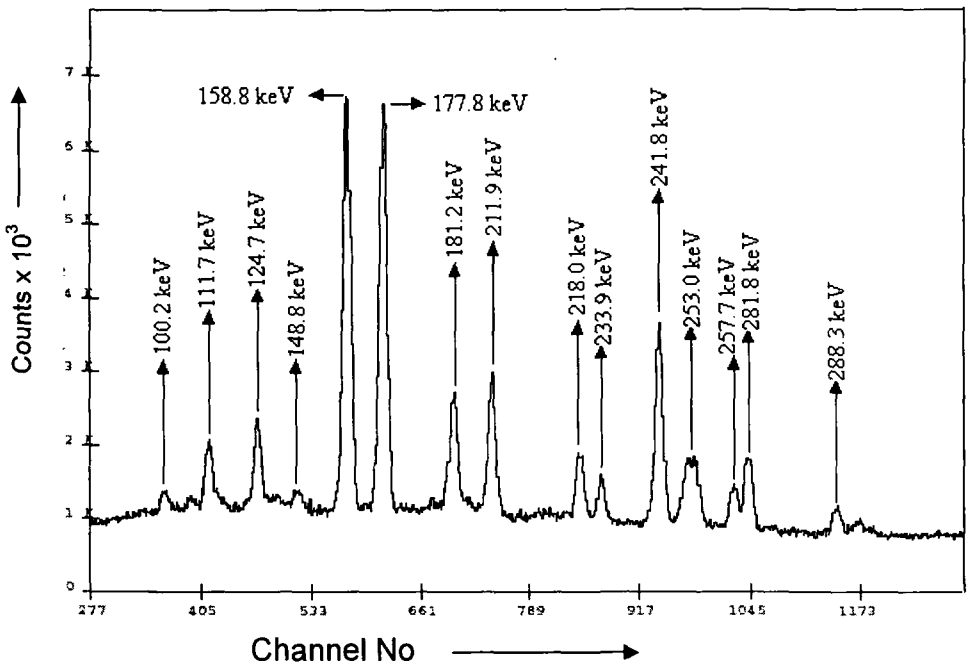

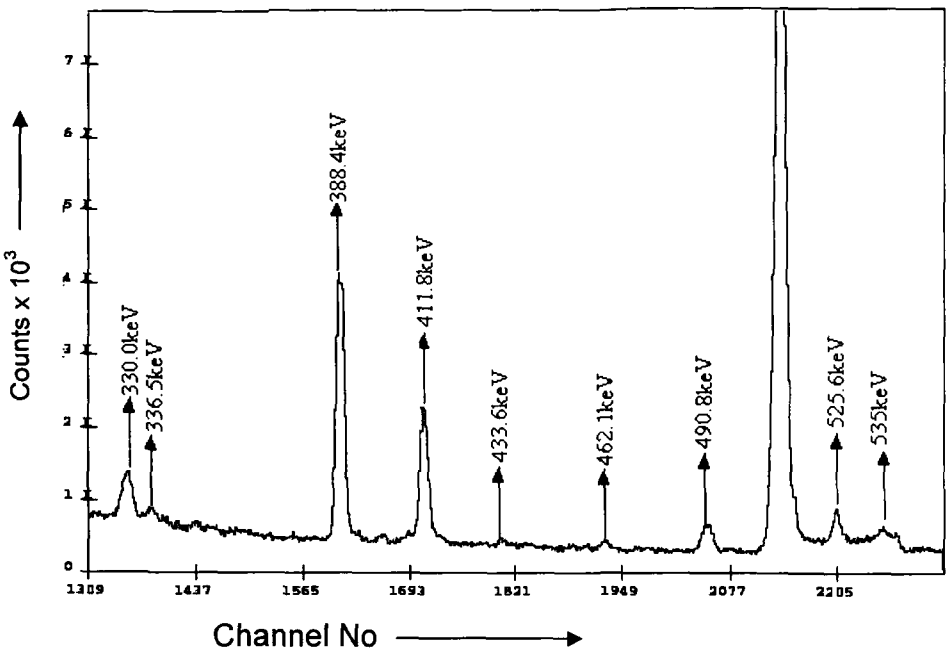

Fig. 2.6.3 Observed γ-rays spectra for $^{16}O + ^{115}In$ system at ≈ 105 MeV.

2.7 Formulation

If a sample containing N_0 number of target nuclei is irradiated by the beam of flux ϕ, the rate of formation of particular activation product is given by,

$$N = N_0 \phi \sigma_r \qquad \ldots\ldots 2.7.1$$

where σ_r is the reaction cross-section for the product nuclei of interest. It may be pointed that the isotopes produced by irradiation are radioactive, and decay simultaneously with their productions. If the stack of the samples has been irradiated for a time t_1, the activity produced in the sample is recorded for time t_3, and the time lapse between stop of irradiation and start of the counting is t_2, the intensity of induced activity after the time t_2 is given as

$$\left[\frac{dN}{dt}\right]_I = \frac{\sigma_r \phi N_0 \{1-\exp(-\lambda t_1)\}}{\exp(\lambda t_2)} \qquad \ldots\ldots 2.7.2$$

and number of nuclei decayed in time t_2 to $(t_2 + t_3)$ is given by

$$C = \frac{N_0 \phi \sigma_r \{1-\exp(-\lambda t_1)\}\{1-\exp(-\lambda t_3)\}}{\lambda \exp(\lambda t_2)} , \qquad \ldots\ldots 2.7.3$$

where λ is the decay constant of the product nuclei and is given by the relation

$$\lambda = \frac{0.693}{t_{1/2}} \qquad \ldots\ldots 2.7.4$$

with $t_{1/2}$ as the half-life of the residual nucleus. If the induced activity is recorded by a detector of geometry dependent efficiency $\epsilon \cdot G$, then the absolute counting rate C and the observed rate A are related as,

$$C = \frac{A}{(\epsilon \cdot G).\theta.K} , \qquad \ldots\ldots 2.7.5$$

where θ is the branching ratio of the characteristic gamma-ray and K is self absorption correction factor for the material of the sample and is given as

$$K = \frac{\{1 - \exp(-\mu d)\}}{\mu d} \qquad \ldots\ldots\ldots 2.7.6$$

where μ is the γ-ray absorption coefficient for the sample and d is the thickness of the sample. Thus from the above equations, we get

$$\sigma_r = \frac{A\,\lambda\,\exp(\lambda\, t_2)}{N_0\,\phi\,\theta\,K(\epsilon\cdot G)\,\{1-\exp(-\lambda\, t_1)\}\{1-\exp(-\lambda\, t_3)\}} \qquad \ldots\ldots\ldots 2.7.7$$

Equation 2.7.7 has been used to calculate the cross-section for the particular reaction product.

In the present measurements, when more than one γ-rays are available for a particular reaction at the same energy then the experimental cross-section is taken as the weighted average of the individual cross-section of these γ-rays. Following formulation has been used for determining the weighted average [10].

If $X_1 \pm \Delta X_1$, $X_2 \pm \Delta X_2$, $X_3 \pm \Delta X_3$, ------ are supposed to be the different measured values of the same quantity X, then the weighted average is given as

$$\overline{X} = \frac{\sum W_i X_i}{\sum W_i} \qquad \ldots\ldots\ldots 2.7.8$$

where $$W_i = \frac{1}{(\Delta X_i)^2}$$

$$\text{The internal error} = \left[\sum W_i\right]^{-1/2} \qquad \ldots\ldots\ldots 2.7.9$$

$$\text{The external error} = \left[\frac{\sum W_i\,(\overline{X} - X_i)^2}{n(n-1)\sum W_i}\right]^{1/2} \qquad \ldots\ldots\ldots 2.7.10$$

The statistical error given in the results is the larger one of the internal and external errors. Based on the above formulation, a computer program NPSIGMA [11] calculates cross-sections at various energies in the present study.

2.8 Recoil range distributions (RRDs)

In the present work, the recoil range distribution (RRD) for various radioactive residues produced in the interaction of ^{12}C beam with ^{93}Nb target nucleus have been measured at ≈ 80 MeV. The typical arrangement of target catcher assembly is shown in Fig 2.8.1. In the irradiation chamber, the target was mounted with Al-backing facing the beam so that the catcher stack immediately followed the niobium layer. The beam energy incident on front Al - surface was 80 MeV in case of ^{12}C+ ^{93}Nb system. After an energy loss of ≈ 3.47 MeV in the Al thickness, the incident beam energy was reduced to 76.53 MeV on the niobium material. A stack of 13 thin Al – catchers of thickness varying from ≈102-113 μg/cm^2 was used to trap the recoiling nuclei. The catcher –thickness used in the present experiment are given in Table 2.8.1. The duration of irradiation was about 4 hours with a beam fluence of ≈ 408.6 μC. The activities induced in each thin catcher were followed off-line for about two weeks using a precalibrated high resolution HPGe detector of 100 c.c. active volume coupled to CAMAC based software FREEDOM [12] at IUAC, New Delhi. The same software was used for analyzing the data.

The experimentally measured cross-sections for particular reaction products in different catcher foils were obtained using equation 2.7.7. In order to obtain the yield distribution as a function of cumulative depth in the catcher stack, the yield in each catcher was divided by its measured thickness. The resulting yield has been plotted against cumulative catcher thickness to obtain the differential recoil range distributions. The measured recoil range distributions for various residues are presented and discussed in Chapters III and V of the thesis.

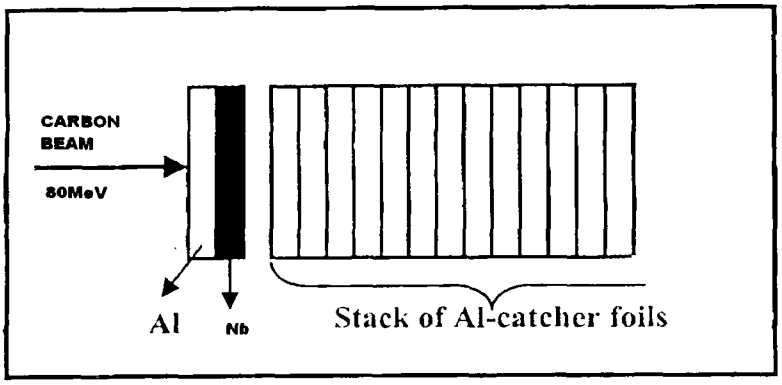

Fig.2.8.1 The Typical arrangements of target catcher assembly used for RRD measurements.

Table 2.8.1.

Catcher thicknesses used for RRD

S. No.	Thickness in μg / cm^2
1	113.1
2	106.6
3	106.6
4	105.6
5	107.3
6	103.2
7	105.9
8	107.4
9	102.3
10	107.4
11	103.4
12	106.4
13	107.8

References

[1] R.C. Koch, Activation Analysis Hand Book, Academic Press, New York and London (1960).

[2] Tauseef Ahmad, M.Phil. Dissertation, A.M.U., Aligarh, India (2006).

[3] I. A. Rizvi, Ph.D. Thesis (Unpublished), A.M.U., Aligarh, India (1988).

[4] B. Wilken and T.A. Fritz, Nucl. Instrum. Methods **138**, 331 (1976).

[5] J. Ernst et al., Z. Phys. **A 308**, 301(1982).

[6] S. M .Qaim, Radio Chimica Acta **25**, 13(1978); Inorg.Nucl.Chem.**36, 239** (1974).

[7] V. Carlo, Activation analysis for Charged particles John Wiley, New York, (1988).

[8] M. Cavinato et al., Phys. Rev. **C 52**, 2577 (1995).

[9] U. Reus and W. Westmeier, Atomic Data and Nucl. Data Tables **29**, 1 (1983).

[10] S.F. Mughahghab, M. Divadeenam and N.E. Holden, Neutron cross-sections, (New York: Academic Press) Vol.1, Part A, **89** (1981).

[11] Avinash Agarwal , Ph.D. Thesis (Unpublished), A.M.U., Aligarh , India (2003).

[12] FREEDOM, Data acquisition and analysis system designed to support the accelerator based experiments at IUAC, New Delhi, India.

Chapter - III

S. No	Systems studied	Energy Range	Coulomb barrier
1.	$^{12}_{6}C+^{93}_{41}Nb\rightarrow ^{105}_{47}Ag$	≈ 47-75 MeV	≈ 44 MeV
2.	$^{12}_{6}C+^{52}_{24}Cr\rightarrow ^{64}_{30}Zn$	≈ 52-80 MeV	≈ 29 MeV
3.	$^{16}_{8}O+^{115}_{49}In\rightarrow ^{131}_{57}La$	≈ 66-105 MeV	≈ 64 MeV

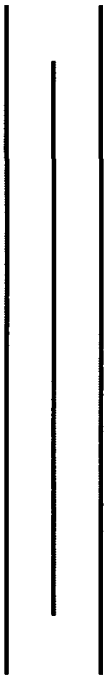

In order to study the complete fusion (CF) and incomplete fusion (ICF) in nuclear reactions induced by ^{12}C and ^{16}O beams, several experiments were carried out for measuring the excitation functions (EFs) in a wide energy range. The systems studied for the EFs measurements are listed in Table 3.1.

Table 3.1

Systems studied for EFs measurements

S. No	Systems studied	Energy Range	Coulomb barrier
1.	${}^{12}_{6}C+{}^{93}_{41}Nb \rightarrow {}^{105}_{47}Ag$	≈ 47-75 MeV	≈ 44 MeV
2.	${}^{12}_{6}C+{}^{52}_{24}Cr \rightarrow {}^{64}_{30}Zn$	≈ 52-80 MeV	≈ 29 MeV
3.	${}^{16}_{8}O+{}^{115}_{49}In \rightarrow {}^{131}_{57}La$	≈ 66-105 MeV	≈ 64 MeV

The excitation functions for thirty reactions namely ^{93}Nb (C, 2n) ^{103}Ag, ^{93}Nb (C, 3n)^{102}Ag, $^{93}Nb(C,4n)^{101}Ag$, $^{93}Nb(C,p3n)^{101}Pd$, ^{93}Nb (C,p4n)^{100}Pd, $^{93}Nb(C,p5n)^{99}Pd$, $^{93}Nb(C,2p2n)^{101}Rh$, $^{93}Nb(C,\alpha n)^{100}Rh$, $^{93}Nb(C,\alpha 2n)^{99}Rh$, $^{93}Nb(C,\alpha p3n)^{97}Ru$, ^{93}Nb (C,αp5n)^{95}Ru, $^{93}Nb(C,2\alpha n)^{96}Tc$, $^{93}Nb(C,2\alpha 2n)^{95}Tc$, $^{93}Nb(C,2\alpha 3n)^{94}Tc$, $^{93}Nb(C, 2\alpha p3n)^{94}$ Mo^{m}, ^{93}Nb (^{12}C,^{13}C)$^{92}Nb^{m}$, $^{52}Cr(C,2n)^{62}Zn$, $^{52}Cr(C, p2n)$ ^{61}Cu, ^{52}Cr (C, p3n)^{60} Cu, ^{52}Cr (C,α3n)^{57}Ni, $^{52}Cr(C,\alpha 4n)^{56}Ni$, $^{52}Cr(C,\alpha p3n)^{56}Co$, $^{52}Cr(C,\alpha p4n)^{55}Co$, $^{52}Cr(C,\alpha 3pn)^{56}Mn$, ^{115}In (O,p3n)^{127}Ba, $^{115}In(O,p4n)^{126}Ba$, $^{115}In(O, \alpha)^{127}Cs$, ^{115} $In(O,\alpha 2n)^{125}Cs$, $^{115}In(O, \alpha p3n)$ ^{123}Xe, and $^{115}In(O, \alpha p5n)^{121}Xe$ have been measured using the stacked foil activation technique. Further, to separate relative contributions of the CF and the ICF, recoil range distributions (RRDs) of several residues ^{101}Pd, ^{100}Pd, ^{99}Rh, ^{96}Tc, ^{95}Tc and ^{94}Tc produced in $^{12}C+$ ^{93}Nb system were also measured at energy ≈ 80 MeV.

In the present work, the various reactions induced by ^{12}C and ^{16}O were observed by detecting the characteristic gamma-lines obtained from the decay of residual nuclei. The possible reaction channels for ^{93}Nb, ^{52}Cr and ^{115}In in the energy range considered in the

present measurement are listed in Tables 3.1, 3.2 and 3.3, respectively. The other details viz., residual nucleus, spin-parity, half-life, gamma ray energies, corresponding absolute intensities and Q-values are also given in the aforesaid Tables. Nuclear data like half-lives, gamma ray energies etc, have been taken from the Table of Isotopes [1] and Nuclear Wallet Card [2]. The Q-values of different reactions have been taken from Ref. [3]. In the list, very weak gamma rays were not included whenever strong gamma rays were available for the same emitting nuclide. We have considered only those gamma rays that gave appreciable activities for the meaningful excitation studies. Description of the different systems and individual reactions are discussed in the following subsections.

3.1 $^{12}C+ ^{93}Nb$ System

Details of each reaction channel in $^{12}C+ ^{93}Nb$ system are discussed as follows:

1. $^{93}Nb (^{12}C, 2n)^{103}Ag$

This reaction produces two unstable isomers of ^{103}Ag. The ground state has half- life 1.10 hour and meta stable state of 5.7 sec. The reaction producing the ground state isomer was studied by considering 118.6 & 148.1 keV γ- rays. The cross-section for the ground state producing reaction is almost equal to the total cross-section for the production of ^{103}Ag isomers due to the activities measured after the decay of meta-stable state and its shorter half- life. The cross-sections of the reaction obtained at different energies are tabulated in Table 3.1.1(a).

2. $^{93}Nb (^{12}C, 3n) ^{102}Ag$

In this reaction two unstable isomers of half- life 12.9 min. and 7.8 min. were produced. The reaction producing the ground state was studied, considering 835.1, 1256.9 & 1581.4 keV γ-rays. Gamma rays having energy 556.6 keV and 719.5 keV are common to both the isomers. However, these peaks can be used in the analysis after the decay of meta stable state activity. The meta stable state of ^{102}Ag shows a 49% isomeric transition to the ground state and the rest decays by β^+ and electron capture. Though separation of cross-section of the two isomers is possible but our experimental conditions restrain it due to high activity of the exposed targets, consequently the counting started about 40 minutes after the irradiation. Therefore, ^{102}Ag cross-section given in Table 3.1.1(a) represents the cross-section of high spin isomer ($^{102}Ag^{g}$) including a contribution of the low spin isomer ($^{102}Ag^{m}$).

Table 3.1

Reactions, spin-parity, Half-life, Identified γ-rays, their intensities and Q-values.

Reactions	Spin-parity (J)$^{\pi}$	Half-life	γ-Energy (keV)	Intensity (%)	Q-value (MeV)
^{93}Nb (^{12}C, 2n)^{103}Ag	$(7/2)^{+}$	1.10h	118.6	31.2	-18.561
			148.1	28.3	
^{93}Nb (^{12}C, 3n)^{102}Ag^{g}	$(5)^{+}$	12.90m	835.1	13.7	-29.452
			1256.9	12.7	
			1581.4	13.7	
^{93}Nb (^{12}C, 3n)^{102} Ag^{m}	$(2)^{+}$	7.80m	556.6	43.0	
			719.5	4.5	
^{93}Nb (^{12}C, 4n) ^{101}Ag	$(9/2)^{+}$	11.10m	261.0	52.0	-38.293
			667.3	9.7	
^{93}Nb (^{12}C, p3n) ^{101}Pd	$(5/2)^{+}$	8.47 h	269.7	6.4	-33.281
			296.3	19.2	
			565.9	3.4	
			590.5	12.0	
			723.9	2.0	
			1289.1	2.3	
^{93}Nb (^{12}C, p4n) ^{100}Pd	$(0)^{+}$	3.63d	126.0	11.0	-41.552
			158.7	2.0	
^{93}Nb (^{12}C, p5n) ^{99}Pd	$(5/2)^{+}$	21.40m	136.2	73.0	-52.663
			263.8	15.0	
			673.9	6.9	
^{93}Nb (^{12}C, 2p2n) ^{101}Rh^{m}	$(9/2)^{+}$	4.34d	306.8	86.0	-30.519
^{93}Nb (^{12}C, αn) ^{100}Rh^{g}	$(1)^{-}$	20.80h	446.2	11.2	-47.699
			539.5	78.4	
			822.5	20.0	
^{93}Nb (^{12}C, α2n) ^{99}Rh^{g}	$(1/2)^{-}$	16.00d	322.4	6.6	
			528.6	40.0	
^{93}Nb (^{12}C, α2n) ^{99}Rh^{m}	$(9/2)^{+}$	4.70h	340.8	69.0	-48.477
			528.1	1.4	
			617.7	11.8	
			1261.0	10.9	
^{93}Nb (^{12}C, αp3n) ^{97}Ru	$(5/2)^{+}$	2.88d	215.7	86.0	-35.024
^{93}Nb (^{12}C, αp5n) ^{95}Ru	$(5/2)^{+}$	1.64h	336.5	70.8	-53.807
			626.9	18.0	
			1096.9	21.2	
^{93}Nb (^{12}C, 2αn) ^{96}Tc^{g}	$(7)^{+}$	4.28d	778.2	99.7	-11.390
			812.5	82.0	
			849.9	98.0	
			1126.8	15.3	
^{93}Nb (^{12}C, 2α2n) ^{95}Tc^{g}	$(9/2)^{+}$	20.00h	765.7	94.0	-22.184
			1073.7	3.8	
^{93}Nb (^{12}C, 2α3n) ^{95}Tc^{m}	$(½)^{-}$	61.00d	204.1	66.2	
			582.1	31.4	
			786.2	9.1	
^{93}Nb (^{12}C, 2α3n) ^{94}Tc^{g}	$(7)^{+}$	4.88h	702.6	99.6	-32.118
			849.7	95.8	
			871.1	99.8	
			916.1	7.6	
^{93}Nb (^{12}C, 2α3n) ^{94}Tc^{m}	$(2)^{+}$	52.00m	871.1	94.2	
			992.7	2.3	
^{93}Nb (^{12}C, 2αp3n) ^{93}Mo^{m}	$(21/2)^{+}$	6.85h	263.1	56.7	-36.755
			684.7	99.7	
			1477.2	99.0	
^{93}Nb (^{12}C, ^{13}C) ^{92}Nb^{m}	$(2)^{+}$	10.15d	934.5	99.0	-38.841

h = hour, m = minute, d = day

Table 3.2

Reactions, spin-parity, Half-life, Identified γ-rays, their branching ratios and Q-values.

Reactions	Spin-parity (J)$^{\pi}$	Half-life	γ-Energy (keV)	Intensity (%)	Q-Value (MeV)
$^{52}Cr(C, 2n)^{62}Zn$	$(0)^{+}$	9.19 h	243.5	2.5	-10.385
			247.0	1.9	
			260.5	1.3	
			394.1	2.2	
			507.6	14.6	
			548.4	15.2	
			596.7	25.7	
$^{52}Cr(C, p2n)^{61}Cu$	$(3/2)^{-}$	3.33h	67.4	3.9	-16.864
			282.9	12.5	
			373.1	2.2	
			588.6	1.2	
			656.0	10.7	
			908.6	1.2	
			1185.2	3.7	
$^{52}Cr(C, p3n)^{60}Cu$	$(2)^{+}$	23.2m	467.3	3.5	-28.574
			497.9	1.7	
			826.3	21.9	
			909.2	2.0	
			952.4	2.7	
			1035.2	3.7	
			1110.5	1.1	
			1293.7	1.9	
			1332.5	88.0	
$^{52}Cr(C,\alpha 3n)^{57}Ni$	$(3/2)^{-}$	1.50 d	127.2	12.9	-25.975
			1377.6	77.9	
$^{52}Cr(C,\alpha 4n)^{56}Ni$	$(0)^{+}$	6.1 d	158.4	98.8	-36.222
			269.5	36.5	
			811.8	86.0	
$^{52}Cr(C,\alpha p3n)^{56}Co$	$(4)^{+}$	77.7d	846.8	99.9	-33.305
			977.5	1.4	
			1037.9	14.1	
			1175.2	2.3	
			1238.3	67.0	
			1360.3	4.3	
$^{52}Cr(C,\alpha p4n)^{55}Co$	$(7/2)^{-}$	17.5h	91.9	1.2	-43.387
			411.4	1.1	
			477.2	20.2	
			803.7	1.9	
			931.2	75.0	
			1316.6	7.1	
			1369.9	2.9	
			1408.4	16.9	
$^{52}Cr(C,\alpha 3pn)^{56}Mn$	$(3)^{+}$	2.58h	846.2	98.9	-30.870

h = hour, m = minute, d= day

Table 3.3

Reactions, spin-parity, Half-life, Identified γ-rays, their branching ratios and Q-values

Reactions	Spin-parity $(J)^{\pi}$	Half-life	γ-Energy (keV)	Intensity (%)	Q-Value (MeV)
$^{113}In(O,p3n)^{127}Ba$	$(1/2)^{+}$	12.74 m	114.7	9.3	-42.960
			180.9	12.4	
$^{113}In(O,p4n)^{126}Ba$	$(0)^{+}$	1.67 h	217.8	4.1	-51.178
			241.0	6.0	
			281.2	3.1	
			328.3	2.1	
			489.4	2.9	
			681.9	4.4	
			993.4	2.4	
			1234.4	2.0	
$^{113}In(O,2p2n)^{127}Cs$	$(1/2)^{+}$	6.25 h	124.8	15.6	-38.754
			287.1	3.4	
			411.8	58.0	
			462.3	4.2	
			587.1	3.5	
$^{113}In(O, \alpha 2n)^{125}Cs$	$(1/2)^{+}$	45.0 m	111.7	8.6	-57.049
			334.9	2.0	
			413.1	5.3	
			524.8	24.0	
$^{13}In(O,\alpha\ pn)^{123}Xe+$	$(1/2)^{+}$	2.08 h	330.2	8.6	-54.532
$^{115}In(O, \alpha\ p3n)^{123}Xe$			899.7	2.4	-26.290
$^{113}In(O, \alpha p3n)^{121}Xe+$	$(5/2)^{+}$	40.10 m	445.4	10.8	-73.394
$^{115}In(O, \alpha p5n)^{121}Xe$					--

h = hour, m = minute, d = day

3 ^{93}Nb (^{12}C, 4n) ^{101}Ag

This reaction has two isomers of ^{101}Ag having half- life 11.1 min. for ground state and 3.1 s for meta-stable state and detected by identifying the γ-rays of 261.0 keV and 667.3 keV. Since the half life of the metastable state is much shorter than that of the ground state, the cross-sections for the ground state producing reaction as obtained above is almost the total cross-section for the production of ^{101}Ag isomers as the activities were measured after the decay of meta stable state. The cross –sections for this reaction obtained at different energies are tabulated in Table 3.1.1(a).

4. ^{93}Nb (^{12}C, p3n) ^{101}Pd

The residue ^{101}Pd (half- life 8.47 hour) was identified by studying 269.7, 296.3, 565.9, 590.5, 723.9 and 1289.1 keV gamma lines. It may also be populated by the β^+ decay of its higher charge isobar precursor ^{101}Ag formed via reaction (C, 4n). However, our calculations confirm that no precursor contribution was found. (See Table 3.1.1(a) for measured cross-sections of ^{101}Pd).

5. ^{93}Nb (^{12}C, p4n) ^{100}Pd

Residual nucleus ^{100}Pd possessing half-life of 3.63 days was identified by γ-lines of 126.0 and 158.7 keV. However, Tomer et al. [4] identified this product by γ-lines of 539.6 keV of 103.0% intensity. This residue may also be populated by its higher charge isobar precursor ^{100}Ag. Two isomers of ^{100}Ag produced during the bombardment, decay with half lives of 2.01 min and 2.3 min to ^{100}Pd. The cross-section of ^{100}Ag isomers expected is smaller than 10 mb [5] and accuracy of EFs for the (C, p4n) reaction is not affected seriously through precursor mode. Determination of ^{100}Ag contribution was not possible as counting was started 40 minutes after the stopping of irradiation. The measured cross-sections are tabulated in Table 3.1.1(b).

6. ^{93}Nb (^{12}C, p5n) ^{99}Pd

Residual nucleus ^{99}Pd has half life of 21.4 min. Gamma- lines of energies 136.2, 263.8 & 673.9 keV were used to characterize this residue. However, other authors [4, 5] used only single γ-ray for the residue. {For measurement of cross-section see Table 3.1.1(b)}

7. ^{93}Nb (^{12}C, 2p2n) $^{101}Rh^{m}$

This reaction populates two isomers of ^{101}Rh having half- lives of ground and meta stable state 3.3 years and 4.34 days respectively. The residue $^{101}Rh^{m}$ is identified by gamma- line of 306.8 keV which is common to both the isomers. Longer half- life of ground state made its cross section negligible so measured cross-section is only due to metastable state .The reaction cross-sections obtained at different energies have been presented in Table 3.1.1(b) .

8. ^{93}Nb (^{12}C, α n) ^{100}Rh

The reaction produces two unstable isomers of Rh namely $^{100}Rh^{g}$ and $^{100}Rh^{m}$ with half-life of ground state as 20.8 hours and meta stable state as 4.6 min. To investigate ^{100}Rh, , γ-lines of 446.2, 539.5 & 822.5 keV have been identified whereas 539.5 keV is common to both the isomers. This peak can be included in analysis after the decay of meta stable state. (See Table 3.1.1(b) for cross-sections).

9. ^{93}Nb (^{12}C, α2n) ^{99}Rh

Two isomers of ^{99}Rh are produced with ground state half life of 16.0 days and that of meta stable state of 4.7 hour. For the ground state the 322.4 keV gamma ray was identified and for the meta stable state intense gamma rays of 340.8, 528.1, 617.7 and 1261.0 keV were studied. The 528.1 keV γ ray is found common to both the isomers hence it has not been taken into consideration. The total cross–sections have been presented in the Table 3.1.1(c).

10. ^{93}Nb (^{12}C, αp3n) ^{97}Ru

The residue ^{97}Ru of half- life as 2.88 days was detected by following the γ-ray of 215.7 keV. Cross–section has been presented in the Table 3.1.1(c).

11. ^{93}Nb (^{12}C, αp5n) ^{95}Ru

The residue ^{95}Ru has half-life of 1.64 hour. Gamma lines of 336.5, 626.9 & 1096.9 keV have been considered for the evaluation of cross-section for ^{95}Ru. The experimental values of cross–section are given in the Table 3.1.1(c).

12. ^{93}Nb (^{12}C, 2α n) ^{96}Tc

This reaction produces two unstable isomers of ^{96}Tc. The half- lives of ground state and metastable state are 4.28 days and 51.5 min. respectively. The reaction producing the ground state was undertaken by considering the 778.2, 812.5, 849.9 & 1126.8 keV γ-rays. The 778.2 keV γ-ray is common to both isomers so this peak can be used in the analysis after the decay of meta stable state activity. In the analysis the 849.9 keV photo peak found associated with (C, 2α3n) reaction so it was not considered at energies above the threshold. The meta stable state of ^{96}Tc decays to the ground state with 98% isomeric transition and 2 % electron capture and β^+ decay. The half-life of metastable state is comparatively shorter thereby making the total cross-section almost equivalent to ground state. The total cross-sections obtained for this reaction are given in Table 3.1.1(c).

13. ^{93}Nb (^{12}C, 2α2 n) ^{95}Tc

This reaction produces two isomers of ^{95}Tc with half-lives of 20.0 hour and 61.0 days. The 765.7 keV γ-ray emitted from the ground state is common to other channel. Therefore, the cross-sections for the (C, 2α2n) ^{95}Tc reaction were measured by considering the 1073.7 keV γ-ray. The metastable state of ^{95}Tc decays to the ground state with 95.8% EC and 0.3% β^+ decay and 3.9% isomeric transition. The main gamma rays obtained from its decay are 204.1, 582.1 and 786.2 keV. The total cross-sections for both the ground as well as meta states are given in Table 3.1.1(d).

14. ^{93}Nb (^{12}C, 2α3 n) ^{94}Tc

Two isomers of ^{94}Tc are produced in this reaction. The ground and metastable states have half- lives of 4.88 hour and 52.0 min. respectively. The ground state has four γ-rays viz., 702.6, 849.7, 871.1 and 916.1 keV whereas the 849.7 keV is common to $^{96}Tc^g$, produced in (C, 2αn) reaction and the 871.1 keV γ-ray is also obtained from the $^{94}Tc^m$. The 871.1 keV γ-ray has also been used in the analysis of ground state producing reaction by counting the activities after several half lives of the meta-stable state. Thus, the cross-sections of the (C, 2α3n) $^{94}Tc^g$ reaction have been measured by considering the 702.6 and 916.1 keV γ-rays. The meta-stable state of ^{94}Tc decays through 72% β^+ and electron capture 28%. The main gamma-rays emitted from its decay are 871.1 and 992.7 keV. The total cross –sections for (C, 2α3 n) ^{94}Tc are presented in Table 3.1.1(d).

15. ^{93}Nb (^{12}C, 2αp3n) $^{93}Mo^{m}$

This reaction produces two isomers of ^{93}Mo with half lives 3.5 x 10^3 years and 6.85 hours. The same residual nucleus was also populated by ^{93}Nb (^{12}C,^{12}B)^{93}Mo. Below the threshold for the (C, 2αp3n) reaction the experimental cross-sections are solely for the ^{12}B reaction .The ground state activity is almost negligible owing to its longer half- life . The meta-stable state was detected through intense γ-rays of 263.1, 684.7 and 1477.2 KeV. The cross–sections for this reaction measured at different energies are shown in Table 3.1.1(d).

16. ^{93}Nb (^{12}C,^{13}C) $^{92}Nb^{m}$

This reaction produces two isomers of ^{92}Nb with half lives 3.2 x10^7 years and 10.15 days, where the latter corresponds to the meta stable state. The ground state activity is negligible due to its much longer half life. The meta stable state has an intense γ-ray of 934.5 keV. The cross-section for (^{12}C, ^{13}C) $^{92}Nb^{m}$ reaction has been measured using the 934.5 keV γ-ray and shown in Table 3.1.1(d).

Table 3.1.1 (a)

Experimentally measured cross-section of residual isotopes in ^{12}C +^{93}Nb system.

Energy	Cross-section (σ ± Δσ) mb							
(E_{lab} ± ΔE)	(^{103}Ag)		(^{102}Ag)		(^{101}Ag)		(^{101}Pd)	
(MeV)	Present	Prev*	Present	Prev*	Present	Prev*	Present	Prev*
46.4 ± 1.43	80.0 ± 9.6		260.3 ± 11.3		1.0 ± 0.2		1.8 ± 0.3	
48.4[a]		18.8[a]		158.6[a]		5.9[a]		
49.4[b]		29.9[b]		143.2[b]				4.2[b]
54.0 ± 1.42	38.2±3.9		615.4 ± 125.3		60.3 ± 6.6		57.8 ± 11.8	
55.9[a]								
56.3[a]		8.8[a]		152.1[a]		61.1[a]		102.8[a]
58.5[b]		12.3[b]		152.7[b]		19.4[b]		183.4[b]
61.2 ± 1.32	7.6±1.4		398.2 ± 46.9		203.4± 26.4		233.7 ± 25.7	
64.6[a]				70.3[a]		104.7[b]		523.0[a]
66.6[b]		5.5[b]		109.9[b]		30.4[b]		271.2[b]
67.8 ± 1.25			180.6 ± 42.2		334.4 ± 40.1		428.7 ± 64.3	
71.6[a]				37.5[a]		109.8[b]		
72.7[b]				46.9[b]		29.1[b]		372.1[b]
73.9 ± 1.08			40.1± 10.3		305.3 ± 30.5		339.9 ± 33.7	
77.4[b]		1.9[b]				18.4[b]		291.6[b]
78.3[a]				8.0[a]		35.5[a]		400.1[a]

[a]Reference [4]
[b]Reference [5]
*Prev [Previous]

Table 3.1.1(b)

Experimentally measured cross-section of residual isotopes in $^{12}C + ^{93}Nb$ system.

Energy ($E_{lab} \pm \Delta E$) (MeV)	Cross-section ($\sigma \pm \Delta\sigma$) mb							
	(^{100}Pd)		(^{99}Pd)		(^{101}Rh)		(^{100}Rh)	
	Present	Prev*	Present	Prev*	Present	Prev*	Present	Prev*
46.4 ± 1.43	4.0 ± 0.1						24.8 ± 2.4	
48.4[a]								27.1[a]
49.4[b]								31.4[b]
54.0 ± 1.42	1.8 ± 0.4						15.2 ± 0.9	
55.9[a]					2.8 ± 0.4			14.4[a]
58.5[b]		6.0[a]						11.4[b]
61.2 ± 1.32		11.1[b]	0.6 ± 0.1			13.5[b]	9.5 ± 1.9	
64.6[a]	2.9 ± 0.5				9.7 ± 1.9			10.7[a]
66.6[b]		46.4[a]						10.8[b]
67.8 ± 1.25		18.7[b]	3.2 ± 0.4			103.1[b]	25.1± 3.6	
71.6[a]	25.6 ± 3.1			1.5[a]	18.4 ± 2.2			30.2a
72.7[b]		159.8[a]						44.1[b]
73.9 ± 1.08		80.0[b]	6.1 ± 0.9			67.4[b]	50.9 ± 7.1	
77.4[b]	113.3 ± 15.9				22.8 ± 2.5			68.6[b]
78.3[a]		166.8[b]		6.5[a]		103.1[b]		120.2[a]

[a]Reference [4]
[b]Reference [5]
*Prev [Previous]

Table 3.1.1(c)

Experimentally measured cross-section of residual isotopes in $^{12}C + ^{93}Nb$ system.

Energy ($E_{lab} \pm \Delta E$) (MeV)	Cross-section ($\sigma \pm \Delta\sigma$) mb							
	(^{99}Rh)		(^{97}Ru)		(^{95} Ru)		(^{96}Tc)	
	Present	Prev*	Present	Prev*	Present	Prev*	Present	Prev*
46.4 ± 1.43	32.3 ± 4.9							
48.4[a]		73.2[a]						8.6[a]
49.4[b]								5.8[b]
54.0 ± 1.42	796.5 ± 119.5				0.3 ± 0.08		13.2 ± 3.8	
55.9[a]		159.8[a]						24.6[a]
58.5[b]		90.4[b]						24.1[b]
61.2 ± 1.32	1152.4 ± 161.3		1.3 ± 0.3		0.7 ± 0.2		56.4 ± 4.5	
64.6[a]		195.5[a]						54.9[a]
66.6[b]		88.4[b]		1.0[b]				32.0[b]
67.8 ± 1.25	1148.9 ± 168.8		17.8 ± 3.9		1.2 ± 0.2		101.2 ± 10.7	
71.6[a]		102.1[a]						
72.7[b]		74.1[b]		13.5[b]				42.0[b]
73.9 ± 1.08	833.3 ± 124.0		97.9 ± 10.2		2.0 ± 0.3		107.3 ± 6.3	
77.4[b]		49.9[b]		100.8[b]				46.0[b]
78.3[a]		95.2[a]						59.1[a]

[a]Reference [4]
[b]Reference [5]
*Prev [Previous]

Table 3.1.1(d)

Experimentally measured cross-section of residual isotopes in $^{12}C + ^{93}Nb$ system.

Energy ($E_{lab} \pm \Delta E$) (MeV)	Cross-section ($\sigma \pm \Delta\sigma$) mb							
	(^{95}Tc)		(^{94}Tc)		(^{93}Mo)		(^{92}Nb)	
	Present	Prev*	Present	Prev*	Present	Prev*	Present	Prev*
46.4 ± 1.43	0.6 ± 0.1		1.3 ± 0.1				1.9 ± 0.3	
48.4[a]		0.6[a]						
49.4[b]		0.9[b]						1.1[b]
54.0 ± 1.42	119.4 ± 9.9		15.1 ± 2.0		1.4 ± 0.1		3.9 ± 0.4	
55.9[a]		2.7[a]		0.3[a]				
58.5[b]		3.3[b]						4.5[b]
61.2 ± 1.32	206.6 ± 59.4				1.8 ± 0.2		5.2 ± 1.2	
64.6[a]		16.6[a]	22.9 ± 2.0	0.6[a]				
66.6[b]		8.9[b]						6.4[b]
67.8 ± 1.25	386.3 ± 52.3		45.9 ± 5.0		3.6 ± 0.5		14.9 ± 1.3	
71.6[a]		48.5[a]		2.2[a]				
72.7[b]		32.5[b]		1.5[b]		1.3[b]		9.8[b]
73.9 ± 1.08	450.9 ± 76.4		58.6 ± 6.0		5.7 ± 0.8		40.7 ± 3.0	
77.4[b]		59.0[a]		6.6[b]		2.4[b]		14.0[b]
78.3[a]		91.6[a]						

[a] Reference [4]
[b] Reference [5]
*Prev [Previous]

3.2 $^{12}C + ^{52}Cr$ System

Details of each reaction channel in the $^{12}C + ^{52}Cr$ system are described as follows:

1. $^{52}Cr(C,2n)^{62}Zn$

This reaction produces unstable ^{62}Zn residual nucleus which decays mainly by electron capture (93.1%) and β^+ (6.9%) with a half-life of 9.19 hour decays to the excited state of ^{62}Cu. The reaction has been studied by considering three major gamma rays viz., 507.6, 548.4 and 596.7 keV. The reaction cross sections obtained for this reaction at five different projectile energies are given in Table 3.2.1(a).

2. $^{52}Cr(C,p2n)^{61}Cu$

The residual nucleus ^{61}Cu being unstable and which decays to the levels of ^{61}Ni by 38% through EC and 62% by β^+ emission. The gamma rays emitted from the product nucleus are enlisted in Table3.2. The reaction has been studied by considering the two major gamma rays viz., 282.9 keV and 656.0 keV at five incident energies. The measured values of the cross sections for this reaction are tabulated in Table 3.2.1(a).

3. $^{52}Cr(C,p3n)\ ^{60}Cu$

This reaction on chromium produces unstable ^{60}Cu residual nucleus which decays dominantly by β^+ (93%) and electron capture (7%) with a half-life of 23.2 minutes to the excited state of ^{60}Ni (unstable isotope). The cross-sections for this reaction have been measured at five incident beam energies by considering the most intense gamma rays viz., 826.3 keV and 1332.5 keV. The reaction cross sections obtained for this reaction at four different projectile energies are given in Table 3.2.1(a).

4. $^{52}Cr(C,\alpha 3n)\ ^{57}Ni$

This reaction produces ^{57}Ni residual nucleus, being unstable and which decays by β^+ emission and electron capture with a half- life of 1.50 days to the exited state of ^{57}Co. The reaction cross sections have been measured using the 127.2 and 1377.6 keV gamma rays. The measured values of the cross-section obtained with the above gamma rays are tabulated in Table 3.2.1(a).

5. $^{52}Cr(C,\alpha 4n)\ ^{56}Ni$

The product nucleus being unstable decays to the levels of ^{56}Co mainly by electron capture (EC). The cross-section for the (C,α4n) reaction have been measured at five different projectile energies using two major gamma rays viz., 158.4 and 811.8 keV. The nuclear spectroscopic data used for this reaction are given in Table3.2 and the cross sections obtained are tabulated in Table 3.2.1(b).

6. $^{52}Cr(C,\alpha p3n)\ ^{56}Co$

This reaction produces ^{56}Co residual nucleus (unstable) which decays by β^+ (19%) and EC (81%) with a half life of 77.7 days. The reaction has been studied by considering the intense gamma rays of 846.8, 1037.9 and 1238.3 keV. The cross sections have been measured at five incident energies using these gamma rays. The reaction cross sections obtained for this reaction are given in Table 3.2.1(b).

7. $^{52}Cr(C,\alpha p4n)\ ^{55}Co$

This reaction on chromium produces unstable ^{55}Co residual nucleus, and which decays to the levels of ^{55}Fe through EC and β^+ emission. The gamma rays of 477.2 and 931.2 keV obtained from the decay of ^{55}Co have been taken into account in the analysis of (C, αp4n) reaction cross sections. The reaction cross sections obtained for this reaction are tabulated in Table 3.2.1(b).

8. $^{52}Cr(C,\alpha 3pn)\,^{56}Mn$

This reaction produces ^{56}Mn residual unstable nucleus whose half- life is 2.58 hr. The cross sections for this reaction have been studied by considering the most intense gamma ray of 846.2 keV. Cross sections obtained for this reaction are tabulated in Table 3.2.1(b).

Table 3.2.1(a)*

Experimentally measured cross-section of residual isotopes in $^{12}C + ^{52}Cr$ system.

Energy $E_{lab} \pm \Delta E$ (MeV)	Cross-section ($\sigma \pm \Delta\sigma$) mb			
	(^{62}Zn)	(^{61}Cu)	(^{60}Cu)	(^{57}Ni)
51.9 ± 0.33	21.2 ± 2.1	433.4 ± 45.5	176.9 ± 25	13.6 ± 2.6
60.3 ±0.29	13.3 ± 0.9	379.6 ± 40.3	86.9 ± 9.5	52.1 ± 3.6
67.8 ± 0.27	9.2 ± 1.0	244.4 ± 29.1	188.9 ± 21	-----
74.6 ±0.26	3.6 ± 0.5	122.3 ± 12.3	181.9± 19	----
80.0 ±0.25	3.0 ± 0.2	42.4 ± 5.5	87.1 ± 7.5	-----

Table 3.2.1 (b)*

Experimentally measured cross-section of residual isotopes in $^{12}C + ^{52}Cr$ system.

Energy ($E_{lab} \pm \Delta E$) (MeV)	Cross-section ($\sigma \pm \Delta\sigma$) mb			
	(^{56}Ni)	(^{56}Co)	(^{55}Co)	(^{56}Mn)
51.9 ± 0.33	--	--	--	--
60.3 ±0.29	59.5 ±14.9	--	--	--
67.8 ± 0.27	73.1 ± 8.9	491.9 ± 85.8	--	76.9 ± 8.7
74.6 ±0.26	86.9 ± 9.3	936.6 ± 66.9	53.8 ± 7.7	161.5 ± 20.4
80.0 ±0.25	94.4 ± 7.4	1728.4 ± 163.5	93.0 ± 25.1	234.3 ± 25.2

*Cross-section values tabulated in Tables 3.2.1(a,b) were measured by us and part of it is the improved version (including errors) of Ref. [6].

3.3 $^{16}O + ^{115}In$ System

The contribution from ^{113}In (4.3%) isotope will be seen in ^{123}Xe and ^{121}Xe evaporation residues. These contributions are maximum at $E_{beam} \leq 80.0$ MeV. In the present work, we rejected this data so that the contributions from the ^{113}In become negligible [7]. Details of each reaction channel in the $^{16}O+^{115}In$ system are described as follows:

1. ^{115}In (O, p3n) ^{127}Ba

The residual nucleus (^{127}Ba) being unstable decays via β^+ (51%) and EC (49%) with a half-life of 12.74 minutes. The reaction has been studied by considering the 114.7 and 180.9 keV gamma rays obtained from the decay of the residual nucleus. The measured values of cross-section for this reaction are presented in Table 3.3.1(a).

2. ^{115}In (O, p4n) ^{126}Ba

This reaction produces ^{126}Ba, unstable nucleus which decays via β^+ and EC to the levels of ^{126}Cs.The reaction has been studied by considering the major gamma rays viz., 217.8, 241.0, 281.2 and 681.9 keV. The reaction cross-sections obtained for this reaction at five different projectile energies are given in Table 3.3.1(a).

3. ^{115}In (O,α) ^{127}Cs

This reaction on indium produces unstable ^{127}Cs residual nucleus which decays dominantly via electron capture EC (96.5%) and β^+ (3.5%) with a half-life of 6.25 hour. Cross-sections for these reactions have been measured by considering 124.8, 411.8, 462.3 and 587.1 keV gamma rays. The cross-sections obtained with different gamma rays are tabulated in Table 3.3.1(a).

4. ^{115}In (O, α2n) ^{125}Cs

The residue ^{125}Cs decays via β^+ (39%) and EC (61%) with a half- life of 45.0 minutes to the levels of ^{125}Xe.The Q-value for this reaction is -57.049 MeV for 2p4n channel and -28.753 MeV for the $\alpha 2n$ channel. The gamma rays of 334.9 keV and 524.8 keV obtained from the decay of ^{125}Cs have been considered in the analysis of (O, α2n) reaction cross-sections. The cross-sections obtained using these gamma rays are given in Table 3.3.1(b).

5. ^{115}In (O, αp3n) ^{123}Xe

This reaction produces ^{123}Xe, unstable nucleus which decays ~~via β$^+$~~ (13%) and EC (87%) with a half-life of 2.08 hour.The residue *^{123}Xe* is formed by the isotopes *^{113}In* and *^{115}In*, via channels αpn and αp3n, respectively. The Q-value for the reaction via ^{113}In isotope for 3p3n channel is -54.532 MeV and for αpn channel is -26.290 MeV. For the isotope ^{115}In, the corresponding Q-values for 3p5n and αp3n channels are -71.248 MeV and -42.952 MeV, respectively. The reaction has been studied by considering the 330.2 and 899.7 keV gamma rays. The cross-sections obtained using these values are tabulated in Table 3.3.1(b).

6. ^{115}In (O, αp5n) ^{121}Xe

The contribution of both the isotopes of Indium (*^{113,115}In*) was seen in ^{121}Xe. The residue ^{121}Xe is formed either by 3p5n channel or by αp3n channel of isotope ^{113}In and/or by 3p7n channel or αp5n channel of ^{115}In. The Q-value for the reaction is -73.394 MeV and -45.0.99 MeV for 3p5n and αp3n channels of ^{113}In, respectively and/or –90.166 MeV for 3p7n channel and –61.871 MeV for αp5n channel of isotope ^{115}In. The cross-sections have been studied by considering the gamma ray of 445.4 keV. Cross-sections obtained using the above gamma ray are given in Table 3.3.1(b).

3.4 Measurement of recoil range distributions (RRDs) in ^{12}C+^{93}Nb system

A separate experiment was performed to measure the distribution of ranges of recoiling residues produced both by the complete and incomplete fusion of ^{12}C at ≈80 MeV. The measure of the yield of the residues produced in a particular reaction is the most accurate way of measuring the reaction cross-section. That may be done by detecting a characteristic γ-ray of the residue in-beam, or off-beam if the residue is radioactive. The off-beam measurements provide by far more accurate results not only because the background in γ-spectra is much smaller, but also because each residue may be identified both through the energy of its characteristic γ-lines and its life- time by measuring the variation with time of activity .

Table 3.3.1(a))*

Experimentally measured cross-section of residual isotopes in $^{16}O + ^{115}In$ system.

Energy $E_{lab} \pm \Delta E$ (MeV)	Cross section [$\sigma \pm \Delta(\sigma)$] (mb)		
	(^{127}Ba)	(^{126}Ba)	(^{127}Cs)
65.8 ± 1.09	465.5 ± 66.9	--	60.8 ± 5.4
74.7 ±1.02	1340.7 ± 240.6	231.9 ± 127.1	572.4 ± 54.3
83.2 ± 0.99	1738.9 ± 252.7	325.5 ± 47.7	1570.5 ± 75.4
90.9 ±0.95	732.5 ± 101.0	728.8 ± 132.0	1619.3 ± 180.7
96.2 ±0.90	1373.9 ± 219.0	913.3 ± 170.2	900.5 ± 75.5
104.2 ± 0.85	--	1781.6 ± 190.4	531.1 ± 60.4

Table 3.3.1(b)*

Experimentally measured cross-section of residual isotopes in $^{16}O + ^{115}In$ system.

Energy $E_{lab} \pm \Delta E$ (MeV)	Cross section [$\sigma \pm \Delta(\sigma)$] (mb)		
	(^{125}Cs)	(^{123}Xe)	(^{121}Xe)
65.8 ± 1.09	210.6 ± 18.9	----------	330.6 ± 33
74.7 ±1.02	163.5 ± 14.9	----------	627.8 ± 62.5
83.2 ± 0.99	194.9 ± 20.5	234.9 ± 19.9	400.9 ± 38.1
190.9 ±0.95	111.2 ± 15.9	134.1 ± 12.5	115.0 ± 8.1
96.2 ±0.90	128.8 ± 19.5	425.2 ± 39.2	110.2 ± 11.9
104.2 ± 0.85	1775.6 ± 198.4	1100.1 ± 99.7	----------

*Cross-section values tabulated in Tables 3.3.1(a,b) were measured by us and part of it is the improved version (including errors) of Ref. [8].

One may measure the RRDs of residues (which depends on their velocity distribution) using a very thin target out of which the residue recoils and a set of thin catchers downstream the target. Such a measurement sheds light on the reaction mechanism: the residues which are formed in a CF reaction having larger recoils than those of residues produced in ICF process or transfer reactions.

The experimentally measured cross-section for a particular evaporation residue in each catcher was obtained using equation (2.7.7) of chapter II. In order to obtain the yield distribution as a function of cumulative depth in catcher stack, the measured cross-section for each evaporation residue in individual catcher was divided by the respective thickness of that catcher. The results of the recoil ranges of six evaporation reaction products at projectile energy ≈ 80 MeV are tabulated in Tables 3.4.

Table 3.4

Measured RRDs for Pd, Rh and Tc isotopes

S. No.	Cumulative Catcher thickness ($\mu g/cm^2$)	Recoil Range (mb / mg-cm^{-2})					
		^{101}Pd	^{100}Pd	^{99}Rh	^{96}Tc	^{95}Tc	^{94}Tc
1.	113.1	14.9	--	3.8	146.7	135.8	11.2
2.	219.8	14.9	32.4	26.7	222.3	202.7	16.3
3.	326.4	14.9	40.5	95.4	101.4	150	12.7
4.	432.0	94.6	113.5	173.3	45.3	91.2	10.9
5.	539.3	303.7	340.5	151.1	21.5	68.9	10.7
6.	642.6	801.6	802.7	119.8	17.2	66.8	11.2
7.	748.6	1095.4	1110.8	97.7	10.7	58.8	13.1
8.	855.9	985.8	981.1	86.3	10.7	50.7	12.2
9.	958.2	512.7	494.9	67.2	8.6	38.5	9.1
10.	1065.5	149.4	113.5	45.8	6.4	34.4	6.5
11.	1276.1	19.9	24.3	3.8	4.3	8.1	1.0
12.	1382.5	14.9	8.1	4.5	2.2	6.1	--
13.	1490.2	--	--	--	--	--	--

3.5 Uncertainties in the measurements

The reliability and utility of experimental data depends on the degree of error related to the particular measurement. The various sources of errors along with the possible ways of their minimization/elimination in the measurement are as follows:

i. The erratic behavior of electronic equipments leads to some errors. It can be minimized by stabilizing the electronic equipments for a few hours before the beginning of the experiment.

ii. The determination of detector efficiency may also produce some errors in the measurement. There may be some contribution to this error owing to any uncertainty in the strength of standard source, statistical count rate of the photo peaks, and in the absolute intensity of the relevant gamma ray. This error may be minimized by careful determination of the detector efficiency and drawing the efficiency curve by fitting the best polynomial using standard software **Origin 6.0**. The maximum uncertainty in the detector efficiency was estimated to be 2%. Error owing to the solid angle effect (<2%) [9] may lead to inaccuracy in the measurement of detector efficiency.

iii. The measurement of target thickness may also bring in some errors which could be minimized by cutting the target foils to the standard sizes and accurately weighing them using a microbalance. The estimated error due to this factor was found less than 1%.

iv. Fluctuations in beam current could also be erratic due to sudden stopping of the beam or fluctuations in beam intensity. The fluctuations were controlled by adjusting the parameter in the Pelletron.

v. Losses of the product nuclei recoiling out of the sample may introduce large errors in the measured cross-sections. These were minimized by counting together the activity induced in the sample and the catcher foils, which were kept just behind the target.

vi. Error in the incident beam energy has been determined by calculating the energy spread in half thickness of the sample with the help of SRIM 2006.

vii. The inaccurate measurement of irradiation time, the time lapse between the stopping of irradiation and beginning of counting as well as counting time may propagate some errors. The estimated upper limit for this error is less than 2% in the present measurement.

viii. In determining the count rate, the dead time of counting introduces an error so in all the cases the dead time was kept less than 10% by suitably adjusting the target-detector distance and the correction for it was applied in the counting rate.

Further, the errors associated with the spectroscopic data like branching ratio and half-life of the product nuclei taken from the Table of radioactive isotopes [1] were not taken into account, because any revision in the spectroscopic data would permit an easy recalculation of the cross-section in future.

The total absolute error in the measured cross-section includes the statistical error in the measured peak areas together with systematic errors. The overall uncertainty in the cross-sections is estimated to be $\approx$ 4-27%.

References

[1] E. Browne and R.B Firestone, Table of Radioactive Isotopes (Wiley, New York, 1986).

[2] J.K.Tuli, Nuclear Wallet Card, National Nuclear Data Centre, Brookhaven National Laboratory, New York, USA (2000).

[3] http://www.nndc.bnl.gov/qcal/.

[4] B.S. Tomer et al., Z. Phys. **A 343**,223 (1992).

[5] P. Misaelides, Radiochim, Acta **28**, 1 (1981).

[6] Anjana Maheshwari, M.Phil.Dissertation, AMU, Aligarh, India, (2007)

[7] S. Mukherjee et al., Int. J. Mod. Phys. **E 15**, 237 (2006).

[8] Meenal Gupta, M.Phil. Dissertation, AMU, Aligarh, India (2007)

[9] R.P. Gardner and K. Varghese, Nucl. Instrum. Methods **93,** 163(1971).

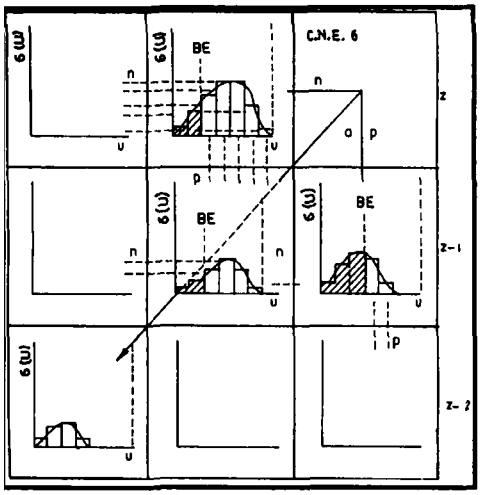

Chapter - IV

COMPUTER CODES

In order to interpret the measurements as described in the chapter III, latest nuclear theories and models have been employed. In case of heavy projectile nucleus, even at low bombarding energy, a large number of different excited configurations are available for the composite system. This is because the average level spacing in the compound nucleus is small compared to the average level- width. The density of quantum mechanical states increases rapidly and becomes very large at higher excitation energy. Moreover, in the emission of particle from the compound nucleus, numerous residual states are formed. In such a situation, a separate study of each state is complex and time consuming. Therefore, statistical models are convenient for the study of nuclear reaction mechanism.

The early models developed by Bethe, Weisskopf and Ewing [1, 2] were based on Bohr's independent hypothesis. These models neglected the angular momentum imparted by the projectile to the composite system and were , therefore, suitable for the study of nuclear reaction mechanism based on light-ion studies as such where the angular momentum effects are insignificant due to the small mass of the projectile at the intermediate energy . In 1952, the models were modified by Hauser and Feshbach [3] to include angular momentum effects in nuclear density expansions and in the theory of compound nuclear reactions. With the advent of heavy-ion beams in late 1950's the modified model of compound nucleus theory was applied to the heavy-ion fusion reactions. Based on the aforesaid models a variety of computer codes have been developed over the years in order to study the nuclear structure and reaction mechanism. These computer codes can now be used to verify the reaction mechanism, to aid in the identification of compound nucleus formation and decay, to determine angular momenta and to search for non-statistical aspects of nuclear structure at higher excitation energies and high angular momentum [4].

In the present work, theoretically calculated excitation functions using computer codes ALICE-91 [5] and PACE2 [6] are compared with the experimental data to extract the nature of reaction mechanism. A brief description of these codes and their input parameters is given in the next two sections.

4.1 Basic Features of the code ALICE-91

The code ALICE-91 can calculate both equilibrium and pre–equilibrium emission cross-section. It is based on the Weisskopf-Ewing model [2] for compound nucleus reaction (equilibrium) while pre-equilibrium emission is stimulated within the framework of Hybrid/geometry dependent hybrid model [7, 8]. In this code the possibility of incomplete fusion has not been taken into account but it can compute statistical fission cross-sections utilizing Bohr-Wheeler approach with angular momentum dependent state and saddle point energies. The code may calculate the reaction cross-section for the residual nuclei having mass ≤ A-11 and atomic number ≤ Z-9 from the compound nucleus (A,Z). Myers-Swiatecki Lysekil mass formula [9] is used for calculating Q-values and binding energies of all the nuclei in the evaporation chain.

The inverse reaction cross-sections used in the code are calculated using optical model [10] subroutines, although code has an option of classical sharp cut off model also. The transmission coefficients are calculated using the parabolic model of Thomas [11] for heavy ions. Like all semi-classical models, ALICE-91 assumes equipartition of energy among the initially excited particles and holes. The important input parameters required in this code are, the level density parameter a, the initial exciton number n_0 and mean free path (MFP) multiplier '*COST*' along with the description of the projectile and target nucleus. The MFP for intranuclear transition rates may be calculated from the optical model of Becchetti and Greenless [12] or from Pauli corrected nucleon-nucleon cross-sections [13, 14]. The MFP multiplier COST is used to adjust the nuclear mean free path in order to reproduce the experimental data. It accounts for the difference, if any, between the calculated and the actual MFPs for two-body residual interactions.

Level densities of residue may be calculated either from the Fermi Gas model or from the constant temperature form. The level density $\rho(U)$ from Fermi gas model is given by [15]

$$\rho(U) \approx (U-\delta)^{-5/4} \exp\left(2\sqrt{a(U-\delta)}\right) \qquad \ldots\ldots 4.1.1$$

where, δ is the pairing term and U is the excitation energy of the nucleus, the level density parameter **a** is taken as A/K, with A being the mass number of the composite nucleus and

K is an adjustable parameter. The level density in the constant temperature form [16] is given as:

$$\rho(U) \propto \frac{1}{T} \varepsilon^{U/T} \qquad \ldots\ldots 4.1.2$$

The differential cross-section $\left(\frac{d\sigma}{d\varepsilon}\right)_v$ for emitting a particle with channel energy ε may be written as (cross-section per unit energy to emit a particle of type v).

$$\left(\frac{d\sigma}{d\varepsilon}\right)_v = \pi \lambda\!\!\!^{-2} \sum_{I=0}^{\infty} (2I+1) T_I \, (2S_v+1) \sum_{l=0}^{\infty} T_v^l(\varepsilon) \sum_{j=|I-l|}^{I+l} \rho(E,J)/D \qquad \ldots\ldots 4.1.3$$

where $\lambda\!\!\!^{-}$ is the reduced de-Broglie wavelength of the incident ion, T_I is the transmission coefficients for the I^{th} partial wave of the incident ion, $\rho(E,J)$ is spin dependent level density for the residual nucleus, D is the integral of numerator over all particles and emission energies, ε the excitation energy of the compound nucleus. S_v is the intrinsic spin of particle v, $T_v^l(\varepsilon)$ is the transmission coefficients for the particle v with K.E. ε and orbital angular momentum l.

In the Weisskopf–Ewing calculations, the nuclear moment of inertia is infinite and hence there is no energy tied to rotation, thus no level density cut off at high spin. This code does not take into account the angular momentum involved in HI reactions. The HI projectile imparts large angular momentum to the composite system having a finite moment of inertia and hence greater rotational energy. Due to nuclear rotation a nucleus with a given angular momentum J, cannot have energy below a minimum value E_j^{min}.

$$E_j^{min} \approx J(J+1)\frac{\hbar^2}{2I} \qquad \ldots\ldots 4.1.4$$

where, I being the moment of inertia of the composite nucleus.

If in the last stages of nuclear de-excitation higher angular momentum of the nucleus inhibits particle emission more than it does γ-ray emission, then, the peak of the excitation functions corresponding to particle emission mode will be shifted to higher energy [17]. A similar shift may also be produced if the mean energy of the evaporated particles increases with increasing nuclear spin. One way of obtaining an estimate of the

particles increases with increasing nuclear spin. One way of obtaining an estimate of the overall energy shift is from the nuclear rotational energy. For a rigid body, the rotational energy E_{rot} [17] is given by,

$$E_{rot} = \left(\frac{m}{M}\right) E_{Lab} \qquad \ldots\ldots\ldots 4.1.5$$

where $\frac{m}{M}$ denotes the ratio of the projectile and target masses and E_{lab} is the incident energy. To account for the large angular momentum imparted to the composite system it is desirable to shift the calculated excitation function by the amount approximately equal to E_{rot}. The pictorial representation for sequence of flow of code ALICE-91 is shown in Fig 3.1.

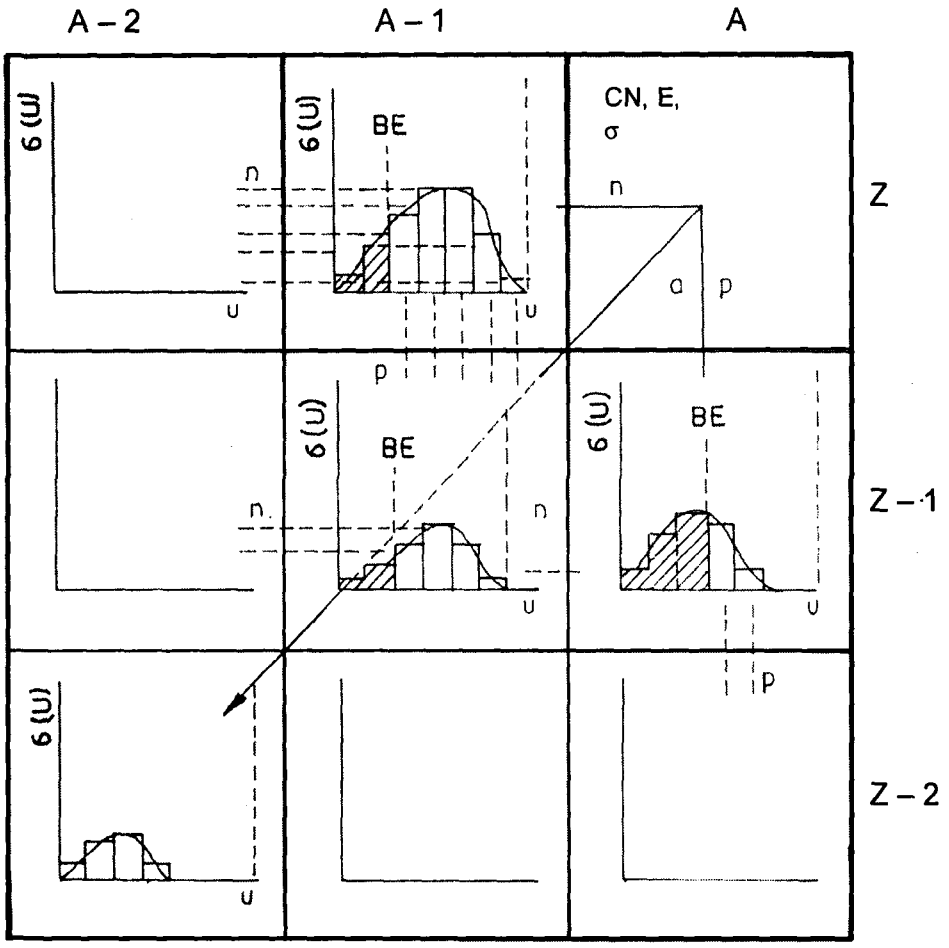

Fig. 3.1. Logic flow of the ALICE-91 code.

4.2 Basic features of the code PACE2

The statistical model code PACE 2 [6] (Projection Angular-momentum Coupled Evaporation, version 2) was derived from a predecessor, code JULIAN [18]. It uses a Monte Carlo procedure to determine the decay sequence of an excited nucleus, using the Hauser- Feshbach formalism. The code PACE 2 [6] is used to calculate the reaction cross-section of highly excited compound nucleus having higher angular momentum. In this code the most of required input parameters have been used as default except the charge and mass of the projectile and target nucleus. Since angular momentum conservation is explicitly taken into account at each step, the calculated excitation functions need not be shifted for rotational energy correction as we have done in case of ALICE-91.

The partial cross-section for compound nucleus formation at angular momentum L and specific bombarding energy is given by

$$\sigma_L = \pi\lambda\!\!\!^{-2}(2L+1)T_L \qquad \ldots\ldots 4.2.1$$

where $\lambda\!\!\!^{-}$ is the reduced wavelength with

$$T_L = [1+\exp(L-L_{max})/\delta]^{-1} \qquad \ldots\ldots 4.2.2$$

where, δ is the diffuseness parameter. L_{max} is determined by total fusion cross- section σ_F given as

$$\sigma_F = \sum_{L=0}^{\infty} \sigma_L \qquad \ldots\ldots 4.2.3$$

The transmission coefficients for the evaporation of light particles (n, p, α) during the first step of de-excitation are obtained by optical model potentials. A special feature of this code is its ability to provide angular distributions of evaporated particles and residues, obtained by tracking the distribution of the angular momentum projection through each cascade. This code contains a summary routine STATIS, which the user can adapt to provide any specific output desired. It may be pointed out that this code carries out only the statistical equilibrium model calculations and does not take PE emission into consideration. The PACE 2 code has been used by many research groups and for many different reactions over the past several years [19-23].

References

[1] H.A. Bethe, Phys. Rev. **50**, 332(1936).

[2] V.F. Weisskopf and D.H. Ewing, Phys Rev. **57**, 472 (1940).

[3] W. Hauser and H. Feshbach, Phys. Rev. **87**, 366(1952).

[4] Avinash Agarwal, Ph.D. Thesis, AMU, Aligarh, India (2003).

[5] M. Blann., ALICE 91, LLNL / IAEA/ NEA Data Bank, France (1991).

[6] A. Gavron, Phys. Rev. **C 21,** 230(1980).

[7] M. Blann, Phys. Rev. Lett. **27,** 337(1971).

[8] M. Blann, Phys. Rev. Lett. **28**, 757(1972).

[9] W. D. Myers and W.J.Swiatecki, Ark.Phys, **36,** 343(1967).

[10] M. Blann, Phys. Rev. **C 21,** 1770 (1980).

[11] T.D. Thomas, Nucl. Phys. **53,** 577 (1964).

[12] F.D. Bacchetti and G.W. Greenles, Phys. Rev. **182,** 1140 (1969).

[13] K. Kikuchi and M. Kawai, Nucl. matter and Nucl. reactions, North Holland Pub. Co. (1968).

[14] M. Blann, Nucl. Phys. **A 213,** 570 (1973).

[15] M. Blann and H. Vonach, Phys. Rev. **C 28,** 1475(1983).

[16] M.Blann, G.Refoo and F.Fabbri, Nucl. Inst. Methods, **A265,** 490(1988).

[17] D. Bodansky, Annu. Rev. Nucl. Sci., **12**, 79 (1962).

[18] M. Hillman and Y.Eyal, Unpublished.

[19] B.S. Tomer et al., Phys. Rev. **C49**, 940(1994).

[20] S. Chakarbarty et al., Nucl. Phys. **A 678,** 355 (2000).

[21] M.K. Sharma et al., Phys. Rev. **C 70**, 044606 (2004).

[22] D. Singh et al., J. Phys. Soc. Jpn.**75**, 104201(2006).

[23] Pushpendra P. Singh et al., Phys. Rev. **C 77**, 014607 (2008).

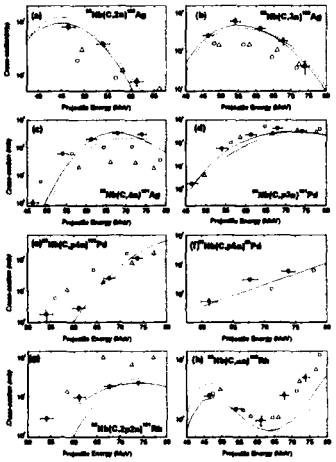

Chapter - V

RESULTS AND DISCUSSION

In order to test the validity of the various nuclear reaction theories and models, an extensive measurement of the excitation functions (EFs) is needed. With this view a total of thirty excitation functions have been measured for the targets ^{93}Nb, ^{52}Cr and ^{115}In. The analysis of EFs has been performed using the computer code PACE 2[1] developed by Gavron for heavy-ion reaction at intermediate energies. To the best of our knowledge, the measurement and analysis of the EFs for ^{52}Cr and ^{115}In are being reported for the first time. However, the EFs for ^{93}Nb were measured by the two groups [2, 3], differ to a large extent; hence precise and accurate measurements are still required. We have also compared our new measurements to show the contrast between our data and available literature values [2, 3] for ^{93}Nb target with the latest version ALICE-91 [4]. Whereas Misaelides [2] had compared the data with the theoretical predictions made by a modified version [5] of the code ALICE [6]. In order to separate the relative contributions of the complete and the incomplete fusion in ^{12}C+^{93}Nb system, measurements of RRDs of various residues at energy ≈ 80 MeV have been made. We will discuss the results of each projectile–target system separately in the later sections.

5.1 Excitation functions for ^{12}C+ ^{93}Nb System

To understand fusion mechanism in the ^{12}C+ ^{93}Nb system , EFs for sixteen reactions viz., ^{93} Nb (C, 2n) ^{103}Ag, ^{93} Nb (C, 3n) ^{102}Ag, ^{93}Nb(C, 4n) ^{101}Ag, ^{93} Nb (C, p3n)^{101}Pd, ^{93} Nb (C, p4n)^{100}Pd, ^{93}Nb (C, p5n)^{99}Pd, ^{93}Nb (C, 2p2n)^{101}Rh , ^{93} Nb (C,αn) ^{100}Rh , ^{93} Nb (C, α2n) ^{99}Rh , ^{93} Nb (C, αp3n) ^{97}Ru, ^{93}Nb (C, αp5n) ^{95}Ru, ^{93}Nb(C,2αn)^{96}Tc, ^{93}Nb(C,2α2n)^{95}Tc,^{93}Nb(C,2α3n)^{94}Tc, ^{93}Nb(C,2αp3n)^{94}Mo^{m} , and ^{93}Nb(^{12}C,^{13}C)^{92}Nb^{m} have been measured at five projectile energies from near Coulomb barrier to well above it. The present measured values have been shown in Figs 5.1.1.1-5.1.1.2 with dark circles. The vertical bars show errors in the measured cross-section values whereas the horizontal bars indicate the spread in the beam energy. The experimental data points of Misaelides [2] and Tomer et al., [3] are represented by open upward triangles and open circles respectively. The theoretical predictions based on ALICE-91[6] and PACE-2 [1] codes have been shown by solid, dash and dot curves for level density parameter constant values 8, 12 and 16, respectively.

5.1.1 Analysis of the experimental results with code ALICE-91

The code ALICE –91 developed by M. Blann [6] accounts for the equilibrium and pre- equilibrium (PE) emission in both the light and heavy ion reactions. It is based on the Weisskopf-Ewing model [7] for the compound nucleus reaction, while the pre-equilibrium emission is stimulated within the framework of Hybrid/geometry dependent hybrid model [8, 9]. In this code the level density parameter *a*, the mean free path multiplier *COST* and initial exciton number n_o are some important input parameters. The level density parameter affects the equilibrium as well as pre-equilibrium component, while the initial exciton number n_o and the mean free path multiplier COST govern the pre-equilibrium component. The level density parameter '*a*' is calculated from the expression $a = A/K$, where K may be varied. The different values of K (8, 12, & 16) and *COST* (3, 6, & 9) were taken into the analysis of the EFs. The effect of variation in parameter K on the calculated EFs is shown in Figs 5.1.1.1(a-j) and 5.1.1.2 (a-f). It is noticed from the figures that the value of K = 16, in general, satisfactorily reproduces the experimental data for all the reactions. The calculated excitations functions are found to be insensitive to the parameter *COST* as is shown in the Fig.5.1.1.2 (g), for the reaction ^{93}Nb (C, 2n).

Moreover, it may be pointed out that the calculated values of excitation functions are shifted towards the lower energy region as compared to the experimentally measured values as shown in Fig. 5.1.1.3(a,b).This is consequence of heavy ions imparting a large angular momentum to the composite nuclear system. The compound systems excited to the same excitation energy formed with incident particles of different masses have appreciably different angular momenta. This, in principle, leads to differences in the excitation functions. As in the last stages of the nuclear de-excitation, the high angular momentum imparted by HI inhibits particle emission more than gamma ray; hence the peak of the excitation functions, corresponding to the particle emission mode, is shifted to the higher energy side [10]. Such a shift could also be produced if the mean energy of the evaporated particles increases with the increasing nuclear spin. The overall estimate of the possible energy shift has been calculated from the E_{rot}, the nuclear rotational energy. In the present work at incident energies 46.4, 54.0, 61.2, 67.8 &73.9 MeV, value of E_{rot} [using equation (4.1.5)] is found to vary from 6.2 to 9.6 MeV. Since the angular momentum effects were

not considered in the Weisskopf – Ewing calculations of the ALICE –91, it is desirable to shift the calculated excitation functions by the amount ≈ E_{rot}. The theoretically calculated EFs after shifting the energy scale by E_{rot}, are found to have a good agreement with the experimental data, noticed from Fig.5.1.1.1(a-g) for ^{93}Nb (C,2n)^{103}Ag, ^{93}Nb (C,3n)^{102}Ag, ^{93}Nb(C,4n)^{101}Ag, ^{93}Nb (C, p3n)^{101}Pd^{93,} Nb (C, p4n)^{100}Pd, ^{93} Nb (C, p5n)^{99}Pd and $^{9\,3}$Nb(C, 2p2n)^{101}Rh. In case of ^{93}Nb(C,αn)^{100}Rh, ^{93}Nb(C,α2n)^{99}Rh, ^{93}Nb(C,αp3n)^{97}Ru, ^{93}Nb(C, αp5n)^{95}Ru, ^{93}Nb(C,2αn)^{96}Tc,^{93}Nb(C,2α2n)^{95}Tc and ^{93}Nb(C,2α3n)^{94}Tc channels, as shown in Figs. 5.1.1.1(h-j) and 5.1.1.2 (a-d), the measured cross-sections were found much higher than those calculated by ALICE-91. The reason may be , these channels are populated not only via the CF of ^{12}C but also through ICF , which are formed due to the fusion of ^{8}Be or α of ^{12}C with ^{93}Nb. As far as ^{93}Nb(C, 2αp3n) ^{93}Mo^{m} and ^{93}Nb (^{12}C, ^{13}C) ^{92}Nb^{m} channels are concerned, the substantial enhancement in the observed cross-sections over their theoretical values has been shown in Figs. 5.1.1.2(e,f). These reactions may be populated via direct reactions and/or incomplete fusion.

5.1.2 Comparison with the previous experimental information

Misaelides [2] compared observations with the theoretical predictions made by a modified version [5] of the statistical model code ALICE [6], using level density parameter of $a = A/15$, whereas Tomer et al. [3] simulated values of cross-section by applying the level density parameter as A/8 $(MeV)^{-1}$ with CASCADE [11]. In our analysis three values of the level density parameter constant viz. 8, 12 &16 have been used. Regarding (^{12}C, xn) reactions(x = 2, 3, 4,) shown in Figs.5.1.1.1(a-c) Misaelides [2] pointed out that the computer code ALICE underestimated the high energy side of the excitation functions in the cases of ^{103}Ag and ^{102}Ag whereas it overestimated the ^{101}Ag cross-section. However, Tomer et al. [3] illustrated that the EFs for the same reactions were well- reproduced by the CASCADE code. But our new measurements are consistent with the level density parameter constant (K = 16) and, therefore, the agreement between the theoretical values predicted by ALICE-91 and the experimental ones is firmly established. With reference to (^{12}C, pxn) reactions (x = 3, 4, 5) Misaelides [2] reported that the good agreement of the experimental and calculated excitation functions indicated that (^{12}C, pxn) reactions proceeded mainly via the compound nucleus formation. Tomer et al. [3] also showed that

pxn products were well-reproduced by the CASCADE code. As may be seen from Fig.5.1.1.1 (d-f), our data agrees with PLD = 16 of ALICE-91. Thus, our findings do not contradict with the conclusions drawn by Misaelides and Tomer et al.

Misaelides [2] had shown a remarkably good agreement between experimental and calculated cross-sections for ^{93}Nb (^{12}C, αp3n) ^{97}Ru reaction in Fig.5.1.1.2 (a), which may be taken as confirmation, that particle evaporation is the dominant mode of the formation of ^{97}Ru in the energy region of interest. This reaction has not been reported by Tomer et al.,[3]. However, our measurements reveal a good agreement between theoretical and experimental values, if E_{rot} shift is not incorporated. But once it is accounted, it results in an enhancement of experimental values in comparison to the theoretical predictions as shown in Figs. 5.1.1.2(a'). This enhancement leads to ICF. However, the application of the E_{rot} is desirable for the reasons discussed above. There is a contradiction between our results and the findings of Misaelides [2] because in our study E_{rot} has been applied. In case of (^{12}C, αp5n) ^{95}Ru, Misaelides [2] stated that the measured cross-sections were obtained in the higher energy region, i.e. above 90 MeV. Tomer et al [3] did not measure this reaction, whereas in our experiment, the values of the cross-section have been found below the incident energy 90 MeV. In fact, there is an enhancement in the cross-section values which is not in agreement either with the theoretical values or with the ones reported by Misaelides (Fig.5.1.1.1j). The enhancement suggests a different mode of reaction from particle evaporation, i.e. ICF.

As far as (^{12}C, αxn) & (^{12}C, 2αxn) channels are concerned, Tomer et al. observed that in the case of αxn channels, ^{100}Rh and ^{99}Rh show higher cross-sections than the CASCADE predictions and for 2αxn channels, ^{96}Tc and ^{95}Tc show higher cross-sections than the calculated values ,while ^{94}Tc data agree with the calculations. Tomer et al. explained these observations in terms of the breakup of the projectile into α and ^{8}Be followed by the fusion of either of the fragments with the target as it is evident from the higher cross-sections for ^{99,100}Rh & ^{95,96}Tc isotopes. Misaelides [2] had termed the above-mentioned channels as transfer reactions. From Figs 5.1.1.2(b, c), it may be seen that for (^{12}C, 2α2n) and (^{12}C, 2α3n) channels , without E_{rot} correction , experimental values of

earlier workers [2] are in good agreement with PLD =16. After applying the E_{rot}, there is an enhancement in EFs which leads to the ICF. In case of $^{93}Nb(^{12}C, \alpha n)^{100}Rh$, as can be seen from Fig.5.1.1.1(h) the agreement between ALICE-91 and experimental values of cross-section exists below 65 MeV and a significant enhancement is found above this energy. This simply means that ^{100}Rh is populated not only via the CF of ^{12}C with ^{93}Nb, followed by the evaporation of an α-particle and one neutron from the excited composite system ^{105}Ag, but may also be formed via ICF .This incomplete fusion can be explained by assuming the breakup of the ^{12}C-nucleus into its fragments viz., ^{8}Be and ^{4}He (α-particle) in the nuclear force field of target nucleus and subsequently one of the fragments ^{8}Be fuses with ^{93}Nb, forming an incompletely fused composite system ^{101}Rh and the unused fragment α-particle moves forward as a spectator.

$$^{12}C\ (^{8}Be + ^{4}He) \rightarrow {}^{8}Be + {}^{93}Nb \rightarrow {}^{101}Rh^{*} \rightarrow {}^{100}Rh + \alpha$$

(α as a spectator)

Thus, the measured activity of ^{100}Rh has contributions from both the CF as well as the ICF channels.

In case of (C, α2n) ^{99}Rh reaction reported values of Misaelides[2] and Tomer et al.[3] are in agreement with the theoretical predictions by ALICE-91, as shown in Fig.5.1.1.1(i), but our experimental values were found to be substantially larger than the ALICE-91 values. Again the cause of this discrepancy may be attributed to the ICF. For (^{12}C, 2α p3n) and (^{12}C, ^{13}C) reactions, Misaelides [2] explained that the production of residues $^{93}Mo^{m}$ and $^{92}Nb^{m}$ is due to reactions with a direct character. An exchange of a neutron with a proton could be the production mechanism of $^{93}Mo^{m}$, whereas, a neutron pick-up would lead to the production of $^{92}Nb^{m}$. The trend in our data shown in Figs. 5.1.1.2(e &f) is also matching with that of Misaelides. Hence, it can be inferred that the two residues populated by direct reactions are not being taken into account by the computer code used.

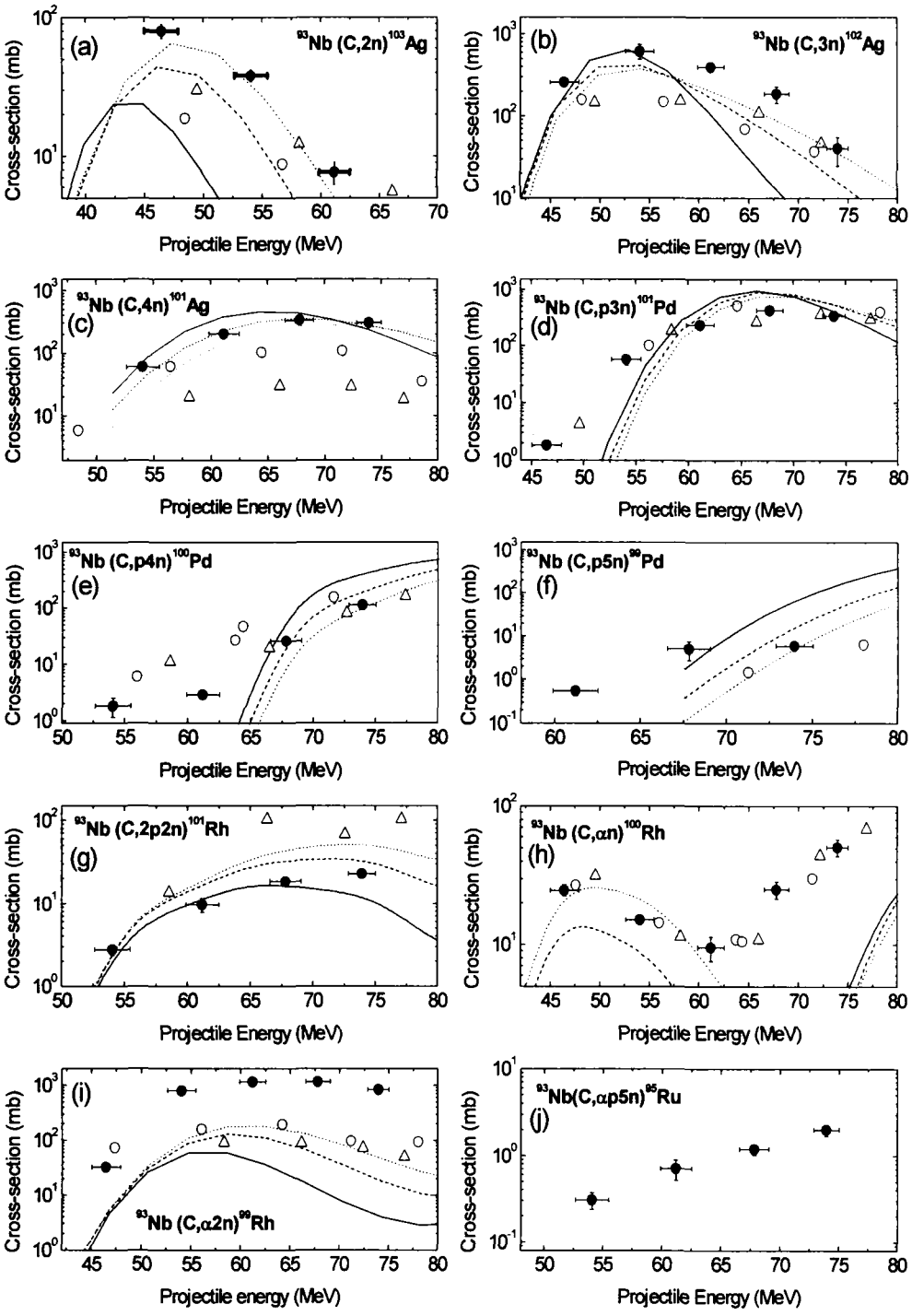

Fig.5.1.1.1 (a-j) Experimentally measured and theoretically calculated EFs using ALICE-91. The dark circles indicate the experimental data points and the solid; dash &dot curves represent the polynomial fit to the ALICE-91 predictions at different level density parameters (8, 12&16). Literature values [2, 3] are also shown by open upward triangles and open circles respectively.

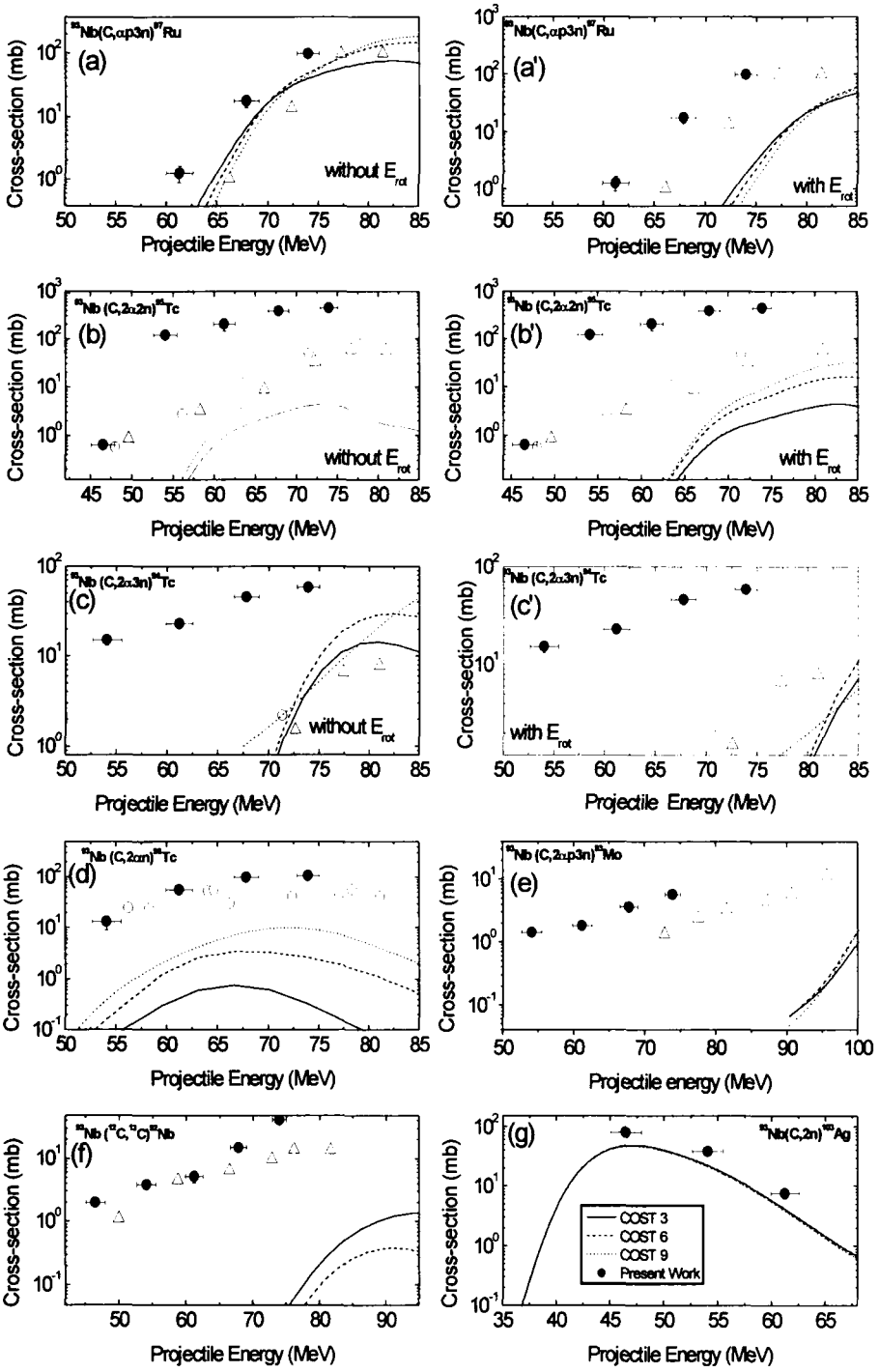

Fig.5.1.1.2 (a-g) Experimentally measured and theoretically calculated EFs using ALICE-91. The dark circles indicate the experimental data points and the solid; dash &dot curves represent the polynomial fit to the ALICE-91 predictions at different level density parameters (8, 12&16). Literature values [2, 3] are also shown by open upward triangles and open circles respectively.

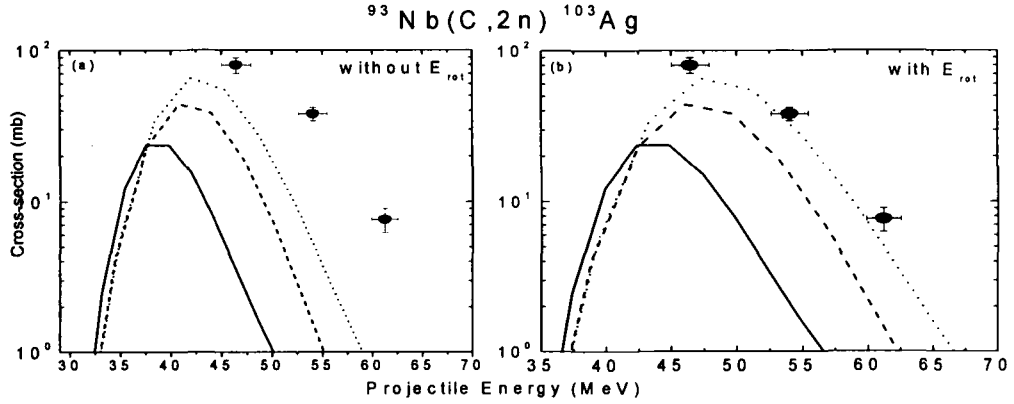

Fig.5.1.1.3 (a-b) Experimentally measured and theoretically calculated EFs using ALICE-91 with and without applying rotational energy shift.

5.1.3 Analysis of the experimental results with code PACE 2

The present measured excitation functions have also been compared with the values calculated using statistical model code PACE2 [1] based on the Hauser- Feshbach formalism. The code uses the Monte Carlo procedure to determine the decay sequence of an excited nucleus and calculates the reaction cross- section of highly excited compound nucleus in the higher angular momentum state. The most of the required input parameters in the code have been used as default except the charge and mass of the projectile and target nucleus. Since angular momentum conservation is explicitly taken into account at each step, the calculated excitation functions need not to be corrected for rotational energy E_{rot}, as done in case of ALICE-91 [6]. In this code the level density , one of the important parameters, has been varied to obtain an agreement with the experimental data .The effect of variation in level density parameter constant designated as PLD (8,12 &16) on calculated EFs for the reaction channels ^{93} Nb (C, 2n) ^{103}Ag, ^{93} Nb (C, 3n) ^{102}Ag, ^{93}Nb(C, 4n) ^{101}Ag, ^{93} Nb (C, p3n)^{101}Pd, ^{93} Nb (C, p4n)^{100}Pd, ^{93} Nb (C, p5n)^{99}Pd, ^{93} Nb (C, 2p2n)^{101}Rh , ^{93} Nb (C, αn)^{100}Rh , ^{93} Nb (C, α2n) ^{99}Rh , , ^{93} Nb (C, αp3n) ^{97}Ru, ^{93} Nb (C, αp5n) ^{95}Ru, ^{93} Nb (C, 2αn) ^{96}Tc, ^{93} Nb (C, 2α2n)^{95}Tc , ^{93}Nb(C,2α3n)^{94}Tc, ^{93}Nb(C,2αp3n)^{94}Mo^{m}, ^{93}Nb(^{12}C,^{13}C)^{92}Nb^{m} is shown in Figs 5.1.3.1 & 5.1.3.2. We notice from the Figs. 5.1.3.1(a-d), that a value of PLD =8, satisfactorily reproduces the measured EFs.

For ^{93}Nb (C, 2n) ^{103}Ag reaction, the evaporation residue ^{103}Ag is expected to be formed via complete fusion of ^{12}C with ^{93}Nb followed by the evaporation of two neutrons from the excited composite system ^{105}Ag. The EFs for the reaction is given in Fig. 5.1.3.1(a). The figure shows that EFs for the product ^{103}Ag are in good agreement with the theoretical predictions, which is a veritable signature of CF. However, measurements of Misaelides [2] and Tomer et al. [3]are slightly suppresed with the theoretical values corresponding to PLD=8 and the present work .With regard to ^{93}Nb (C, 3n) ^{102}Ag, from the Fig. 5.1.3.1(b), it is seen that EFs for the product ^{102}Ag are well reproduced with the theoretical predictions, which leads to CF, as expected. Nevertheless, earlier values [2, 3] are somewhat less than our measurements and theoretical predictions. The variation of cross-sections with energy for this channel ^{93}Nb (C, 4n) ^{101}Ag as shown in Fig. 5.1.3.1(c), shows that PACE-2 calculations remarkably reproduce the measured cross-section with the same trend. This excellent agreement between measured and theoretical values indicates that the CF plays a role in the population of ^{101}Ag. In lower energy region, reported values by Tomer et al. [3] almost agree with PLD = 8, but in higher energy region (above 55 MeV) values by Misaelides[2] and Tomer et al.[3] are smaller but the trend is almost same.

In case of ^{93}Nb (C, p3n) ^{101}Pd, the possibility of formation of evaporation residue ^{101}Pd may be via complete fusion of ^{12}C with ^{93}Nb followed by the evaporation of a proton and three neutrons from the excited composite system ^{105}Ag. The residual nucleus ^{101}Pd may also be populated by the β^+ decay of its higher charge isobar precursor ^{101}Ag formed via reaction ^{93}Nb (C, 4n). Thus, the measured activity of ^{101}Pd has contribution from both the independent production and from precursor decay. But our calculations demonstrate the absence of precursor contribution .The measured EFs for this reaction is shown in Fig. 5.1.3.1(d). The cross-section increases with the increase in energy and attains a maximum, followed by falls off with the further increase in the energy as the other channels open up. Another feature of this plot is good agreement with the earlier measured values [2, 3]. As far as ^{93}Nb (C, p4n) ^{100}Pd and ^{93}Nb (C, p5n) ^{99}Pd reactions are concerned, our new measurements are consistent with theoretical predictions for PLD equal to 8. But other values [2, 3] are not in good agreement either with PACE-2 calculations or measured values by us. From the Figs. 5.1.3.1(a-f), it can be seen that x n (x = 2, 3&4) and p x n (x = 3, 4 & 5) products are

formed via de-excitation of the compound nucleus formed in CF.

In ^{93}Nb (C, 2p2n) ^{101}Rh reaction, the evaporation residue ^{101}Rh may be formed by the complete fusion followed by the evaporation of 2 proton and 2 neutrons from excited composite system ^{105}Ag. This residual nucleus ^{101}Rh may also be populated via ICF of ^{8}Be fragment and unused fragment α-particle moving forward as a spectator. Thus, the measured activity of ^{101}Rh may be significant to both the CF and ICF channels. The EFs for this reaction are shown in Fig. 5.1.3.1(g) which indicates good agreement with PACE 2 calculations and the experimental data, thereby indicating a contribution of only CF. But Misaelides' values [2] match at ≈58 MeV and go higher above it. This data [2] may have contribution from ICF. The EFs for the reaction^{93}Nb (C, αn) ^{100}Rh is shown in Fig. 5.1.3.1(h). An agreement between PACE-2 predictions and experimental values exist below 65 MeV and above this energy, significant enhancement of cross-section is found. This simply indicates that the ^{100}Rh is populated via CF and ICF of ^{8}Be fragment. Earlier measurements [2, 3] fairly agree with the present ones and theoretical values. However, no such interpretations were given in earlier analyses [2, 3]. From the figure 5.1.3.2 (a), we notice the enhancement of cross-section in^{93}Nb (C, α2n) ^{99}Rh compared to that found from PACE-2 values. This means that in addition to CF, ICF is also playing a role in population of ^{99}Rh radionuclide. But other observed values [2, 3] match with theoretical predictions. Misaelides [2] and Tomer et al. [3] predicted CF for this channel while our analysis confirms the presence of ICF component in production mechanism. This may be due to the fact that they might have not considered both ground and meta state contributions. Regarding ^{93}Nb (C, αp3n) ^{97}Ru reaction, from Fig. 5.1.3.2(b), it is seen that our measured cross-sections are higher than the theoretical predictions done by PACE-2. We are not getting any data for cross-section up to 65 MeV from PACE-2; on the contrary we have measured it experimentally. This can be explained by the ICF of ^{8}Be fragment with ^{93}Nb followed by the emission of proton and three neutrons from the excited composite system ^{101}Rh and unused fragment α-particle which moves forward as a spectator. The trend of data reported by Misaelides[2] also nicely matches with the present work. For ^{93}Nb (C, αp5n) ^{95}Ru reaction, we report experimental values in energy region, as shown in Fig.5.1.3.2(c). Misaelides [2] obtained cross-section values for this reaction in the higher energy region

and argued that the residues ^{97}Ru and ^{95}Ru are populated via CF by comparing the results with ALICE [5] code. But once the comparison of the results reported by Misaelides[2] with code PACE 2 is made, significant enhancement is observed in higher energy region [as shown in Fig.5.1.3.2 (b,c)].This enhancement over the theoretical values may be explained in terms of ICF process. Hence, the conclusion drawn in the previous subsection 5.1.2 is further verified.

As far as ^{93}Nb (C, 2αn) ^{96}Tc, ^{93}Nb (C, 2α2n) ^{95}Tc and ^{93}Nb (C, 2α3n)^{94}Tc reactions are concerned, our measured cross-sections are substantially higher [shown in Fig.5.1.3.2 (d-f)] than the ones calculated using PACE 2 and other values available in the literature [2,3]. This simply indicates that these radio- nuclides are populated via ICF. The observations made above indicate that ICF occur even at energy as low as 6 MeV/nucleon. In case of ^{93}Nb (C, 2αp3n) ^{93}Mo^{m} reaction, residue ^{93}Mo^{m} may be populated via different routes, mainly CF, ICF /PE and direct reactions. Theoretical values of PACE-2 are negligible in this energy region, thus not shown in the Fig 5.1.3.2(g). The trend of data reported by Misaelides [2] and our measurements agrees well but values differ approximately by an order of magnitude. This discrepancy between our measurement and Misaelides reported values may be due to the residue being populated in addition to direct reaction. However, PE is not observable when measured values are compared with ALICE-91 code. Consequently, this residue may be populated via ICF and direct reactions. Regarding ^{93}Nb (^{12}C, ^{13}C) ^{92}Nb^{m} reaction, ^{92}Nb^{m} may be populated via neutron pick up channel. The data trend of Misaelides and our measurements matches fairly but experimental values found to be substantially larger than those of model code PACE-2 [as shown in Fig.5.1.3.2 (h)]. This difference in cross-section values cannot be the uncertainty in measurement and thus may be attributed to direct reaction. Hence, the arguments presented by Misaelides for these residues ^{93}Mo^{m}, ^{92}Nb^{m} are supported by our new measurements. In the light of the above results and discussion, it may be stated that our new measurements, somewhere, serve as supplement/complement and sometimes better than or at least as good as the previous literature values [2, 3].

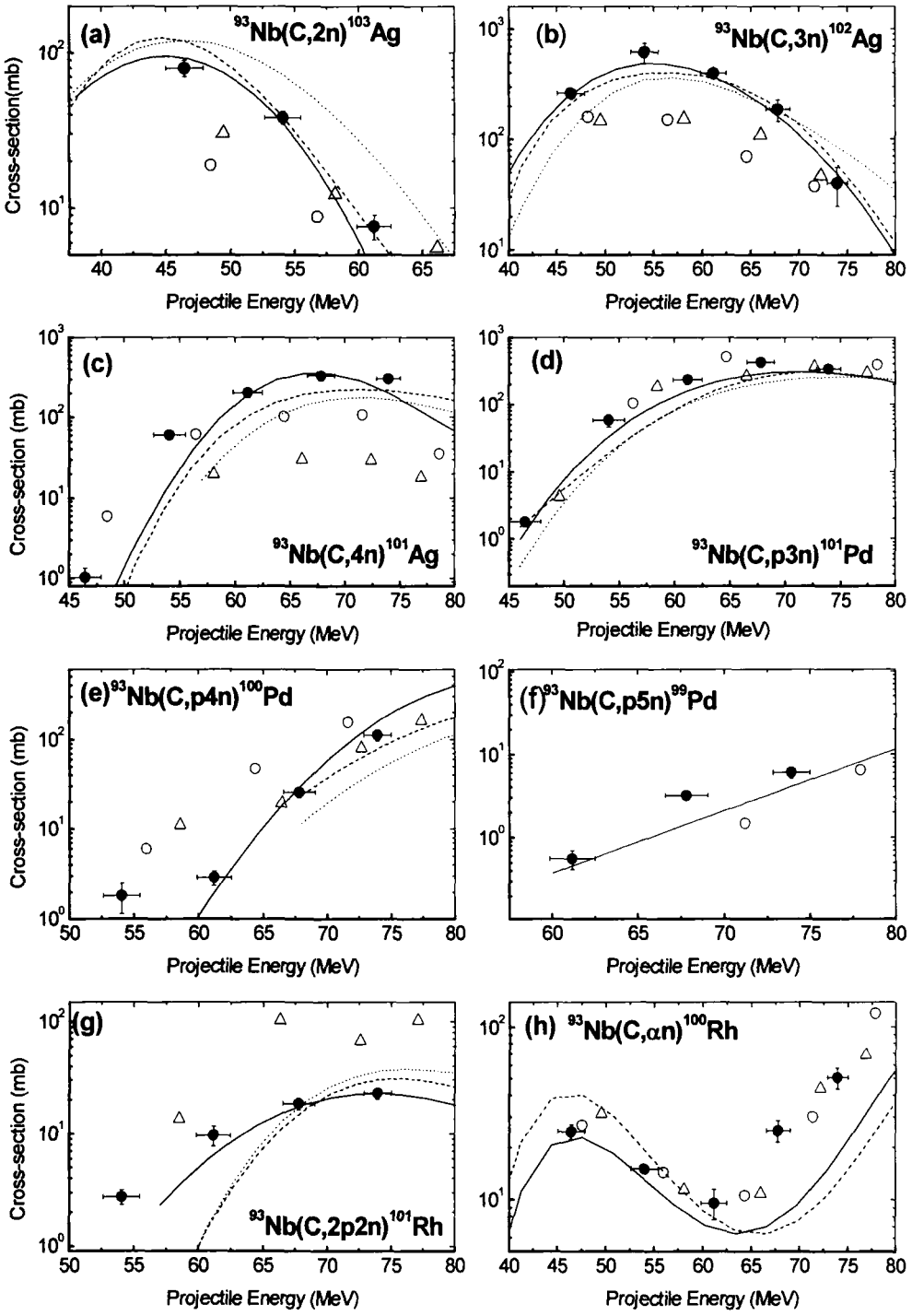

Fig.5.1.3.1 (a-h) Experimentally measured and theoretically calculated EFs using PACE-2. The dark circles indicate the experimental data points and the solid; dash &dot curves represent the polynomial fit to the PACE-2 predictions at different level density parameters (8, 12&16). Literature values [2, 3] are also shown by open upward triangles and open circles respectively.

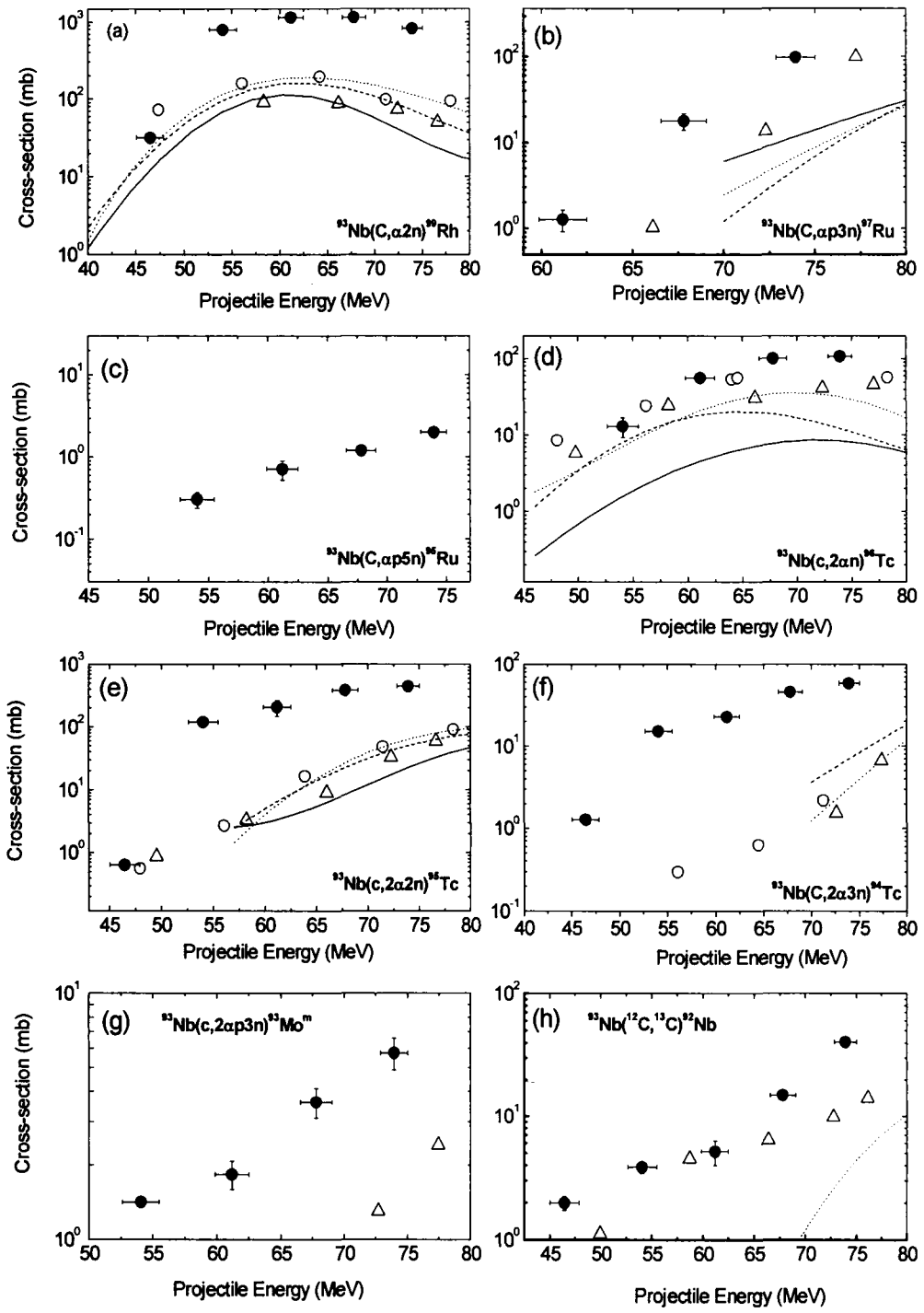

Fig.5.1.3.2 (a-h) Experimentally measured and theoretically calculated EFs using PACE-2. The dark circles indicate the experimental data points and the solid; dash &dot curves represent the polynomial fit to the PACE-2 predictions at different level density parameters (8, 12&16). Literature values [2, 3] are also shown by open upward triangles and open circles respectively.

5.2 Excitation functions for $^{12}C+ ^{52}Cr$ System

In the present work, the excitation functions (EFs) for carbon-induced reactions on chromium have been experimentally measured in the energy range from 52.2 to 80.0 MeV. The reactions studied at five projectile energies were $^{52}Cr(C,2n)^{62}Zn$, $^{52}Cr(C,p2n)^{61}Cu$,$^{52}Cr(C,p3n)^{60}Cu$,$^{52}Cr(C,\alpha 3n)^{57}Ni$,$^{52}Cr(C,\alpha 4n)^{56}Ni$,$^{52}Cr(C,\alpha p3n)^{56}Co$,$^{52}Cr(C,\alpha p4n)^{55}Co$, and $^{52}Cr(C,\alpha 3pn)^{56}Mn$. To the best of our knowledge, no earlier measurements for these reactions are available in the literature.

5.2.1 Analysis of experimental results with code PACE 2

In the code PACE 2, the level density parameter given by a = A/ K, where, A is the mass number of the compound nucleus and K is a free parameter, is one of the important parameters. The value of K(PLD) may be varied to match the experimental data. A value of PLD = 8 (default value), is found to satisfactorily reproduce the measured EFs, in general, in the previous case of $^{12}C+ ^{93}Nb$ system. Hence in the case of $^{12}C+^{52}Cr$ system, we have chosen K=8 only in our calculations of EFs using code PACE2.

Regarding ^{52}Cr (C, 2n) ^{62}Zn reaction [shown in Fig. 5.2.1(a)] the trend in our data nicely matches with the theoretically evaluated EFs. Hence the residue ^{62}Zn will be populated via CF channel as expected. With reference to (C, p2n) and (C, p3n) reaction channels, measured EFs are much higher than the one theoretically predicted, but the trend is almost the same. These channels may also be populated by β^+ emission and/or electron capture (EC) of higher charge precursor. The measured activity of these channels may also have the contribution from the precursor decay. The contribution due to the precursor decay could not be separated, due to the short half –lives of precursor isobars. Thus, the observed enhancement in the Fig.5.2.1 (b-c) shows the cumulative cross-sections of the residues ^{61}Cu and ^{60}Cu, respectively.

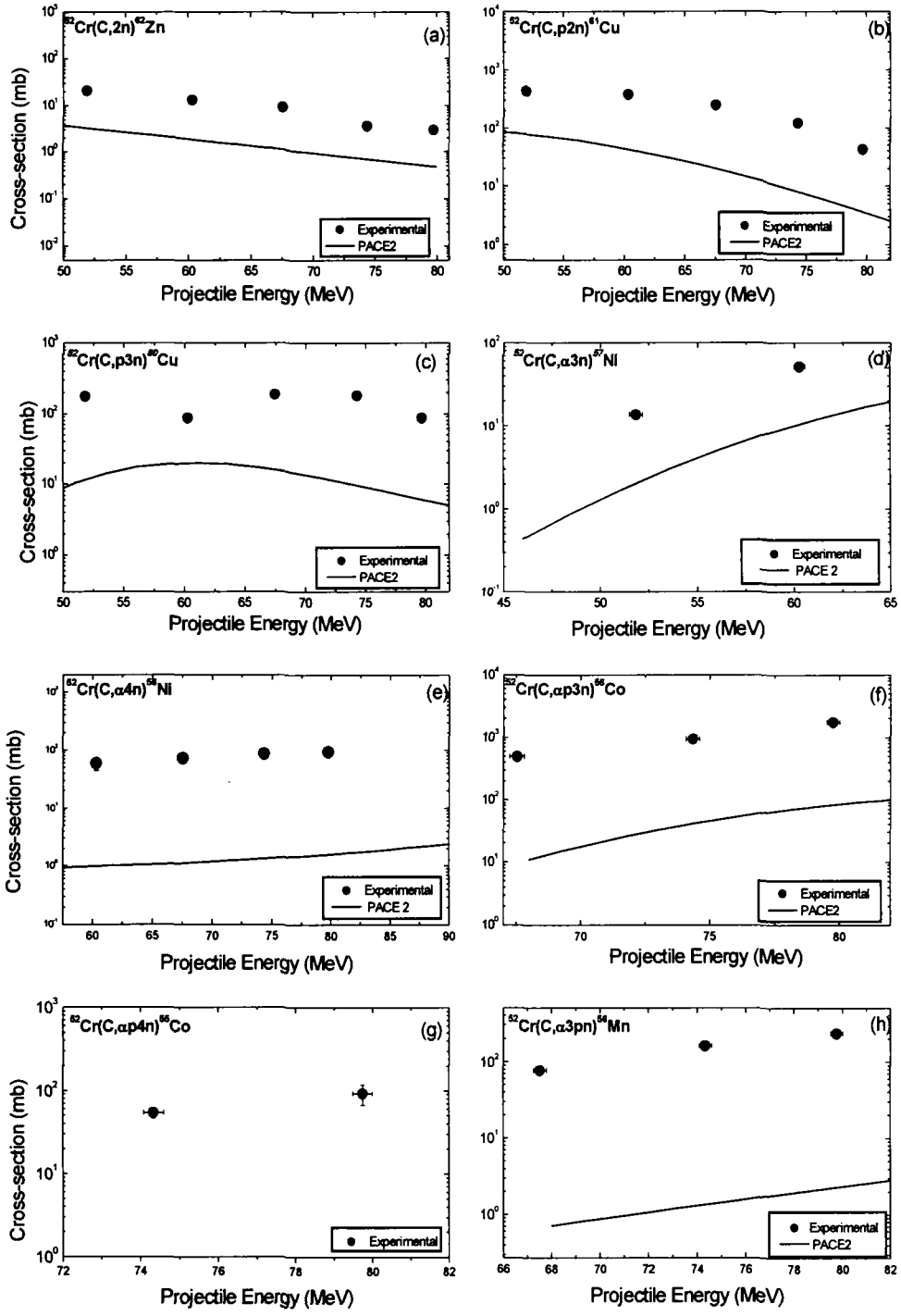

Fig. 5.2.1(a-h) Experimentally measured and theoretically calculated EFs using code PACE2 (PLD=8)

In case of the reactions $^{52}Cr(C,\alpha 3n)^{57}Ni$, $^{52}Cr(C,\alpha 4n)^{56}Ni$, $^{52}Cr(C,\alpha p3n)^{56}Co$, $^{52}Cr(C,\alpha p4n)^{55}Co$ and $^{52}Cr(C,\alpha 3pn)^{56}Mn$, the theoretical values from code PACE2 give substantially small cross-sections as shown in Figs. 5.2.1(d-h).The enhancement of the cross-section indicates that these channels are not populated by CF of ^{12}C followed by evaporation of neutron, proton and alpha particles but may be due to ICF reaction of ^{12}C with ^{52}Cr. Theoretical calculations for PACE2, however, do not take the incomplete fusion process into account. The discrepancy in the experimentally measured excitation functions and the calculated counter parts may be attributed to the above-mentioned ICF processes [12].

5.3 Excitation functions for $^{16}O+ ^{115}In$ System

The excitation functions measured for $^{115}In(O,p3n)^{127}Ba$, $^{115}In\ (O,p4n)^{126}Ba$, $^{115}In\ (O,\alpha)^{127}Cs$, $^{115}In\ (O, \alpha 2n)^{125}Cs$, $^{115}In\ (O, \alpha p3n)^{123}Xe$, and $^{115}In\ (O, \alpha p5n)^{121}Xe$ reactions are depicted in figures 5.3.1 with solid circles. To the best of our knowledge, no earlier measurements are available in the literature; therefore, we are the first to report these reactions.

5.3.1 Analysis of the experimental results with code PACE 2

We have chosen level density parameter constant (PLD=8, default value) in the evaluation of EFs using code PACE2 as in the case of $^{12}C+^{52}Cr$ system. It is evident from the Fig. 5.3.1(a-b) that the experimentally measured excitation functions for the reactions $^{115}In\ (^{16}O, p3n)\ ^{127}Ba$ and $^{115}In\ (^{16}O, p4n)^{126}Ba$ are much higher than the theoretical predictions based on PACE2, but the trend is almost the same. The residue $^{127\text{-}126}Ba$ may also be populated by β^+ emission and/or electron capture (EC) of higher charge precursor isobar $^{127\text{-}126}La$ populated via the neutron channel. The measured activity of these residues may also have the contribution from the precursor decay. The contribution due to the precursor decay could not be separated due to the short half- lives of the precursor isobars. Thus, the observed enhancement in the Fig. 5.3.1(a-b) shows the cumulative cross-sections of ^{127}Ba and ^{126}Ba residues.

In case of reactions $^{115}In(^{16}O, \alpha)$ and $^{115}In(^{16}O, \alpha 2n)$, the theoretical predictions of the code PACE2 have substantially small cross sections as compared to the measured ones shown in Figs. 5.3.1(c-d). This considerably higher discrepancy with the

experimentally measured cross sections compared to the theoretical calculations may be explained in terms of the contribution coming from the ICF of the ^{16}O ion. It may be assumed that ^{16}O ion breaks up into ^{12}C and ^{4}He fragments under the nuclear field of the target nucleus and only one of the fragments i.e., ^{12}C fuses (^{4}He moves along the beam direction) with the target nucleus forming the excited composite system $^{127}Cs^*$, leading to the formation of the residual nuclei ^{127}Cs and ^{125}Cs respectively. However, theoretical calculations from PACE 2, do not take this ICF process into account. Thus, the discrepancy between the experimentally measured excitation functions and the theoretically calculated counterparts may be attributed to the above-mentioned ICF processes.

As far as ^{115}In (^{16}O, $\alpha p3n$) ^{123}Xe reaction is concerned, the agreement between PACE 2 predictions and experimental values exist below 90 MeV and above this energy significant enhancement of cross-section is found. This simply indicates that this ^{123}Xe is populated by not only via CF of ^{16}O with ^{115}In but may also be formed via ICF of ^{12}C fragment followed by emission of one proton and three neutrons form the excited composite system.

For the $^{115}In(^{16}O, \alpha p5n)^{121}Xe$ reaction, theoretical prediction of PACE 2 gives negligible cross sections while the measured ones are substantial as shown in Fig. 5.3.1(f). This much higher discrepancy of experimentally measured cross sections as compared to the theoretical calculations may again be explained in terms of the contributions coming from the incomplete fusion of ^{16}O. The higher cross sections in case of ^{115}In (^{16}O, $\alpha p5n$) reaction may be explained assuming that ^{12}C (if ^{16}O breaks up into ^{12}C and ^{4}He fragments) fuses with the target nucleus and emits one proton and five neutrons. Since, theoretical calculations from PACE 2 do not take the ICF process into account, it may be inferred that a significant part of the reaction in these cases goes through the ICF [13].

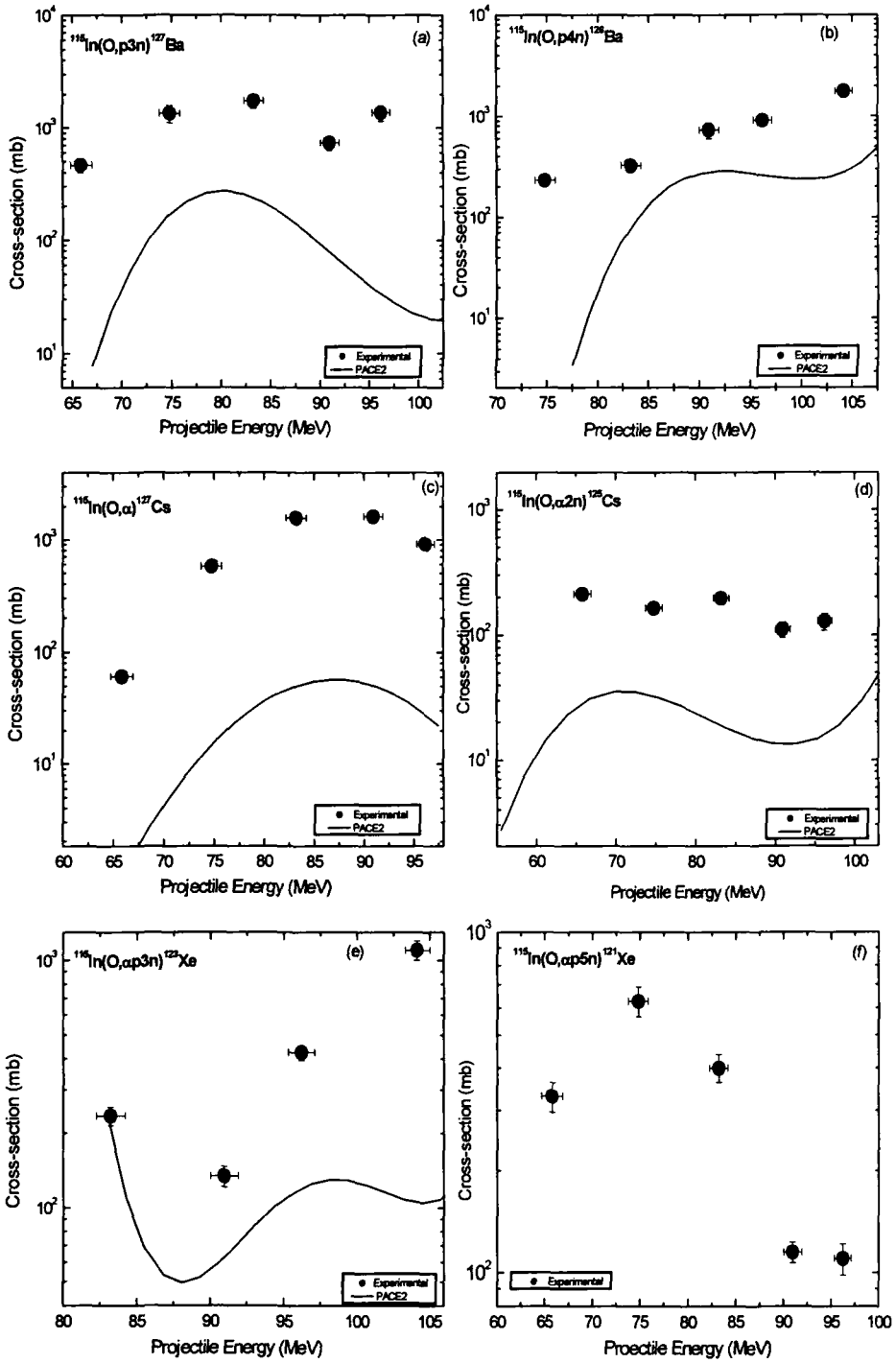

Fig 5.3.1(a-f) Experimentally measured and theoretically calculated EFs using code PACE2 (PLD=8).

5.4 Results of Recoil Range Distributions (RRDs)

In the previous subsection 5.1.1, the enhancement of the EFs by several orders of magnitude was observed as compared to the theoretical calculations in the alpha emission channels i.e. ^{93}Nb(C, α2n) ^{99}Rh , ^{93}Nb(C,2αn)^{96}Tc, ^{93}Nb (C, 2α2n)^{95}Tc , ^{93}Nb(C,2α3n)^{94}Tc. In order to further confirm the complete and incomplete fusion reaction mechanism and to separate the contribution of these reaction processes in ^{12}C + ^{93}Nb system, the forward recoil range distributions of various reaction products have been measured at projectile energy ≈ 80 MeV. The measured values of recoil ranges of evaporation residues as a function of cumulative thickness of catcher foils are shown in Fig. 5.4.1(a-f). The measured values are shown by solid squares and the size of the square indicates the magnitude of errors. The solid lines guide the eye to the experimental data. As can be seen from these figures, at a given value of incident projectile energy, only one peak is observed in the recoil range distributions for ^{101}Pd and ^{100}Pd isotopes. However, the recoil range distributions of ^{101}Pd, ^{100}Pd populated via reactions (C, p3n) and (C, p4n) show only one peak, and are Gaussian in nature. One peak in the recoil range distribution clearly indicates that palladium products are formed solely via the complete fusion process, followed by the evaporation of n and/or p. The recoil range distributions for evaporation residues formed via reactions (C, α2n), (C, 2α2n), and (C, 2α3n), show two separate peaks, one corresponding to the CF and the other at a relatively lower value of range. These peaks clearly indicate that the residues are not only formed by the CF process but by some other process in which the linear momentum transfer is less than as found in case of complete fusion process. This is possible only when a fragment of the projectile fuses with the target and the rest moves with velocity almost equal to that of the projectile, leading to less momentum transfer. The two separate peaks in the recoil range distribution clearly indicate that these reaction products are not only formed by the complete fusion process but partly by the incomplete fusion also.

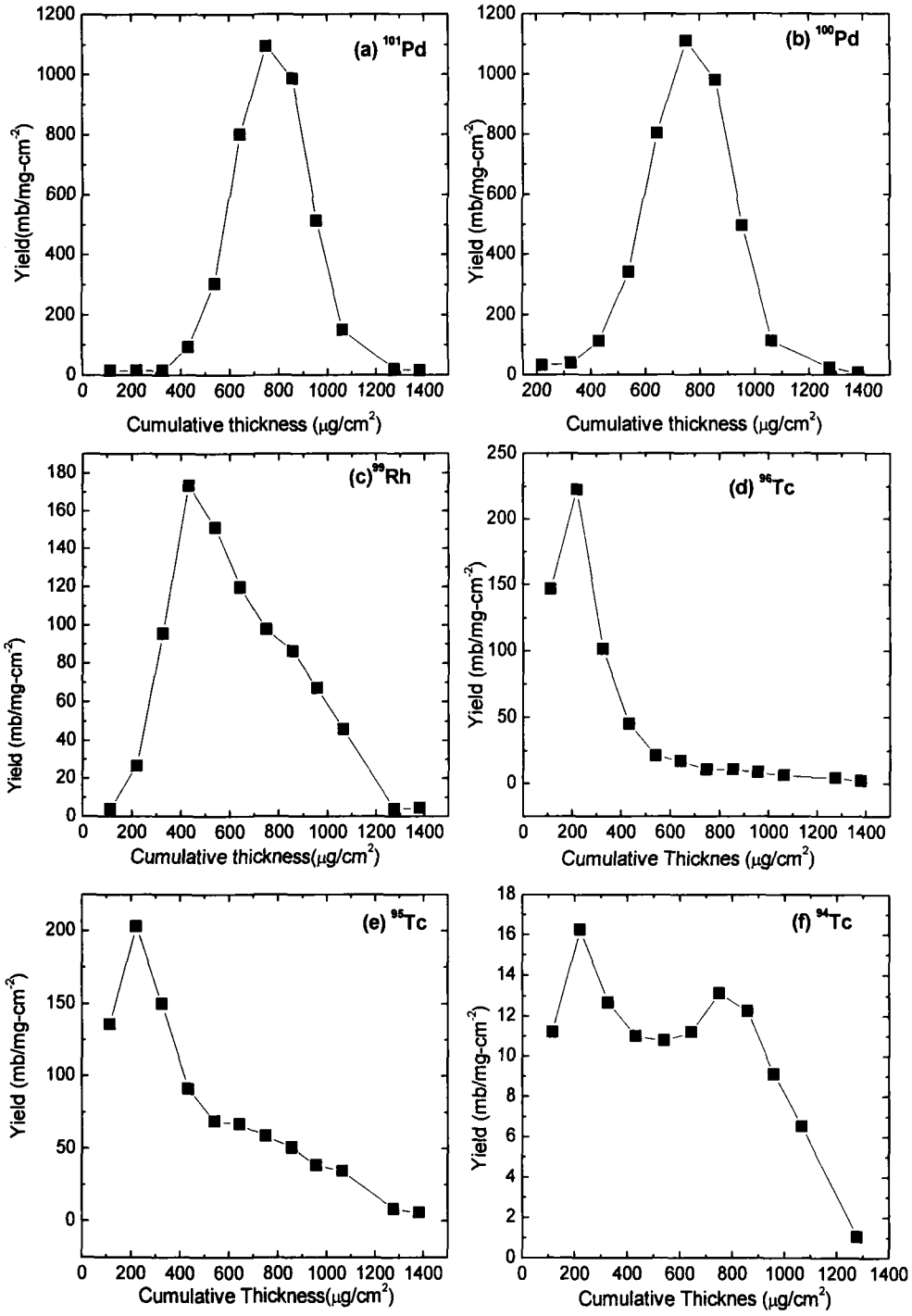

Fig.5.4.1(a-f). The experimentally measured RRDs for various radioactive residues produced in the ^{12}C+ ^{93}Nb system at ≈ 80 MeV are shown. The solid lines are guides to the experimental data.

Further, the relative contributions of the complete and incomplete fusion in the production of a particular reaction product may be computed by fitting the experimentally measured RRDs with Gaussian peaks using the ORIGIN software. The yield curves of evaporation residues obtained from RRDs are assumed to be Gaussian in nature and may be given as [14]

$$Y = Y_0 + \frac{A}{\sqrt{2}\,\pi\,\omega_A^2} e^{-(R-R_p)^2/2\omega_A^2}, \qquad \text{---------5.4.1}$$

where Rp is the most probable mean range, ω_A is the width parameter (Full Width at Half Maximum) of the recoil range distribution, and A is the area under the peak. Further, the normalized yield Y may be estimated by the chi square fit to the experimentally determined production yield at different catcher foil thicknesses and may be represented as follows:

$$\chi^2 = \frac{1}{m-p-1}\{Y(A) - Y_0(A)\}^2 \qquad \text{-------- 5.4.2}$$

The value of the chi square (χ^2) was minimized in this analysis using a non-linear least-square fit routine, keeping the width parameter w_A and most probable mean range (Rp) of the evaporation residues as a free parameter.

Moreover, as indicated in Figs5.4.1(c-f), such cases in which the residues show more than one RRD component, the experimentally measured normalized yields have been fitted using the multi-peak option in a way similar to mentioned above. The contribution of different fusion components (^{12}C, ^{8}Be and ^{4}He) have been obtained by way of dividing the area under the peak of the corresponding fusion component by the total area associated with the experimental data. The percentage contributions coming from the different complete and/or incomplete-fusion components are deduced in such a way for the residues populated in ^{12}C+ ^{93}Nb systems are indicated in Figs.5.4.2(c-f), along with their corresponding channels.

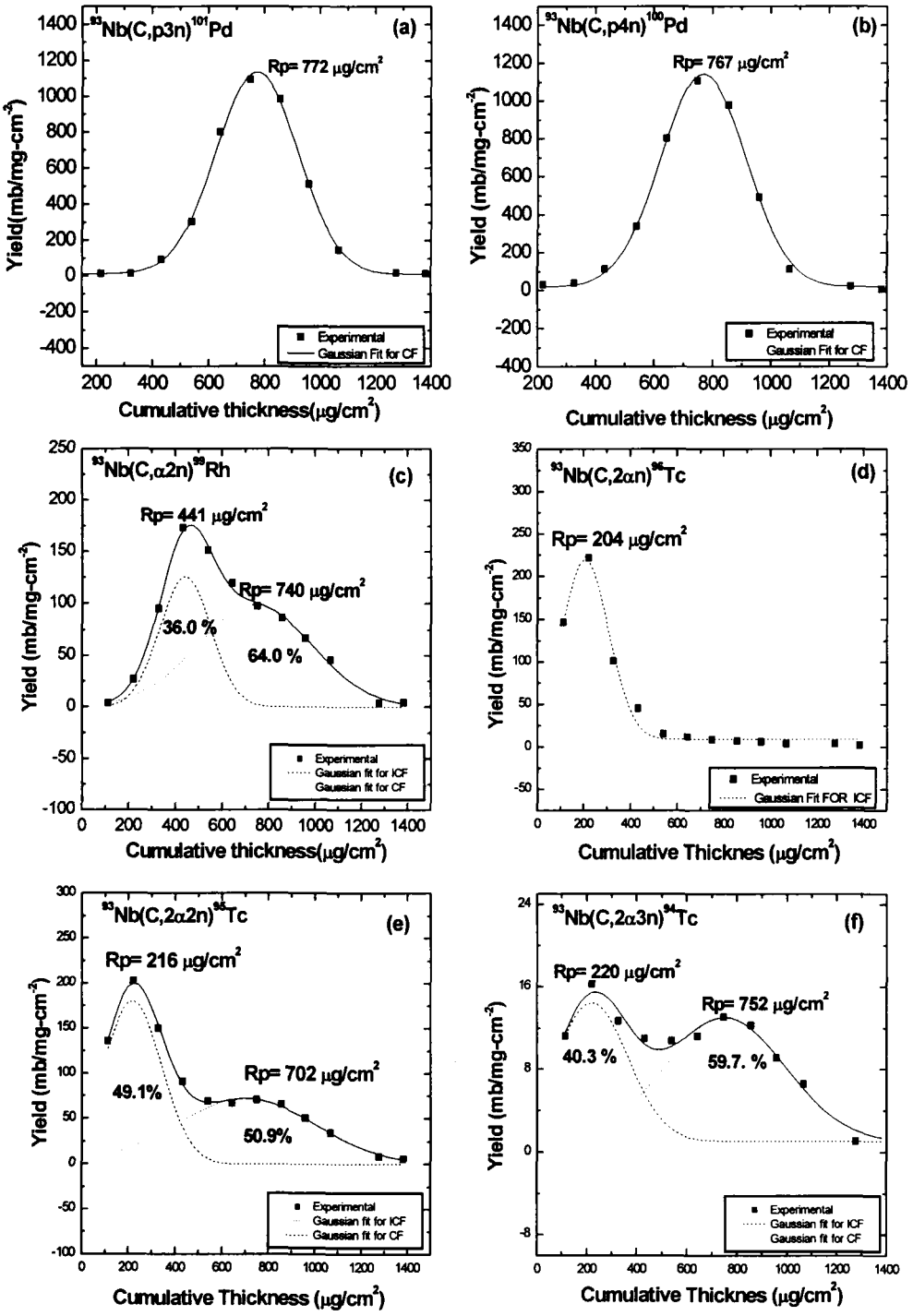

Fig5.4.2(a-f) Gaussian fit to the experimentally measured RRDs.

5.4.1 Discussion of the experimental results of RRDs

As can be seen from Figs 5.4.2(a-b), the RRDs for ^{101,100}Pd isotopes produced via (^{12}C, p3n) and (^{12}C, p4n) channels respectively have a peak at only one value of cumulative catcher thickness (≈770 μg/cm^2). The RRDs of Pd isotopes are Gaussian in nature, having peaks at a thickness corresponding to the expected recoil range of the composite nucleus ^{105}Ag in aluminum, calculated using the classical approach and the stopping power tables of Northcliffe and Schilling [15], meaning hereby that these products are formed by the complete fusion process only, followed by the evaporation of n and/or p. However, for the reaction ^{93}Nb(C,α2n)^{99}Rh [Fig5.4.2(c)],the RRDs has two peaks, one at a relatively lower value of cumulative catcher thickness ≈ 441 μg/cm^2 (due to ^{8}Be fusion) and the other at ≈ 740 μg/cm^2 (due to ^{12}C fusion) respectively. The incomplete fusion contribution in this case is found to be 36.0 % with an uncertainty of 5%. Regarding the ^{93}Nb(C,2αn)^{96}Tc reaction , the RRD show a dominant low range component due to the ICF of an α particle (peak at ≈204μg/cm^2) while a long range tail as shown in Fig. [5.4.2(d)] demonstrates almost a negligible CF part.

In case of reactions ^{93}Nb(C,2α2n)^{95}Tc and ^{93}Nb(C,2α3n)^{94}Tc, shown in Figs.5.4.2(e-f) , the RRDs have two peaks; one is at relatively lower values of catcher thickness ≈ 216/220 μg/cm^2(due to α fusion) and the other at ≈ 702/750 μg/cm^2(due to ^{12}C fusion). The relative contribution of the ICF [as indicated in Figs5.4.2 (e,f)] of α particle in the population of ^{95}Tc and ^{94}Tc residues is found to be ≈49.1% and 40.3% respectively.

In light of the above facts, it may be concluded that the ICF plays an important role in the heavy–ion reactions. A detailed study on the angular distribution of projectile-like fragments may provide important additional information on the incomplete fusion reaction dynamics.

References

[1] A Gavron, Phy. Rev. **C. 21,** 230 (1980).

[2] P. Misaelides, Radiochim, Acta **28**, 1 (1981).

[3] B.S. Tomer et al., Z. Phys. **A 343**, 223 (1992).

[4] M. Blann, ALICE-91, LLNL/IAEA/NEA Data Bank France,(1991).

[5] I.S Grant, Private communication.

[6] M. Blann, J. Bisplinghoff, Report -3494-27(1975). University of Rochester. N.Y.

[7] V.F. Weisskopf and D.H. Ewing, Phys. Rev. **57,** 472 (1940).

[8] M. Blann, Phys. Rev. Lett. **27,** 337 (1971).

[9] M. Blann, Phys. Rev. Lett. **28**, 757 (1972).

[10] D. Bodansky, Ann. Rev. Nucl. Sci. **12,** 79 (1962).

[11] F. Puhlhofer, Nucl. Phys. **A 280,** 267(1977).

[12] Anjana Maheshwari, M.Phil.Dissertation, AMU, Aligarh, India, (2007)

[13] Meenal Gupta, M.Phil. Dissertation, AMU, Aligarh, India (2007)

[14] P.P Singh et al., Eur. Phys. J. **A34**, 29 (2007).

[15] L.C. Northcliffe and R.F. Schilling, At. Data Nucl. Data Tables **A7**, 264(1970).

List of Publications

1. *Study of some excitation function in $^{12}C + {}^{59}Co$ system*
   Avinash Agarwal, I.A. Rizvi, **Tauseef Ahmad**, Anjana Maheshwari, Rakesh Kumar, K.S. Golda, B.K. Yogi and A.K. Chaubey
   DAE-BRNS Symposium on Nuclear Physics Vol. **46B**, 234 (2003).

2. *A glimpse of forward recoil range distribution of ERs in $^{12}C + {}^{59}Co$ at 6 MeV/A*
   Avinash Agarwal, I.A. Rizvi, **Tauseef Ahmad**, Anjana Maheshwari, Rakesh Kumar, K.S. Golda, B.K. Yogi and A.K. Chaubey
   DAE-BRNS Symp. on Nucl. Phys. Vol. **46B,** 286 (2003).

3. *Measurement and analysis of cross-sections for Ne induced reactions with Vanadium at 4-7 MeV/A*
   Avinash Agarwal, I.A.Rizvi, **Tauseef Ahmad,** A. Maheshwari, Meenal Gupta, S.S. Ghugre, A.K. Sinha and A.K. Chaubey
   Proceedings of the 50th Symposium on Nuclear Physics Vol. **50,** 319 (2005).

4. *Study of some evaporation residues identified in $^{12}C+{}^{93}Nb$ system Below 7 MeV/A*
   Tauseef Ahmad, I.A. Rizvi, Avinash Agarwal, Rakesh Kumar, K.S. Golda and A.K. Chaubey
   Proceedings of the DAE-BRNS Symp. on Nucl. Phys. Vol. **51**, 423 (2006).

5. *Study of some incomplete fusion reactions in $^{12}C+{}^{93}Nb$ System at Pelletron energies*
   Tauseef Ahmad, I.A. Rizvi, Avinash Agarwal and A.K. Chaubey
   Proceedings of the DAE Symp. on Nucl. Phys. Vol. **52**, 313 (2007).

6. *Incomplete and complete fusion reactions in the interaction of $^{16}O + {}^{115}In$ system: A study of excitation functions*
   Avinash Agarwal, Meenal Gupta, I.A. Rizvi, **Tauseef Ahmad**, Anjana Maheshwari, Rakesh Kumar and A.K. Chaubey
   Proceedings of the DAE Symp. on Nucl. Phys. Vol. **52**,389 (2007).

7. *Measurement and analysis of excitation function in $^{12}C + ^{52}Cr$ system*

I.A. Rizvi, Anjana Maheshwari, Avinash Agarwal, **Tauseef Ahmad**, Meenal Gupta and A.K. Chaubey

Proceedings of the DAE Symp. on Nucl. Phys. Vol.**52**, 395 (2007).

8. *A study of Recoil Range Distributions (RRDs) for various residues populated in $^{12}C + ^{93}Nb$ system*

Tauseef Ahmad, I.A. Rizvi, Avinash Agarwal and A.K. Chaubey

Submitted to DAE-BRNS Symp. on Nucl. Phys. (2008).

9. *Excitation functions for some evaporation residues identified in the interaction of ^{20}Ne and ^{93}Nb at moderate excitation energies.*

Avinash Agarwal, I.A. Rizvi, Meenal Gupta, **Tauseef Ahmad**, S.S.Ghugre, A.K. Sinha and A.K.Chaubey

Submitted to DAE-BRNS Symp. on Nuclear Physics (2008)

10. *Reaction Mechanism in the $^{12}C + ^{93}Nb$ system through excitation functions below 7 Mev/nucleon*

Tauseef Ahmad, I.A. Rizvi, Avinash Agarwal, Rakesh Kumar, K.S. Golda and A.K. Chaubey

Submitted to Phys. Rev. C.

11. *Proton induced reactions on Niobium*

I.A.Rizvi, Avinash Agarwal, **Tauseef Ahmad** and A.K.Chaubey

Submitted to Romanian Reports in Physics.

DAE-BRNS SYMPOSIUM ON NUCLEAR PHYSICS

CONTRIBUTED PAPERS VOLUME 46B(2003)

BHABHA ATOMIC RESEARCH CENTRE
MUMBAI

DECEMBER 8-12, 2003

Editors
P. Singh
Bency John

Organised by
BOARD OF RESEARCH IN NUCLEAR SCIENCES
DEPARTMENT OF ATOMIC ENERGY
GOVERNMENT OF INDIA

Study of Some Excitation Functions in $^{12}C + ^{59}Co$ System

[1] Avinash Agarwal, [2] I. A. Rizvi, [3] Tauseef Ahmad, [3] Anjana Maheswari, [4] Rakesh Kumar, [4] K. S. Golda, [5] B. K. Yogi and [3] A. K. Chaubey

[1]Department of Physics, Bareilly College Bareilly 243 005, India
[2]Department of Physics, Addis Ababa University, Addis Ababa, P.O.Box 1176, Ethiopia
[3]Department of Physics, A. M. U. Aligarh 202 002, India
[4]Nuclear Science Centre, New Delhi – 110 067, India
[5]Department of Physics, Govt. College Kota, India

E-mail: avi_ag@rediffmail.com

The study of nuclear reaction mechanism in heavy ion induced reactions has been of great interest over the past decade. Measurement of excitation functions served as a powerful tool for the understanding of reaction mechanism.

At the energies of projectile near the coulomb barrier the reactions are dominated by compound nucleus formation, but as the energy of projectile is increased incomplete fusion (ICF) of the projectile starts competing with the complete fusion (CF). In ICF reactions, only a fragment of the projectile fuses with the target. An important feature of these reactions is the emission of light particles at forward angles with approximately beam velocity.

As a part of program to study the complete and incomplete fusion reactions in heavy ion induced reactions we have studied the reactions induced by $^{12}C^{5+}$ in ^{59}Co. The experiment has been performed using 15UD Pelletron facility of NSC New Delhi. Thin targets of specpure cobalt (thickness ~ 350 $\mu g/cm^2$) were prepared on 2 mg/cm^2 aluminum backing using vacuum evaporation technique. Individual targets of Cobalt were irradiated at energies ranging from 60 – 80 MeV. The beam current was around 20 nA. The flux of heavy ions was measured using a Faraday cup and charge integrator. To crosscheck the flux and in order ton align beam line in scattering chamber two monitors (SSB detectors) were also placed at $\pm$ 10^0 to the beam line. Activates induced in targets-catcher assemblies were measured using HPGe gamma detector with associated electronics and PC coupled through CAMAC. All the decay parameters of the nuclei studied here were taken from Table of Radio Active Isotopes by Browne and Firestone(*). The method of calculation of cross-sections is described in details in our earlier paper(2). The excitation functions for the reactions $^{59}Co(C, p3n)^{67}Ge$, $^{59}Co(C, \alpha p3n)^{63}Zn$ and $^{59}Co(C, 2\alpha 2n)^{61}Cu$ have been measured in the present work. The measured excitation functions are compared with the theoretically calculated values using CASCADE(3) and ALICE-91 (4) codes, and results are as shown in figures.

CASCADE code gives cross-sections based on compound nucleus formation only while ALICE-91 code gives compound nucleus and compound nucleus plus pre-equilibrium contributions. Our measurements do not match with the CASCADE code calculations. The results obtained using ALICE-91 code for pre-equilibrium plus compound nucleus are also not matching

with our results, which shows that the processes other than compound nucleus formation and pre-equilibrium decay are playing an important role at these energies. The large difference in our measured and calculated values gives clear signatures of incomplete fusion at these energies.

References:

1. E. Browne and Firestone, Table of Radioactive Isotopes (Wiley, New York, 1986)
2. Avinash Agarwal, I. A. Rizvi, and A. K. Chaubey Phys. Rev. C63, 34605 (2002)
3. F. Puhlhofer, Nucl. Phys. A280, 267 (1977)
4. M. Blann, ALICE-91 LLNL/IAEA/NEA Data Bank, France (1991)

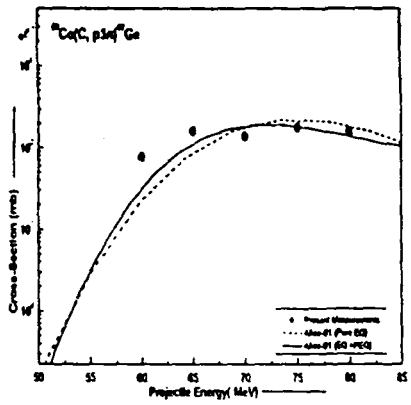

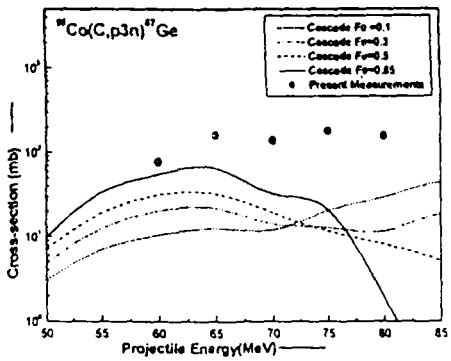

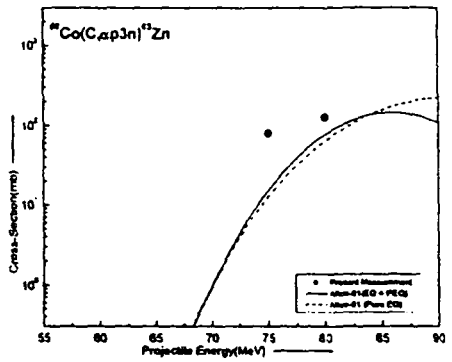

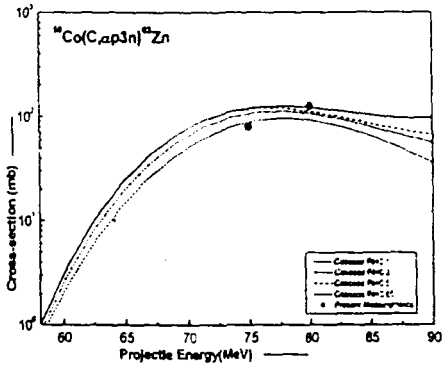

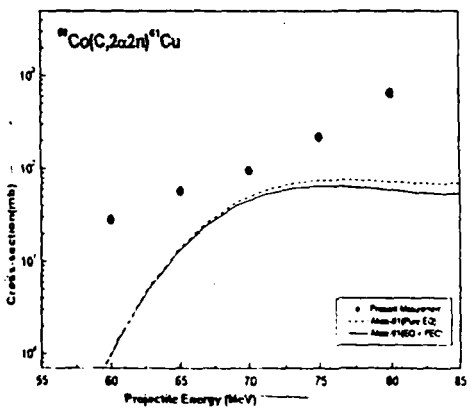

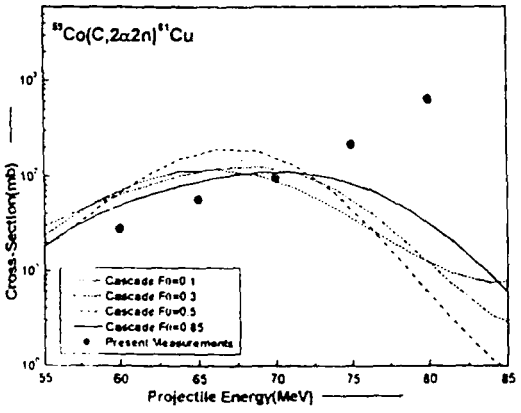

A Glimpse of Forward Recoil Range Distribution of ERs in $^{12}C + ^{59}Co$ at 6 MeV/A

[1] Avinash Agarwal, [2] I. A. Rizvi, [3] Tauseef Ahmad, [3] Anjana Maheswari, [4] Rakesh Kumar, [4] K. S. Golda, [5] B. K. Yogi and [3] A. K. Chaubey

[1]Department of Physics, Bareilly College Bareilly 243 005, India
[2]Department of Physics, Addis Ababa University, Addis Ababa, P.O.Box 1176, Ethiopia
[3]Department of Physics, A. M. U. Aligarh 202 002, India
[4]Nuclear Science Centre, New Delhi – 110 067, India
[5]Department of Physics, Govt. College Kota, India

E-mail: avi_ag@rediffmail.com

Preliminary studies of excitation functions of various evaporation residues (ERs) indicates that Heavy ion induced reactions may take place by some other modes except through complete fusion (1). Considerable enhancement of the measured excitation functions in comparison to theoretical predictions obtained by computer codes ALICE-91 and CASCADE, indicates that various reaction channels are not only populated by complete fusion followed by evaporation of neutrons, protons and alpha particles but also by some other process, which may be incomplete fusion of ^{12}C with ^{59}Co.

In order to have further confirmation the measurement of Forward Recoil Range Distribution (FRRD) of evaporation residues produced in the reaction is mandatory. In this present work we have measured the FRRD of ERs at 75 MeV projectile ($^{12}C^{5+}$) energy. The experiment was performed using General Purpose Scattering Chamber (GPSC) facility at Nuclear Science Centre, New Delhi. The stack consisting of a self-supporting target of ^{59}Co (thickness ~ 200 nm) followed by a series of thin aluminum catcher foils (thickness ~70 – 100 μg /cm^2) was irradiated for ~24 hrs. The induced activities in catcher foils were followed offline using pre - calibrated HPGe detector coupled to CAMAC based FREEDOM data acquisition system. ERs produced were identified using their characteristic gamma rays adopted from Table of Isotopes (2). The other experimental details can be found elsewhere (3). The measured values of recoil range plotted against cumulative thickness of catcher foils for various residual isotopes are shown in figure. It can be seen from figs. (A) and (B) that only one peak is observed in the FRRD for ^{67}Ge and ^{67}Ga isotopes, produced by (C, p3n) and (C, 2p2n) reaction channels. One peak in the FRRD clearly indicates that these products are formed solely via complete fusion only. The recoil range distribution for ERs formed via reactions (C, αn), (C, α2n), (C, αp3n) and (C, 2α2n) show two separate peaks, as shown in figs (C – F). One corresponds to complete fusion and the other at relatively lower value of range indicates incomplete fusion. This clearly shows that these residues are not only formed by complete fusion process but by some other means in which the linear momentum transfer is less than that in case of complete fusion process. This is possible only when a fragment of the projectile fuses with the target and rest moves with the same velocity

almost as that of incident projectile, leading to less momentum trainsfer, which is Incomplete fusion.

References

1. Avinash Agarwal et .al. Proceeding DAE Sysmp. on Nuclear Physics M S University Tirunelveli Dec. 26 – 30, 2002 Vol.45B p .246
2. E. Browne and Firestone, Table of Radioactive Isotopes (Wiley, New York, 1986)
3. Avinash Agarwal, Ph.D Thesis Aligarh Muslim University Aligarh 2003. Unpublished

Figues showing the measured values of recoil range distribution for various residual isotopes produced at 75 MeV projectile energy

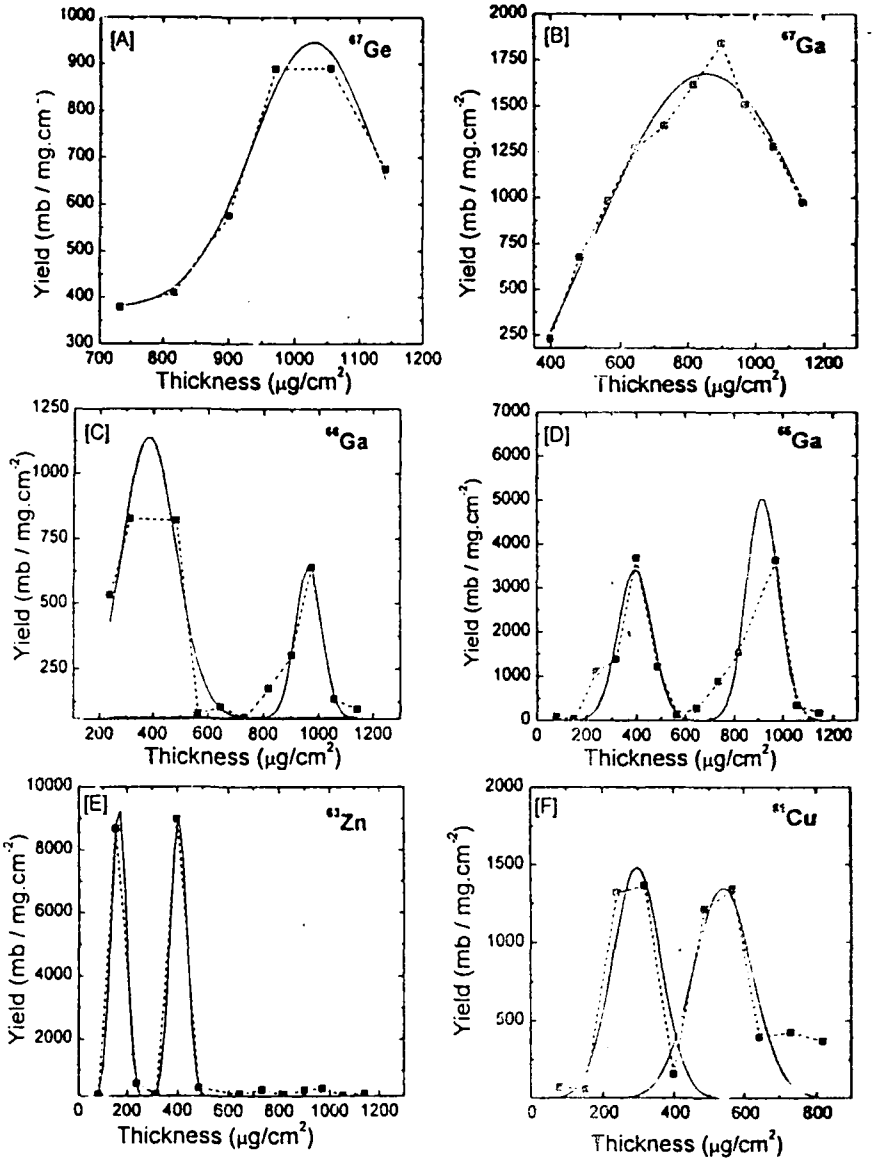

DAE-BRNS 50th Symposium on Nuclear Physics

Invited Talks and Contributed Papers **Volume 50 (2005)**

Bhabha Atomic Research Centre, Mumbai

December 12 - 16, 2005

Editors
S. Kailas
Suresh Kumar
L. M. Pant

Sponsored by
Board of Research in Nuclear Sciences
Department of Atomic Energy
Government of India

Measurement and analysis of cross-sections for Ne induced reactions with Vanadium at 4 - 7 MeV/A

Avinash Agarwal [1*], I. A. Rizvi [2], Tauseef Ahmad [2], A. Maheshwari [2], Meenal Gupta [2], S. S. Ghugre [3] A. K. Sinha [3] and A. K. Chaubey [4]

[1] *Department of Physics, Bareilly College Bareilly 243 005, INDIA*

[2] *Department of Physics, Aligarh Muslim University Aligarh 202 002, INDIA*

[3] *UGC DAE Consortium For Scientific Research, Kolkata Centre Kolkata 700 098, INDIA*

[4] *Department of Physics, Addis Ababa University Addis Ababa,P.O.Box 1176, ETHIOPIA*

* *email: avi_ag@rediffmail.com*

It is well established that the reaction cross-section in reactions of light heavy ions is dominated by the mechanism of fusion/evaporation. However it has long been realized that in addition to complete fusion (CF), various incomplete fusion (ICF) processes may contribute significantly to the yields of evaporation residues. Inamura et al (1) was the first who identified incomplete fusion as a mechanism. The various incomplete fusion processes occur for incident partial waves generally higher than those involved in complete fusion, but that the window in *l*- space associated with the different processes overlap to a considerable extent.

In the present paper we have made an attempt to understand the reaction mechanisms involved in the interaction of $^{20}Ne^{6+}$ with ^{51}V. The experiment has been performed using Cyclotron facility of Variable Energy Cyclotron Centre (VECC) Kolkata (INDIA). Thin target foils of vanadium (thickness 1.19 – 1.50 mg/cm^2) were prepared by rolling at the target laboratory of VECC. In the present measurement the stacked foil activation technique was used. The target foils and aluminum foils which works as energy degrader as well as catcher were chosen in such a way that the desired energy of the projectile would be available on a particular target. The stack of target and degrader foils was irradiated with 145 MeV diffused $^{20}Ne^{6+}$ beam. The flux of the heavy ions was measured by using the Faraday cup and charge integrator. After irradiation the activities induced in target catcher assemblies were measured using HPGe gamma ray detector associated with required electronics and MCA. All the decay parameters of the nuclei studied here have been adopted from Table of Radioactive Isotopes by Browne and Firestone (2). The computational information is described in detail in our earlier report (3).

The cross –sections for the production of ^{66} Ga, ^{65} Ga, ^{64} Zn, ^{63} Zn, ^{51} Cu, ^{56} Ni and ^{52} Mn have been measured in the present work. The theoretical estimation of the cross – sections for the evaporation residues of interest, produced by complete fusion were obtained using the Monte Carlo simulation code PACE-2 (4). In the calculation the optical model parameters for emitted light particles (n, p, α) were taken from Perey and Perey (5). The fusion cross –sections were calculated following the prescription of Bass (6). The level density parameter is one of the important quantities. The variation of cross –section for different values of level density parameter (K) has also been studied in present work.

The measured excitation functions with theoretical

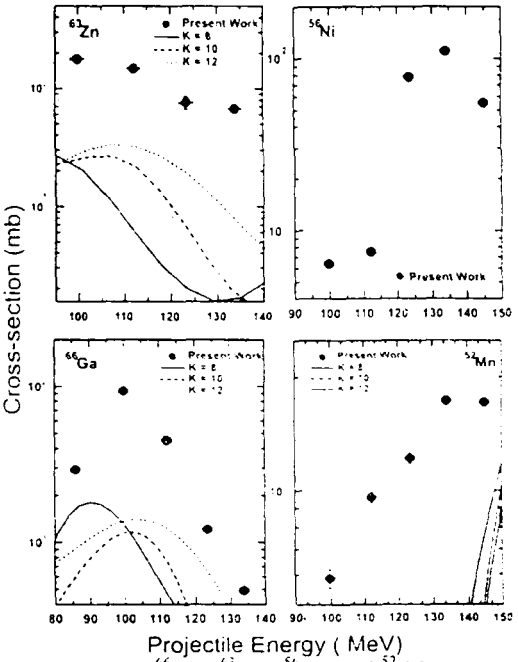

predictions for ^{66} Ga, ^{63} Zn, ^{56} Ni and ^{52} Mn as representative cases are shown in figures. From Figures we see that there is substantial difference between our measured and theoretically calculated values. The significant enhancement of cross – sections clearly indicated the presence of some other process in the population of these radioisotopes, which can be incomplete fusion. In order to confirm this, measurements of forward recoil range distribution of residual isotopes is still needed.

References

[1] T. Inamure, M. Ishihara, T. Fukuda, T. Shimoda and H. Hiruta. Phys. Lett. **68B** (1977) 51

[2] E. Browne and R. B. Firestone. *Table of Radioactive Isotopes* (Wiley, New York) 1986.

[3] Avinash Agarwal, I. A. Rizvi, and A. K. Chaubey . Phys. Rev. **C63** (2002) 34605

[4] A. Gavron Phys. Rev. **C21** (1980) 230

[5] C. M. Percy and F. G. Percy . At. Data and Nucl. Data Tables **17** (1976) 1.

[6] R. Bass. Phys. Rev. Lett. **39** (1997) 265

Proceedings of the DAE – BRNS

SYMPOSIUM ON NUCLEAR PHYSICS

Invited Talks and Contributed Papers Volume 51 (2006)

The Maharaja Sayajirao University of Baroda
Vadodara
December 11 -15, 2006

Editors
S. Kailas
Suresh Kumar
S. Santra

Sponsored by
Board of Research in Nuclear Sciences
Department of Atomic Energy
Government of India

Study of Some Evaporation Residues Identified in ^{12}C +^{93}Nb System Below 7 MeV/ A

Tauseef Ahmad[1*], I.A. Rizvi[1], Avinash Agarwal[2], Rakesh Kumar[3], K.S.Golda[3] and A.K.Chaubey[4]

[1]*Department of Physics, Aligarh Muslim University, Aligarh- 202002, INDIA*
[2]*Deptartment of Physics, Bareilly College Bareilly- 243005, INDIA*
[3] *Inter University Accelerator Centre, Aruna Asaf Ali Marg, New Delhi - 110067, INDIA*
[4]*Deptartment of Physics, Addis Ababa University, Addis Ababa, P.O.Box 1176, ETHIOPIA*
* *email: tau_ad@rediffmail.com*

Introduction

As a part of our programme to study the reaction mechanism i.e. Complete and In-complete fusion (CF & ICF) / PE emission in heavy ion induced reactions, an attempt has been made to measure the excitation function (EF) (i.e. cross-section versus incident energy) for ^{12}C+ ^{93}Nb system at Pelletron energies. Since excitation functions provide clues for the reaction mechanism, it serves as a powerful tool to understand the reaction mechanism properly. For instance, the slowly descending tail of the excitation function is a direct signature of pre-equilibrium emission. The importance of the excitation function also lies in the fact that with ever increasing use of radioactive isotopes in various applied fields, there is a growing demand to provide the knowledge of the excitation functions of nuclear reactions in order that the production of selected isotopes could be maximized. The excitation functions of nuclear reactions leading to suitable products are very important to be known for the yields of products before its Thin Layer Activation (TLA) application in a particular material. The measurement of excitation functions has been done using activation technique. This technique is popular for its sensitivity, selectivity and simplicity. The main advantage of this technique is the possibility of measuring EFs for the production of large number of residues in a single irradiation, thereby reducing beam time requirements. In this technique, activities induced by radioactive fragments in the target and catcher assemblies are measured by off-line spectroscopy. The experiment was carried out at the Inter University Accelerator Centre (IUAC). New Delhi, India.

Experimental Details

Self-supporting ^{93}Nb targets of thickness ~2.02 mg/ cm^2 were prepared by rolling natural niobium of purity better than 99.9%. The target thickness was determined by gravimetry. A stack of five samples of ^{93}Nb was irradiated by ^{12}C beam of energy 75 MeV. The irradiation was performed in General Purpose Scattering Chamber (GPSC) having facility of in vacuum transfer of targets. The two surface barrier (SSB) detectors were also kept at ± 10° to the beam direction to monitor the flux of the incident beam. The stack of samples was irradiated for nearly six and half-hours keeping in view the half-lives of radioisotopes of interest. The charge states of beam was 6^+ with beam current 25 nA to 30 nA. The irradiated samples were taken out from the GPSC and the activities induced in samples were recorded by using a HPGe detector coupled with PC.The detector was pre-calibrated using standard γ - sources of known strength. The evaporation residues were identified using the characteristic γ - rays as well as half-lives. A list of identified various residues produced by different reaction channels are presented in Table-1. All the decay parameters of residues studied here have been adopted from Table of Radioactive Isotopes by Browne and Firestone [1]. The formulation used to find out cross-sections is described in detail elsewhere [2]. The errors in the measured cross-sections may be introduced because of the uncertainty in determining the efficiency of detector, the dead time of the detector, uncertainty in determining the number of nuclei in the sample, fluctuations in beam current etc. The reported value is the weighted average [2] of the various cross-section

values so obtained. The statistical error given in the results is the larger one of the internal and external errors [2]. In general these errors are less than 12%.

Table- 1 Nuclear spectroscopic data used for this work

ERs	Channel	Half Life	γ-Energy (keV)	Inten. (%)
^{103}Ag	(C, 2n)	1.10 h	118	31.2
^{101}Pd	(C, p3n)	8.5 h	296	19.2
^{100}Rh	(C,αn)	20.8 h	539	78.4
^{98}Rh	(C,α3n)	8.7 m	652	96.0

Results and Discussion

In order to understand fusion mechanism in heavy ion interactions, excitation functions for reaction channels viz ^{93}Nb(C, 2n)^{103}Ag, ^{93}Nb(C, p3n)^{101}Pd, ^{93}Nb(C, αn)^{100}Rh & ^{93}Nb(C, α 3n)^{98}Rh have been experimentally measured at five energies from near coulomb barrier (43.5 MeV) to well beyond it. The size of experimental data point (closed circles) includes the magnitude of the estimated error. The measured results of EFs are compared with the predictions of Monte Carlo simulation using the code PACE2 [3] as shown in figures. The level density parameter is one of the important quantities in this code. The variation of cross-section for different values of level density parameter designated as PLD has also been studied in the present work [4]. The other input parameters in the programme were used as default values. Theoretical model parameters for emitted light particles were taken from Perey and Perey [5] for alpha, proton & neutrons. The fusion cross-sections were calculated by following the prescription of Bass [6].

Conclusion

From figures it is observed that EFs of products ^{103}Ag, ^{101}Pd show the good agreement with the theoretical values calculated using PACE2, which is veritable signature of CF. On the other hand some of the α - channels like (C, αn) and (C, α3n) show a substantial difference between our measured and theoretically calculated values. The significant enhancement of cross-section clearly indicates the presence of some other process in the population of these radioisotopes, which can be incomplete fusion. In order to confirm this, measurements of Recoil Range distribution and particle gamma coincidence studies are required.

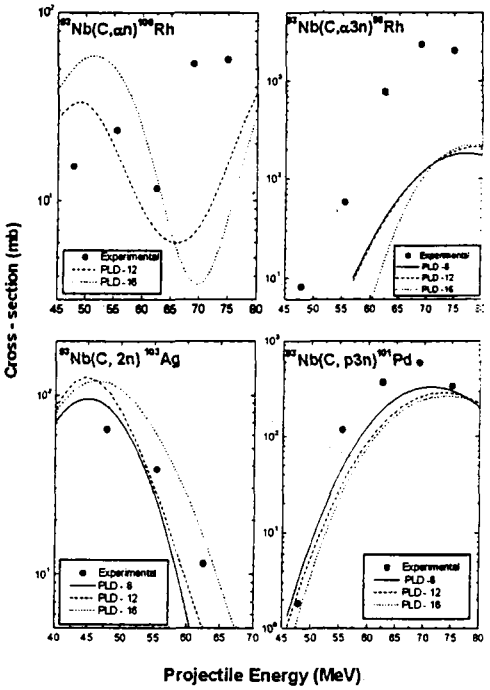

Acknowledgments

The authors are thankful to the Director, IUAC, New Delhi for extending the facilities for carrying out the experiment. We also thank the Chairman, Department of Physics, A.M.U. for providing the necessary facilities.

References

[1] E.Browne and Firestone. Table of Radioactive Isotopes (Wiley, New York) 1986.
[2] Avinash Agarwal, I.A. Rizvi and A.K.Chaubey. Phy. Rev. C 65 (2002) 34605.
[3] A. Gavron, Phys. Rev. C 21(1980) 230.
[4] Tauseef Ahmad, M.Phil. Dissertation (2006) AMU, Aligarh, India
[5] C.M.Perey and F.G.Perey At. Data and Nucl.data Tables 17 (1976) 1.
[6] R.Bass.Phys.Rev. Lett. 39 (1997) 265.

Proceedings of the
DAE SYMPOSIUM ON
NUCLEAR PHYSICS

Invited Talks and Contributed Papers Volume 52 (2007)

Sambalpur University
Jyotivihar, Burla, Orissa
December 11 -15, 2007

Editors
R. K. Choudhury
A. K. Mohanty
S. Santra

Sponsored by
Board of Research in Nuclear Sciences
Department of Atomic Energy
Government of India

Study of some incomplete fusion reactions in $^{12}C+^{93}Nb$ system at Pelletron energies

*Tauseef Ahmad[1], I.A.Rizvi[1], Avinash Agarwal[2] and A.K.Chaubey[3]

[1]*Department of Physics, AMU, Aligarh. -202002, INDIA*
[2]*Department of Physics, Bareilly College Bareilly-243005, INDIA*
[3]*Department of Physics, Addis Ababa University, P.O.Box 1176 Addis Ababa, ETHIOPIA*

* *email: tau_ad@rediffmail.com*

Introduction

Recent experiments on heavy ion reaction mechanism indicate that complete fusion (CF) gives way to incomplete fusion even at energies slightly above the coulomb barrier [1,2]. In case of ICF reactions only a fraction of projectile fuses with the target nucleus that leads to excited incompletely fused composite system and the unused part moves forward with almost same velocity as that of incident projectile as spectator. The excited in-completely fused composite system gives rise to final reaction products after unusual modes of de-excitation. Several models have been proposed to explain ICF reactions. The Sum rule model of Wilczynski et al [3] predicts that ICF mainly takes place in peripheral collisions and is localized in the input angular momentum space above the critical angular momentum for CF. Few models have proposed to explain some of the important characteristics of ICF reaction dynamics but many aspects like linear momentum, multiplicity associated with process, and dependence on beam energy is not fully explored. In order to understand ICF reaction dynamics, more experimental data covering a wide range of periodic table and energy are required. Cross-section data of such products are also required to determine the optimum irradiation conditions for the production of RIBs. Keeping in view the above specialties of ICF, the excitation functions for the residues $^{100-98}Rh$, ^{97}Ru, $^{95-94}Tc$ occurring in $^{12}C + ^{13}Nb$ system have been measured in the projectile energy range about 47-75 MeV using activation technique followed by off line gamma spectrometry. The comparison of experimentally measured EFs has been made with predictions of ALICE- 91 code [4].

Experimental Details

Self-supporting ^{93}Nb targets of thickness ~2.02 mg/ cm^2 were prepared by rolling natural niobium of purity better than 99.9%. The target thickness was determined by gravimetry. A stack of five samples of ^{93}Nb was irradiated by ^{12}C beam of energy 75 MeV. The irradiation was performed in General Purpose Scattering Chamber (GPSC) having facility of in vacuum transfer of targets. The two surface barrier (SSB) detectors were also kept at $\pm$ 10° to the beam direction to monitor the flux of the incident beam. The stack of samples was irradiated for nearly six and half-hours keeping in view the half-lives of radioisotopes of interest. The charge states of beam was 6^- with beam current 25 nA to 30 nA. The irradiated samples were taken out from the GPSC and the activities induced in samples were recorded by using a HPGe detector coupled with PC. The detector was pre-calibrated using standard γ - sources of known strength. The evaporation residues were identified using the characteristic γ - rays as well as half-lives. All the decay parameters of residues studied here have been adopted from Table of Radioactive Isotopes by Browne and Firestone [5]. The formulation used to find out cross-sections is described in detail elsewhere [6]. The errors in the measured cross-sections may be introduced because of the uncertainty in determining the efficiency of detector, the dead time of the detector, uncertainty in determining the number of nuclei in the sample, fluctuations in beam current etc. The reported value is the weighted average of the various cross-section values so

obtained. The statistical error given in the results is the larger one of the internal and external errors. In general these errors are less than 12%.

Results and Discussion:

In the present contribution, EF_s for the radioactive residues produced via the reactions ^{93}Nb (C, αn)^{100}Rh , ^{93}Nb (C, α2n) ^{99}Rh , ^{93}Nb (C, α3n) ^{98}Rh , ^{93}Nb (C, αp3n) ^{97}Ru, ^{93}Nb (C, 2α2n) ^{95}Tc , ^{93}Nb (C, 2α3n) ^{94}Tc have been measured. The measured results of EFs are compared with the predictions of ALICE-91. This code has been developed by M. Blann, to account for the equilibrium as well as pre-equilibrium (PE) emission in light and heavy ion reactions. In this code the level density parameter *a*, the mean free path multiplier *COST* and initial exciton number n_o are some of the important input parameters. The level density parameter *a* is calculated from the expression *a* = A/K where, A is the mass number of the compound nucleus and K is a level density parameter constant designated as PLD, which can be varied. Calculations have been performed for different values of PLD (8,12,16) and *COST* (3,6,9).The effect of variation of the parameter PLD on calculated EFs is presented in Figs 1,2 &4. It can be seen from the same Figs that in α-emission channels the significant enhancement of cross-section has been found [7].This leads to new mode of reaction termed as ICF. Further it has been observed that the calculated excitations functions are insensitive to the parameter *COST*. As a representative case the effect of variation of parameter *COST* on the calculated EF for the reaction ^{93}Nb (C, 2n) ^{103}Ag is shown in Fig3.

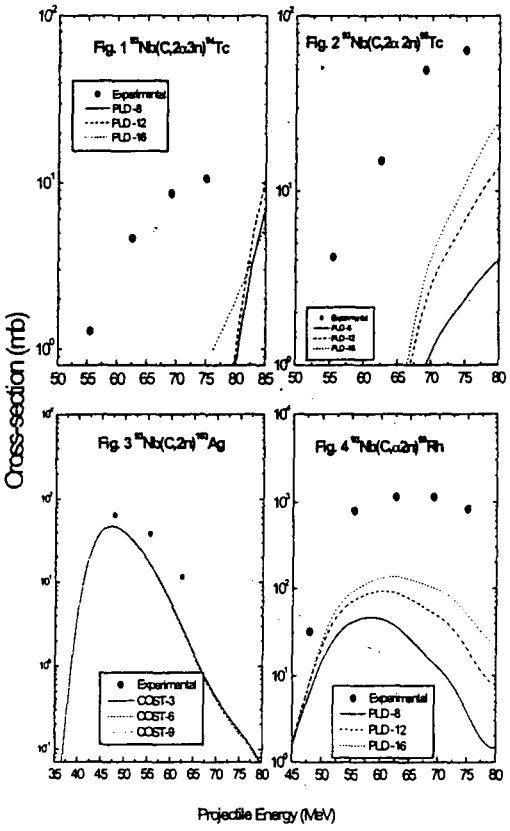

Acknowledgements

We would like to thank IUAC personnel especially Mr. Rakesh Kumar and Ms. K. S. Golda for their assistance in our experiment. Thanks are due to Pelletron crew for providing good quality beam. We also thank the Chairman, Department of Physics, AMU, Aligarh for providing the research facility.

References

[1] S. Chakrabarty et al, Nuclear Physics **A678**, 255 (2000)

[2] M. K. Sharma et al, Phys. Rev. **C70,** 044606 (2004).

[3] J.Wilczynaski, et al, Nucl Phys. **A373**, 109 (1982).

[4] M. Blann, ALICE-91, LLNL/IAEA/NEA Data bank France (1991).

[5] E.Browne and Firestone, Table of Radioactive Isotopes (Wiley, New York) 1986.

[6] Avinash Agarwal et al, Phy.Rev.C**65** (2002) 34605

[7] Tauseef Ahmad et al, Proceedings of DAE-BRNS symo.**51** (2006) 423-424.

Incomplete and complete fusion reactions in the interaction of $^{16}O + ^{115}In$ system: A study of excitation functions

*Avinash Agarwal[1], Meenal Gupta[2], I. A. Rizvi[2], Tauseef Ahamad[2], Anjana Maheshwari[2], Rakesh Kumar[3] and A. K. Chaubey [4]

[1]*Department of Physics, Bareilly College, Bareilly - 243 005, INDIA*

[2]*Deptartment of Physics, Aligarh Muslim University, Aligarh – 202 002, INDIA*

[3]*Inter University Accelerator Centre, Aruna Asaf Ali Marg, New Delhi - 110067, INDIA*

[4]*Deptartment of Physics, Addis Ababa University, P.O. Box 1176, Addis Ababa , ETHIOPIA*

* *email: avibcb@gmail.com, avi_ag@rediffmail.com*

Introduction

Investigations of different reaction mechanisms involved in the heavy ion induced reactions e.g., Complete fusion (CF), Incomplete fusion (ICF), direct reactions, transfer reactions etc. have been a point of core interest at entrance channel energies as low as 5 MeV/A. Recent studies report the breakup of ^{12}C, ^{16}O, and ^{20}Ne into ^{4}He, ^{8}Be and ^{12}C projectile fragments and their subsequent fusion with the target [1–5]. As a part of our ongoing program to understand CF and ICF reaction mechanisms, we have made an attempt to measure the excitation functions for the evaporation residues (ERs) identified in the interaction of $^{16}O + ^{115}In$ system. In the present report the excitation functions (EFs) for seven evaporation residues produced in the interaction of considered projectile target system have been measured using activation technique, followed by off line gamma ray spectroscopy. This technique provides in the simplest and fastest way the comprehensive and at the same time detailed information we are looking for.

Experimental Details

The experiment was performed at the Inter University Accelerator Centre (IUAC) New Delhi. Spectroscopically pure natural indium i.e., ^{115}In (95.7%) + ^{113}In (4.3%) of thickness 1mg/cm^2 was evaporated onto aluminum baking of thickness ~ 2mg/cm^2. The stacks comprising of target foils and suitable energy degraders were irradiated in the General purpose scattering chamber having in-vacuum transfer facility at IUAC for about 8 hrs. The total charge collected was 1062 μC. The activities produced in the target catcher assembly were followed offline using pre-calibrated HPGe detector with associated electronics and data acquisition system FREEDOM. The various ERs were identified by their characteristics γ-rays and decay curve analysis. The Detailed analysis of the data was done using FREEDOM in offline mode. The excitation functions for various evaporation residues have been calculated using the formulation given elsewhere [6].

Results and Discussion

The excitation functions for the evaporation residues ^{127}Ba, ^{125}Ba, ^{127}Cs, ^{125}Cs, ^{123}Xe, ^{121}Xe and ^{120}Ir have been measured in the energy range ≈ 4 MeV/A to 7 MeV/A. To the best of our knowledge no earlier measurements are available in the literature. The decay channels studied are tabulated in table given below. As it is pointed out in the table, the contribution from ^{113}In isotope (4.3%) will be seen in the residues ^{123}Xe, ^{121}Xe and ^{120}I. These contributions are maximum at projectile energy ≤ 45 MeV. In the present work we rejected this data so that the contributions from ^{113}In become negligible. The experimentally measured values of EFs have also been compared with those calculated using theoretical model code ALICE-91. The effect of level density parameter PLD with initial exciton number 16(8+8 +0) and cost 3 is studied.

ERs	Decay channel	Half-life
^{127}Ba	^{115}In(O,p3n)^{127}Ba + Precursor ^{127}La	12.70 min
^{126}Ba	^{115}In(O,p4n)^{126}Ba	100.00 min.
^{127}Cs	^{115}In(O.α)^{127}Cs	6.25 hrs.
^{125}Cs	^{115}In(O.α2n)^{125}Cs	46.70 min.
^{123}Xe	^{113}In(O.αpn)^{123}Xe +^{115}In(O.αp3n)^{123}Xe	2.08 hrs.
^{121}Xe	^{113}In(O.αp3n)^{121}Xe +^{115}In(O.αp5n)^{121}Xe	40.10 min.
^{120}I	^{113}In(O.2αn)^{120}I +^{115}In(O.2α3n)^{120}I	53.00 min.

The experimentally measured values along with theoretical predictions are shown in figures. It is evident from figure that the experimental values of EFs for ^{127}Ba are much higher than the theoretical predictions, but the trend is almost same. This residue may also populate from the decay of its higher charge precursor isobar ^{127}La. The independent yield of ^{127}Ba could not be calculated as the EFs for ^{127}La are not measured because of very small half life of ^{127}La. For reaction residue ^{126}Ba, as seen from figure, the experimental data is in good agreement with theory up to 90 MeV and after that the data points are higher as compared to theory. It is also found that the excitation functions for ^{127}Cs , ^{125}Cs , ^{123}Xe, ^{121}Xe and ^{120}I ERs the measured EFs are much higher than the theoretical predictions.

Conclusion

The comparative study of experimentally measured EFs with theory show considerable enhancement in cross-sections for some isotopes indicating that the process other than Compound nucleus decay play important role in the production of these residues. This large difference gives clear signature that the role of ICF for these channels is important in the considered energy range, which can be further confirmed by Recoil Range Distribution (RRD) and particle gamma coincidence measurements.

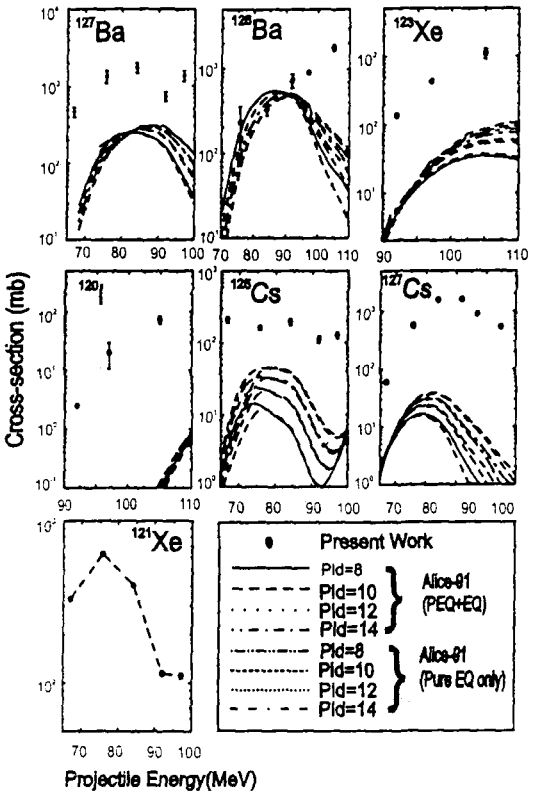

Acknowledgements

The financial assistance to one of author (AA) from DST, New Delhi in the form of Fast Track Young Scientist scheme vide project ref. SR/FTP/PS-08-2006 is highly acknowledged.

References

[1] S. Mukherjee, A. Sharma, S. Sodaye, A. Goswami and B. S. Tomar. Int. Jour. Mod. Phys. E. **15**(2006) 237.

[2] M. K. Sharma, Unnati, B. P. Singh, R. Kumar, K.S. Golda, H. D. Bhardwaj and R. Prasad, Nucl. Phys. A **776** (2006) 83.

[3] R. Tripathi , K. Sudarshan, A. Goswami, R. Guin and A. V. R. Reddy Phys. Rev. C **74** (2006) 014610

[4] E.Z. Buthelezi, F. Cerutti, E. Gadioli, G. F. Steyn, A. Pepe, S. H. Connell and A. A. Cowley Eur. Phys. J. A. **28** (2006) 193.

[5] D.Singh, M. A. Ansari, R. Ali, N.P.M. Sathik and M. Ismail. J. Phy. Soc. Japan 75 (2006) 104201.

[6] Avinash Agarwal, I. A. Rizvi and A. K. Chaubey . Phys. Rev. C **65** (2002) 034605

Measurement and analysis of excitation functions in $^{12}C + ^{52}Cr$ system

*I.A. Rizvi[1], Anjana Maheshwari[1], Avinash Agarwal[2], Tauseef Ahmad[1], Meenal Gupta[1] and A.K. Chaubey[3]
[1]Department of Physics, Aligarh Muslim University, Aligarh-202 002, INDIA
[2]Department of Physics, Bareilly College, Bareilly-243 005, INDIA
[3]Department of Physics, Addis Ababa University, P.O. Box 1176, Addis Ababa, ETHIOPIA
email: *isarrizvi@hotmail.com

Introduction

The study of fusion of heavy ions (HI) has been the topic of significant interest to nuclear physicists for the past several years. With the availability of heavy ion beams of suitable energy range, the interest has renewed in the recent past. The HI fusion reactions are very important to study the nuclei at high excitation and high spin states. HI induced reactions with projectile energies closed to coulomb barrier are dominated by compound nucleus and direct reactions. As the projectile energy is increased compound nucleus formation is hindered and incomplete fusion (ICF) starts competing with the complete fusion (CF). In ICF reactions only a part of the projectile fuses with the target nucleus, while rest of it escapes with nearly the same velocity as that of incident ion mainly in forward cone. Further, as the excitation energy is increased it is quite possible that the nuclear particles are evaporated prior to the attainment of equilibrium process. This phenomenon is known as pre-equilibrium (PE) Process Thus, in HI interaction ICF and PE processes may lead to the enhancement of cross-sections for certain channels.

Recent literature [1,2] reports the importance of CF, ICF as well as PE emission in HI reactions at energies around coulomb barrier. As a part of our on going program to study CF, ICF and PE emission in HI reactions, the excitation functions (EFs) for six reactions produced in $^{12}C+^{52}Cr$ system have been measured in the energy range about 52.0 to 80.0 MeV. The experiment was performed at the Inter-University Accelerator Centre (IUAC), New Delhi, India.

Experimental Details

Targets of enriched isotope of ^{52}Cr (83.79%) of thickness 364.32 $\mu g/cm^2$ were prepared by vacuum evaporation technique at the Target Division of IUAC, New Delhi, India. The staked foil activation technique was employed. The stack comprising of five target foils with energy degraders was irradiated by $^{12}C^{6+}$ beam of energy 80.0 MeV at the IUAC, New Delhi, India. The irradiation was done in the General Purpose Scattering Chamber (GPSC), having in vacuum transfer facility. The irradiation time of about 4 hours was chosen according to the half-lives of evaporation residues of interest. The total charge collected was around 456 μc. The incident energy of ^{12}C on each foil in the stack was calculated from the software 'SRIM' version 2003 [3].

After irradiation and cooling, a 100cc HPGe detector (resolution 2 keV for 1332 keV γ ray of ^{60}CO) coupled to PC based data acquisition system having software "FREEDOM" was used for recording spectra of residual activity induced in the individual foil. Energy and efficiency calibrations were done using a standard ^{152}Eu gamma point source of known strength by keeping it at the target position. The expression used for computing the experimentally measured cross-sections is taken from reference[4].

Results and Discussion

In the present work, the EFs for carbon-induced reactions on chromium were experimentally measured in the energy range

about 52.0 to 80.0 MeV. The reactions studied at five projectile energies were $^{52}Cr(C,2n)^{62}Zn$, $^{52}Cr(C,p2n)^{61}Cu$, $^{52}Cr(C,p3n)^{60}Cu$, $^{52}Cr(C,\alpha p3n)^{56}Co$, $^{52}Cr(C,\alpha p4n)^{55}Co$ and $^{52}Cr(C,\alpha 3pn)^{56}Mn$. To the best of our knowledge no earlier measurements are available in literature. The EFs have also been calculated theoretically using computer code ALICE-91 [5]. The effect of variation of PLD on the calculated EF, for the reaction $^{52}Cr(C,p2n)^{61}Cu$ is shown in Fig.1. It is evident from Fig. 1 that the value of PLD equal to 22 reproduces the experimental data for this reaction. To see the effect of variation of 'COST' on EFs, calculations have been performed for different values of COST (4,6,8). As a representative case the effect of variation of parameter 'COST' on the calculated EFs for the reaction $^{52}Cr(C,p3n)^{60}Cu$ is shown in Fig.2. Further, it has been noticed that effect of 'COST' variation is negligible in HI induced EFs.

The effect of variation of exciton number (n_0) for the reaction $^{52}Cr(C,p3n)^{60}Cu$ is shown in Fig. 3. It may be pointed out that a set of k=22, n_0=12 with COST=6 gives satisfactorily reproduction of the magnitude of experimental data for the reactions $^{52}Cr(C,p2n)^{61}Cu$ as shown in Fig. 4 while chosen set of parameters do not reproduce the same for the reaction $^{52}Cr(C,\alpha p3n)^{56}Co$ as displayed in Fig. 5. For the $^{52}Cr(C,\alpha p3n)^{56}Co$ reaction, the theoretical predictions of code ALICE-91 give substantially small cross-sections as compared to the measured cross-sections as shown in Fig. 5. The enhancement of the cross-section indicates that these channels are not reproduced by complete fusion of ^{12}C followed by evaporation of neutron, proton and alpha particles but also by some other process, which may be incomplete fusion of ^{12}C with ^{52}Cr.

Since the angular momentum effect have not been considered in the present version of ALICE-91 code for pure Weisskopf–Ewing calculations, it is obvious to shift the calculated EFs by the amount ≅12.0-18.5 MeV. It has been found that the code ALICE-91 calculations satisfactorily reproduce the experimental data when the energy scales of the calculated EFs are shifted by respective E_{Rot} values. It is very clear from Figs. 4 & 6 that the EFs for the reaction $^{52}Cr(C,p2n)^{61}Cu$ is in good agreement with the calculated values after taking into account the rotational energy shift.

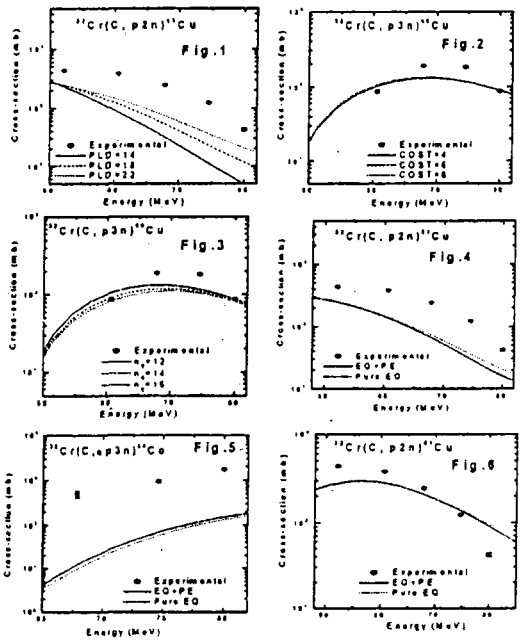

Conclusion

It was found that in some reaction channels i.e. $^{52}Cr(C,2n)^{62}Zn$, $^{52}Cr(C,p2n)^{61}Cu$ & $^{52}Cr(C,p3n)^{60}Cu$ there is a good agreement between theoretical and experimental values. However, in alpha emission channels i.e. $^{52}Cr(C,\alpha p3n)^{56}Co$ $^{52}Cr(C,\alpha p4n)^{55}Co$ and $^{52}Cr(C,\alpha 3pn)^{56}Mn$ reactions there is a significant enhancement in the cross-section values which leads to a new mode of reaction termed as ICF. In order to have further confirmation of ICF and to find out relative contribution of CF and ICF in a particular reaction channel, more detailed experiments for the measurement of energy spectra of emitted particles are required.

References

[1]. D. Singh, M. Afzal Ansari, R. Ali, N.P.M. Sathik and M. Ismail, J. Phy. Soc. Japan **75** (2006) 104201.

[2]. Manoj Kumar Sharma, Unnati, B.P. Singh, Rakesh Kumar, K.S. Golda, H.D. Bhardwaj and R. Prasad, Nucl. Phy. **A776** (2006) 83.

[3]. J.F. Ziegler and J.P. Biersack, SRIM 2003 (SRIM.com).

[4]. Anjana Maheshwari, M.Phil Dissertation, A.M.U., Aligarh, India (2007).

[5]. M. Blann, ALICE-91 LLNL/IAEA/NEA, Data Bank, France (1991).